AN ABSTRACT OF THE DISSERTATION OF

Matthew R. Slattery for the degree of Doctor of Philosophy in Toxicology presented on June 5th, 2019.

Title: A Nano-sized Dose of Toxicology: Elucidating the Disconnect Between Nanomaterial Dosimetry and Biological Effects.

Abstract approved: _____

Stacey L. Harper

Nanotechnologies continue to permeate a multitude of industries, with diverse applications ranging from pesticides to fuel additives. The unusual behavior of nanomaterials that drives their innovation also complicates the job of toxicologists tasked with assessing their potential environmental and public health impacts. This dissertation investigates the underlying reasons for uncertainty associated with the biological effects of nanomaterials. Chapter 2 and Chapter 3 focus on nanoparticles present in commercially available pesticide formulations and assess how particle size influences the environmental risk of a pesticide's active ingredient. These studies reveal a size-specific effect on the toxicity of the nanoparticles despite normalized concentrations of active ingredient and highlight the potential for nanoparticles to mask the hydrophobic behavior of some chemicals. In Chapters 4 and 5, the focus shifts to soybeans and their microbiome as they respond to soils amended with cerium oxide nanoparticles. Utilizing metagenomic software to analyze large data sets and predict changes in ecological functionality, these companion chapters correlate plant growth with bacterial community structure and emphasize the atypical dose-response relationship of nanoparticles in terrestrial systems. Further, they address importance of acknowledging the difference between pristine and aged nanoparticle exposures. This body of work demonstrates the capacity for nanomaterials to confound toxicological assessment if the disconnect between nanomaterial dosimetry and biological response is not accounted for.

A Nano-sized Dose of Toxicology: Elucidating the Disconnect Between Nanomaterial Dosimetry and Biological Effects

by
Matthew R. Slattery

A DISSERTATION

submitted to

Oregon State University

in partial fulfillment of
the requirements for the
degree of

Doctor of Philosophy

Presented June 5th, 2019
Commencement June 2019

Doctor of Philosophy dissertation of Matthew R. Slattery presented on June 5th, 2019.

APPROVED:

Major Professor, representing Toxicology

Head of the Department of Environmental and Molecular Toxicology

Dean of the Graduate School

I understand that my dissertation will become part of the permanent collection of Oregon State University libraries. My signature below authorizes release of my dissertation to any reader upon request.

Matthew R. Slattery, Author

ACKNOWLEDGEMENTS

The author expresses sincere appreciation to the following people:

Stacey Harper, for your mentorship and unwavering support from the beginning, all while enduring your own tremendous hardship. Your patience was instrumental in helping me find my own (nonlinear) path, and your steadfast optimism kept the dream alive.

Bryan Harper, for never failing to produce a smile while preaching the cyclical nature of science (experiment, fail [many times], learn, repeat). Your excitement in tackling new problems is contagious and I'd be lucky to take some of that with me moving forward.

Jay Reichman, for the many hours spent at the bench and in the office unravelling the molecular mysteries of the sequencing world. Stories about the old days of science, and musings about the modern ones, went a long way to reignite my academic passions.

Craig Marcus, for sharing your extraordinary knowledge and enthusiasm of all things toxic, from Paracelsus to pesticides. Thanks for letting me step in to conclude my PhD coursework the same way that it began: with open-minded dialogue from a room of passionate toxicologists.

My fellow graduate students, for reminding me nobody is truly alone along the arduous path to a PhD. I'm grateful for your superb company at the bench, in classrooms, on coastlines, and – most importantly – on the dance floor.

My family, for their genuinely unconditional support and giving me every opportunity to pursue my academic goals.

CONTRIBUTION OF AUTHORS

Matthew R. Slattery is the primary author and responsible for all components of this dissertation except as follows:

Stacey L. Harper and Bryan J. Harper assisted with study design, interpretation of Chapters 2 and 3, as well as the editing of all Chapters.

Vince L. Cataldi conducted the *Daphnia* toxicity tests in Chapter 3.

Jay R. Reichman assisted with DNA processing and data interpretation in Chapters 4 and 5.

TABLE OF CONTENTS

TABLE OF CONTENTS (continued)

TABLE OF CONTENTS (continued)

LIST OF FIGURES

LIST OF FIGURES (Continued)

LIST OF FIGURES (Continued)

LIST OF TABLES

Chapter 1 Introduction

Since the beginning of the environmental movement in the 1960's, the research and management of environmental contaminants has focused on small molecules that interact with biological systems. As toxicology evolved as a discipline, the relationship between the environmental concentration of a chemical and the magnitude of an organism's response became a cornerstone of environmental protection. The toxicologists' assumption is that dose makes the poison, such that higher doses exert stronger effects. Recently, nanomaterials have challenged the predictability of this relationship, namely because they necessitate supplemental information and consideration for accurate prediction. Understanding when, how, and why nanomaterials violate the dose-response assumption is critical to effective management of nanotechnologies and may help to expand their utility.

1.1 Nanomaterial production and application

Nanomaterials are available in a virtually infinite variety of shapes, sizes, compositions, and surface chemistries. While some agencies such as the International Organization for Standardization define nanomaterials as having a size of 1 to 100 nm in at least one dimension, this definition is arbitrary considering that nanomaterials do not suddenly gain or lose unique properties at 100 nm (Stone 2010). Instead, it is useful to view nanomaterials for their iconic features, including (but not limited to) their extremely high surface area to volume ratio, colloidal behavior, chemical reactivity, and propensity for transformation. For example, the surface area to volume ratio is considered a crucial component of interaction between nanomaterials and biological targets (Nel 2009) while environmental transformations can fundamentally alter the surface reactivity of a nanoparticle (Lowry 2012).

Given the limitless range of nanomaterials available for manufacture, they see an equally wide breadth of applicability. Pesticides, cosmetics, coatings, electronics, food products, textiles, and fuel additives are among the multitude of products that take advantage of nanomaterial features.

In this dissertation, two seemingly distant applications of nanotechnologies are investigated: pesticides and fuel additives.

These categories are unified by their toxicological relevance to agricultural practices. Obviously, pesticides have an important role within modern pest management practices. Research into nano-enabled pesticide products shows great promise for improving the efficacy of current active ingredients (Kah 2018). Nonetheless, governing agencies are determining how to regulate the emerging role of nanotechnology in the pesticide industry.

The link between fuel catalysts and agricultural systems may seem less relevant without additional context. The nanomaterial used in fuel catalysis is a cerium oxide (CeO_2) nanoparticle (CeNP) that aids in the combustion of diesel fuel. These CeNPs are highly resistant to degradation or dissolution (Cornelis, 2014). They survive the combustion process and are ejected into the atmosphere with the rest of the combustion byproducts and settle into soils where they can accumulate up to 1 mg kg^{-1} along roadways (Park 2008). This vector of contamination is relevant for farmers who operate diesel machinery on their property or farms near roadways. Additionally, CeNPs that find their way to wastewater plants are likely to accumulate in biosolids (Barton 2014), which are in turn applied to farming soils as fertilizer.

1.2 Nanotoxicology nuances and needs

Nanotoxicology as a discipline continues to grow with the increasing presence of nanomaterials in our modern world. Due to fundamental differences between nanomaterials and small molecules, many of the conventional protocols developed for toxicological assessments are not compatible for probing nanopesticides or CeNPs. Merely quantifying a nanoparticle in an environmental sample presents a major challenge. While small molecules can be isolated using liquid or gas chromatography and subsequently quantified on a mass spectrometer or similar molecular detection instrument, nanomaterials require a different approach. For example, you cannot isolate a nanoparticle passing through a liquid chromatography column if its passage is

blocked by the column pores and attempting to vaporize a nanoparticle is simply ineffective and likely to create problems for gas chromatographs.

Even if separating and isolating nanoparticles was logistically simple, determining the mass of a nanoparticle disregards other vital properties that dictate their behavior. Metrics including particle number and surface area have equal or greater importance than mass with respect to nanomaterial toxicity (Teeguarden 2006).

The subsequent chapters are case studies that highlight the shortcomings of conventional toxicology approaches when assessing the environmental impacts of nanomaterials. For Chapters 2 and 3 covering nanopesticides, the validity of longstanding metrics of chemical mobility and toxicity are investigated for their effectiveness on nano-enabled formulations. Small modifications to assessment protocols may resolve some of the incompatibilities between nanomaterials and pesticide risk assessment. At the very least, it is important to acknowledge the potential for idiosyncratic or unexpected biological responses to nanopesticides.

Similarly, Chapters 4 and 5 point out the relevance of experimental shortcomings in prior CeNP research and implement new study designs intended to capture a more holistic picture of nanomaterial impacts to terrestrial organisms. In these cases, more attention is paid to atypical nanoparticle concentration-response relationships and the importance of particle aging in determining biological effects. These ideas have gained momentum in the nanotoxicology literature in recent years, but these studies combine modern sequencing technology with the evolving notions of nano-biological interactions.

References Cited

1. Barton, L. E., Auffan, M., Bertrand, M., Barakat, M., Santaella, C., Masion, A., … Bottero, J. Y. (2014). Transformation of pristine and citrate-functionalized CeO2 nanoparticles in a laboratory-scale activated sludge reactor. Environmental Science and Technology, 48(13), 7289–7296. https://doi.org/10.1021/es404946y
2. Kah, M., Kookana, R. S., Gogos, A., & Bucheli, T. D. (2018). A critical evaluation of nanopesticides and nanofertilizers against their conventional analogues. Nature Nanotechnology, 13(8), 677–684. https://doi.org/10.1038/s41565-018-0131-1
3. Lowry, G. V., Louie, S. M., & Ma, R. (2012). Transformations of Nanomaterials in the Environment. Frontiers of Nanoscience, 7, 55–87. https://doi.org/10.1016/B978-0-08-099408-6.00002-5
4. Nel, A. E., Mädler, L., Velegol, D., Xia, T., Hoek, E. M. V, Somasundaran, P., … Thompson, M. (2009). Understanding biophysicochemical interactions at the nano-bio interface. Nature Materials, 8(7), 543–557. https://doi.org/10.1038/nmat2442
5. Park, B., Donaldson, K., Duffin, R., Tran, L., Kelly, F., Mudway, I., … Martin, P. (2008). Hazard and risk assessment of a nanoparticulate cerium oxide-based diesel fuel additive - A case study. Inhalation Toxicology, 20(6), 547–566. https://doi.org/10.1080/08958370801915309
6. Stone, D., Harper, B. J., Lynch, I., Dawson, K., & Harper, S. L. (2010). Exposure assessment: Recommendations for nanotechnology-based pesticides. International Journal of Occupational and Environmental Health, 16(4), 467–474. https://doi.org/10.1179/oeh.2010.16.4.467
7. Teeguarden, J. G., Hinderliter, P. M., Orr, G., Thrall, B. D., & Pounds, J. G. (2007). Particokinetics in vitro: Dosimetry considerations for in vitro nanoparticle toxicity assessments. Toxicological Sciences, 95(2), 300–312. https://doi.org/10.1093/toxsci/kfl165

PESTICIDE ENCAPSULATION AT THE NANOSCALE DRIVES CHANGES TO THE HYDROPHOBIC PARTITIONING AND TOXICITY OF AN ACTIVE INGREDIENT

Matthew R. Slattery, Bryan J. Harper, Stacey L. Harper

Nanomaterials
MDPI, St. Alban-Anlage 66, 4052
Basel, Switzerland
Published in volume 9, issue 1.

Chapter 2 Pesticide Encapsulation at the Nanoscale Drives Changes to the Hydrophobic Partitioning and Toxicity of an Active Ingredient

2.1 Abstract

Given the costs associated with designing novel active ingredients, new formulations focus on the use of other ingredients to modify existing formulations. Nano-sized encapsulated pesticides offer a variety of enhanced features including controlled release and improved efficacy. Despite the presence of nano-sized capsules in current use pesticide formulations, the analytical and toxicological implications of encapsulation are uncertain. To explore this issue quantitatively, we fractionated the capsules of a commercially available encapsulated insecticide formulation (γ-cyhalothrin active ingredient) into two size ranges: a large fraction (LF), with an average hydrodynamic diameter (HDD) of 758 nm, and a small fraction (SF), with an average HDD of 449 nm. We developed a novel extraction method demonstrating a time-dependent inhibition of γ-cyhalothrin from capsules for up to 48 hours. An acute immobilization test with a freshwater macroinvertebrate (*Ceriodaphnia dubia*) revealed that the SF was significantly more toxic than both the LF and the free γ-cyhalothrin treatment (EC_{50} = 0.18 µg/L, 0.57 µg/L, and 0.65 µg/L respectively). These findings highlight that encapsulation of γ-cyhalothrin mitigates hydrophobic partitioning in a time-dependent manner and influences toxicity in a size-dependent manner. Recognizing the analytical and toxicological nuances of various nano-sized capsules can contribute to innovation in pesticide formulations and may lead to more comprehensive pesticide regulation.

2.2 Introduction

More than 55 billion dollars are spent every year on pesticides [1], reflecting their enormous economic and agricultural importance. While pesticide products are typically composed of many chemicals, in the United States they are regulated according to their active ingredients – the primary drivers of their targeted toxicity. Development and registration of a novel active ingredient is costly and requires up to 2 years of review [2]. This incentivizes manufactures to implement other ingredients (also known as inert ingredients) when reformulating pesticides rather than create new active ingredients. Other ingredients in pesticide products face less regulatory scrutiny, sparking contention over their capacity to modify a pesticide's risk to non-target organisms [3-6]. Nonetheless, reformulation of existing active ingredients is a common practice in the pesticide industry, as indicated by the multitude of distinct products containing identical active ingredients.

Among the innovative formulations available on the market, encapsulated pesticides offer a variety of desirable features that include reduction in human exposure to active ingredients, controlled release, longer residual concentrations, elimination of organic solvents, and increased efficacy [7-9]. Encapsulation technologies utilize a three-dimensional barrier that surrounds active ingredients, shielding them from immediate interaction with their surrounding chemical environment. However, these capsules may also result in incompatibilities with current pesticide risk assessments. For example, chemical descriptors for hydrophobicity (K_{OW}, the octanol-water partitioning coefficient) and soil sorption (K_d, the soil adsorption coefficient) may not be reflective of an active ingredient once encapsulated [10]. Pesticide fate and transport models are highly dependent on these descriptive parameters of active ingredients and can suffer from significant uncertainty when these values are inaccurate [11,12].

Further complicating our understanding of encapsulation technologies, capsules in the nanoscale (1 – 1000 nm) are garnering attention in pesticide literature [13-16] and have been observed in current-use formulations [17,18]. Nano-encapsulated formulas capitalize on the sheer diversity of nanomaterials available, including polymers, lipids, mesoporous silica, clay, and other materials

[19-21]. In addition to many capsule compositions, the size of nanoscale capsules is likely a relevant factor in pesticide formulations, given that nanoparticle size is typically a driving factor in their colloidal behavior and increased relative surface area [22]. While nano-specific effects are recognized in pesticide formulations [23], little is known about the influence of capsule size at the nanoscale.

As nano-encapsulation technologies infiltrate the pesticide market, it is important to note that nano-enabled products can display anomalous behavior when compared to their conventional counterparts [23] and present unique incompatibilities with pesticide regulation [24]. This has drawn concern over integration with current legislative framework [25]. Pyrethroid-based active ingredients appear to be particularly responsive to behavior modifications resulting from nano-enabled formulations [23]. The effects associated with both nano-enabled and encapsulated pesticides could exacerbate discrepancies between expected and observed concentrations, especially when combined as a nano-encapsulated formulation. A quantitative method to assess the extent of capsule-based interference on hydrophobic partitioning would help address concerns that encapsulation renders conventional descriptors such as KOW misleading. Additionally, supplementing this data with toxicity data is necessary to address the demand for comparisons between nano-enabled pesticide formulations and their conventional counterparts [23].

This study sought to investigate these issues by (i) isolating and separating nano-sized capsules from a current-use pyrethroid-based insecticide using centrifugation and passive settling, (ii) designing a novel, time-dependent extraction technique intended for laboratory extraction and hydrophobic comparison of active ingredients and their encapsulated counterparts, and (iii) conducting an acute toxicity test to compare the response of a freshwater macroinvertebrate, *Ceriodaphnia dubia*, to freely suspended and nano-encapsulated active ingredients.

2.3 Materials and Methods

2.3.1 Chemicals

A commercially available, EPA registered capsule suspension insecticide (EPA Reg. No. 67760-104-53883) with 5.9% γ-cyhalothrin was used. Analytical standard grade γ-cyhalothrin [3-(2-chloro-3,3,3-triuoro-1-propenyl)-2,2-dimethyl,cyano(3-phenoxyphenyl) methyl ester], 98.5% purity (CAS number 68085-85-8) was purchased from Crescent Chemical Company (Islandia, NY, USA). Hexane (CAS number 110-54-3) was purchased from Avantor Performance Materials, Inc. (Center Valley, PA, USA).

2.3.2 Preparation of Capsule Fractions from Commercial Product

The encapsulated pesticide formulation used here is sold as a concentrated product (59.9 g γ-cyhalothrin/L according to the label) which was diluted with ultrapure Milli-Q water (Milli-Q Gradient A10 water purification system equipped with a Q-Gard® 2 and a Quantum™ IX Ultrapure Organex cartridge, Millipore Corp., Billerica, MA, USA) to a 100 mg/L stock. In order to isolate the pesticide capsules in the formula and reduce the presence of other ingredients, 10 mL aliquots of the stock were centrifuged for 30 min at 7000 g with a benchtop Eppendorf 5430 centrifuge (Hamburg, Germany), creating a capsule pellet. Carefully, 9 mL of the resulting supernatant was removed from each aliquot and replaced with Milli-Q water, then vortexed to resuspend the capsule pellet to form the unfractionated (UF) samples. To separate the UF capsules into two distinct size ranges, the UF samples were centrifuged again for 7 mins at 1400 g. This produces a supernatant containing the small fraction (SF), while the large fraction (LF) was generated by resuspending the capsule pellet in Milli-Q water. To ensure that the capsules remained in suspension and did not form aggregates over time, the SF and LF samples were set undisturbed in the dark for 48 h before carefully collecting the top 5 mL of the settled SF and LF samples, which was stored in a glass vial at 4 ºC for later analysis.

2.3.3 Capsule Characterization

The hydrodynamic diameter (HDD), zeta potential, and polydispersity index (PDI) of the three fractions (UF, SF, and LF) were measured in triplicate by dynamic light scattering (DLS) using a Zetasizer Nano ZS (Malvern Instruments, LTD., Worcestershire, UK) at 25 ºC. Statistical differences between fractions were determined with a one-way ANOVA. Analysis were considered significantly different at $p \leq 0.05$. The size and morphology of capsules was verified using an FEI Quanta 600 FEG (FEI CO., Hillsboro, OR, USA) scanning electron microscope (SEM) operating at 10 kV using samples prepared by dropping 20 µL of each fraction onto a Si substrate and drying before imaging.

2.3.4 Quantification and Partitioning of γ-cyhalothrin

An Agilent Technologies 7820A GC equipped with an Agilent Technologies 7963A Automatic Liquid Sampler, electron capture detector (ECD), and 25 m × 0.32 mm ID BPX35 column was used to quantify γ-cyhalothrin in test samples. Standard grade γ-cyhalothrin was run at 0.05, 0.1, 1.0, and 2.5 mg/L to produce a calibration curve and verify retention times at the beginning of every run. Solutions of LF and SF were diluted with Moderately Hard Water (MHW) to approximately 1 mg/L for γ-cyhalothrin quantification. MHW was prepared according to the Environmental Protection Agency (EPA) recipe [26]. The LF and SF solutions were compared against a free γ-cyhalothrin (FC) treatment, prepared by adding γ-cyhalothrin suspended in acetone to MHW such that the concentration of γ-cyhalothrin was 1 mg/L and the concentration of acetone was 1 mL/L. Then 600 µL of hexane was mixed with 600 µL of LF, SF, or FC in 1.5 mL gas chromatography (GC) vials in triplicate. Vials were placed on a SCILOGEX MX-T6-S Analog Tube Roller set to 30 rpm for 2 minutes (0 h), 1, 6, 24, 48, or 72 h. After agitation, 500 µL of hexane was aspirated from the vials and diluted with 500 µL of fresh hexane in a new GC vial for analysis. Preliminary studies demonstrated complete recovery of γ-cyhalothrin from the full formulation (quantification of γ-cyhalothrin by GC-ECD that matched concentrations listed on the product label) at 72 h, and therefore γ-cyhalothrin recovery is presented as a percentage of the 72 h concentration. A two-way ANOVA analysis was used to compare γ-cyhalothrin recovery among capsule type and extraction time. Analyses were considered significantly different at $p \leq 0.05$.

2.3.5 Daphnid Immobilization Assay

C. dubia less than 24 h old were provided by the Aquatic Toxicology Laboratory at Oregon State University, cultured in MHW according to EPA specifications [26]. Toxicity assessments at 48 h used immobility of *C. dubia* as an endpoint, defined as no observable swimming action for 15 seconds under gentle agitation of the test vessel (although the heart may still be beating or antennae moving). A total of five treatments were tested: MHW control, 1 mL/L acetone control (in MHW water), FC, SF, and LF. The γ-cyhalothrin concentrations in the FC, SF, and LF stock solutions were verified by GC-ECD before dilution with MHW to concentrations of 0.006, 0.017, 0.05, 0.45, 1.35, 4.05, and 12.5 µg/L. For each treatment and control, 10 *C. dubia* were placed individually in glass vials with 2 mL of their respective solution. There were two experimental replicates per concentration and control, for a total of 20 neonates per treatment. The test period was 48 h under 18 h light period with full-spectrum lights and the water temperature remained at 20 ºC.

A one-way ANOVA was used to compare differences between experimental replicates. We used the drc package in R, version 3.0-1, to generate a two-parameter log-logistic model of the *C. dubia* dose-response curve that was compared pairwise using a one-way ANOVA. Estimates of the EC50 (concentration required for 50% immobilization) for the FC, LF, and SF treatments were calculated using drc. These estimates were compared using a one-way ANOVA test. Analyses were considered significantly different at $p \leq 0.05$.

2.4. Results and Discussion

2.4.1. Capsule Isolation, Fractionation, and Characterization

The SEM images of the UF, LF, and SF show a collapsed, spherical capsule morphology in all fractions (Fig 2.1). Presumably, the capsules collapse once dried and placed in the vacuum of the SEM chamber. In aqueous suspension, this may be a cavity where the capsule payload is located.

According to the pesticide's marketing materials, the capsules are designed to dispense γ-cyhalothrin in two stages [27]. There is an initial rapid release from the disruption of thin-walled capsules, followed by a slow release through thick-walled capsules that preserve the active ingredient for multiple weeks. Variability in wall thickness could not be verified by the SEM, though the shape and structure of the capsules is aligned with this description.

We compared the diameter of the capsules, indicated by the average hydrodynamic diameter (HDD); their electrophoretic mobility, indicated by the zeta potential; and their heterogeneity, indicated by the polydispersity index (PDI). The HDD of all fractions was less than 1000 nm, and each fraction was significantly different from the others, ranked in increasing order as SF < UF < LF (Table 1). This demonstrates that the fractionation method employed here successfully separated the UF into two distinct nanoscale capsule fractions. While previous studies have investigated differences between micro- and nano-capsules [17], this study benefits from comparisons within the nanoscale to better understand the relative importance of capsule size when formulated below 1000 nm.

When comparing heterogeneity, the PDI of all three treatments were below 0.3 (Table 1), indicating a suitably monodisperse sample for DLS measurement. The UF was significantly different from the LF, which would be expected if the fractionation process was successfully separating the UF into increasingly homogenous nanoscale capsule fractions. This was corroborated by the SEM images, in which the UF (Fig. 2.1A) shows the greatest diversity of capsule sizes. Zeta potential was not different for any of the capsule treatments (Table 2.1).
It is noteworthy to mention that the 48 h settling period was necessary to allow particularly large capsules (>1000 nm) to settle out of suspension. This is important for accurate DLS measurements, which can be disrupted by the presence of settling particles in a sample. The settling process also ensured that the LF and SF capsules were stable in suspension throughout the duration of a 48 h static aquatic exposure. We determined that the LF and SF together constitute approximately 2% of the total γ-cyhalothrin contained in the full pesticide formulation. This suggests that the nano-sized capsules are not a majority constituent of the original product

although 2% could be an underestimate due to the potential loss of capsules during the fractionation process.

The isolation and fractionation method employed here is simple and scalable, and allowed us to reliably separate capsules according to their size. Processes like this can be used to investigate other encapsulated formulas, facilitating further research into the effects of capsule size with different capsule compositions or active ingredients. Further, separation processes during manufacturing could be leveraged by the pesticide industry to develop tightly controlled formulations with specific sizes for novel applications.

2.4.2. γ-cyhalothrin Partitioning

Recovery of free γ-cyhalothrin, determined by GC-ECD quantification of γ-cyhalothrin after the extraction process, was immediate and consistent from 0 to 72 h (Fig 2.2), indicating uninhibited hydrophobic partitioning of free γ-cyhalothrin out of the aqueous sample and into hexane. This is unsurprising considering that pyrethroids are deliberately designed to be hydrophobic to minimize their transport in water [27]; thus, γ-cyhalothrin's extremely low solubility in water (<3 µg/L) and high solubility in hexane (>500 g/L) is expected to drive strongly hydrophobic behavior.

In contrast, γ-cyhalothrin recovery from the LF and SF was less than 3% at 0 h (Fig 2.2). The recovery of these encapsulated treatments increased over time, plateauing around 48 h. There was a significant difference between both encapsulated treatments and the FC at 0, 6, and 24 h. This suggests that initially, only a small fraction of the total γ-cyhalothrin in the LF and SF is freely available for partitioning into the nonpolar phase. This agrees with the notion of an internal capsule cavity that contains a bulk of the active ingredient, and the percentage of surface bound and freely dissolved γ-cyhalothrin is less than 3% at 0 h. As time progresses from 0 to 48 h, the capsules degrade until all the γ-cyhalothrin is released. Preliminary trials showed consistently low recoveries of γ-cyhalothrin at 0 h for SF and LF samples that were multiple days old, suggesting that the capsules are relatively stable in aqueous solution without the presence of

a nonpolar extraction solvent. Interestingly, there were no significant differences in γ-cyhalothrin recovery between the LF and SF at any point, suggesting that these capsules interfere with hydrophobic partitioning similarly regardless of their size.

Interpreting these findings with respect to pesticide regulation highlights potential inconsistencies with regulatory strategies focused on the behavior of active ingredients. For example, implementing KOW in pesticide transport modeling is meant to account for the hydrophobic partitioning of the active ingredient. However, we have shown that encapsulation can inhibit the hydrophobic behavior of a pyrethroid for up to 48 h when in the presence of a nonpolar phase. This time-dependency may be an important consideration when modeling pesticide transport in the days following an application, when the hydrophobicity of an active ingredient is still shielded by the capsules. For example, γ-cyhalothrin may be more mobile during a rainfall event for the first two days when formulated in nano-sized capsules. While the capsules are assumed to release the relatively immobile γ-cyhalothrin into the desired area over time, a risk assessment may not address the movement of the capsules themselves prior to the release of γ-cyhalothrin. Determining the fate and transport of the capsules themselves is complicated by both the proprietary nature of capsule composition and the challenges associated with distinguishing engineered nanoparticles from complex environmental media.

The time-dependent extraction method utilized here allowed us to make quantitative comparisons between encapsulated products and their freely suspended counterparts. It uses a non-carcinogenic solvent, minimal sample preparation, and low sample volumes. Developing methodology like this is a necessary step towards understanding how the fate and behavior of pesticides can be altered by nano-sized encapsulated formulations. Building on these methods and screening additional capsule designs will address the current shortage of data regarding nano-enabled pesticides [25]. It is possible that existing shortcomings in nanopesticide regulation affect our ability to mitigate environmental exposures of hydrophobic active ingredients, especially in light of the widespread contamination of pyrethroids in surface waters that exceed regulatory thresholds and predictions [29]. Such discrepancies between modeled and measured environmental pyrethroid concentrations could indicate that current risk assessments are

inadequate for accurate predictions about active ingredients. One approach to resolving this issue may be to incorporate an initial kinetics step that accounts for the release of an active ingredient from its nanoparticle carrier. Notably, this step will be susceptible to factors beyond the typical concentration and rate coefficients delineated by the active ingredient, given that the physiochemical parameters of the pesticide are not informative of the capsule diameter or thickness.

2.4.3 Size-dependent Immobilization of *C. dubia*

In our 48 h immobilization test with *C. dubia*, the response from control treatments was 10% or less. The lack of response from the acetone control affirmed that acetone was a suitable carrier solvent for γ-cyhalothrin in our FC samples, allowing for exposures above the pyrethroid's solubility limit. There was no significant difference between experimental replicates, so response data was aggregated.

The *C. dubia* showed a dose-dependent response to the FC, SF, and LF exposures as modeled by a two-parameter, log-logistic regression (Fig. 2.3). The SF showed the highest toxicity (EC50 = 0.18 µg/L), followed by the LF (EC50 = 0.57 µg/L) and the FC (EC50 = 0.65 µg/L) (Fig 2.4). The SF, but not the LF, was significantly more toxic than the FC. This indicated a size-dependent effect on toxicity. Considering the proprietary nature of the capsule composition, it is impossible to eliminate a synergistic or additive effect due to the capsules themselves – a capsule only control is impossible without cooperation with the manufacturer. However, if the LF and SF capsules have identical chemical makeup, the insignificant difference between the LF and the FC makes synergistic effects unlikely. If the capsules themselves indeed elicited a toxic response, there are many biocompatible capsule materials available for use as nano-carriers [30] that might eliminate capsule toxicity.

When accounting for slope, all three modeled curves were significantly different from each other. The slope of the response curves increases in order of LF < SF < FC. The increased response variability observed in the LF and SF samples, as indicated by their lower slope values,

could be explained by changes in the distribution of γ-cyhalothrin throughout the exposure solution. In the case of FC treatment, γ-cyhalothrin molecules are evenly dispersed throughout the water with the carrier solvent, facilitating a relatively consistent exposure to the *C. dubia* as it swims through the water column. For the LF and SF, γ-cyhalothrin is mostly associated with the capsules rather than freely suspended, and therefore γ-cyhalothrin exposure to *C. dubia* is probably limited to encounters with the capsules. Assuming a large capsule contains more γ-cyhalothrin than a small capsule, there are fewer LF capsules than SF capsules for a given concentration (treatments were normalized by γ-cyhalothrin content, not capsule count). Therefore, the LF treatment had fewer capsules in suspension than the comparable SF treatment, which would exacerbate the increased response variability associated with capsule-mediated exposures.

The three-dimensional structure of capsules could also play a role in the toxic response. Cladocerans like *C. dubia* use mesh sieves on their appendages to ingest particles ranging from approximately 100 to 5000 nm in diameter as adults, with the preferential uptake occurring near 500 nm [31]. Given that the neonates used in this study are smaller than adults, a preferential uptake of particles under 500 nm is sensible and may result in increased ingestion of the SF when compared to the LF. One study found that nano-encapsulation increased the overall uptake of a pyrethroid in earthworms, but most of the active ingredient remained in the gut rather than being internalized [32]. If this were the case for the *C. dubia*, encapsulation could prevent a toxic response by preventing internalization of γ-cyhalothrin. However, there is evidence that smaller nanoparticles are more readily taken up in the closely related genus *Daphnia* [33], in which case capsules may increase γ-cyhalothrin internalization if sufficiently small. This notion is supported by the observed increased in toxicity from the SF. If capsule leakage is the mechanism for release, small pesticide capsules would release active ingredients more rapidly than large capsules [34]. Our partitioning experiment did not suggest a difference in γ-cyhalothrin release rate between SF and LF, though enzymatic degradation of capsules in the gut of *C. dubia* could affect the capsule integrity.

Finally, the stability of the capsules in suspension could be influenced by the neonates. While our preparation of the SF and LF samples involves a 48 h settling period before conducting the immobilization assay, the *C. dubia* could exert an effect on the particle stability. Other researchers have found that protein exudates from *Daphnia* can prompt the agglomeration of nanoparticles within a matter of hours [35]. Agglomeration of the pesticide capsules could cause them to drop out of suspension and sink to the bottom of the water column where they are unlikely to be ingested by filter feeders. Agglomeration state could not be determined here because DLS is not sensitive enough to verify the size of the pesticide capsules at the low particle concentrations used in our toxicity assessments.

2.5 Conclusions

Innovations in pesticide formulation are important for manufacturers, who benefit from the economic opportunity associated with pesticide sales, as well as other stakeholders concerned with environmental impacts caused by pesticide use. The advantages of encapsulation technologies should not be understated, and combining these features with the recent developments in nano-enabled products is becoming a fruitful area of research. As these investigations continue, it would be mutually beneficial for risk assessors and pesticide manufacturers to minimize the barriers of proprietary technology so that studies like this can result in more effective products that reduce environmental impacts. With the litany of nanoscale capsule designs available, identifying and describing their effects on active ingredients is an important pathway towards innovative pesticide products. In future studies, attention to the rates of release and desorption of active ingredients from nanoparticle carriers, and subsequent incorporation into risk assessment frameworks, will be a valuable contribution to predicting the fate of nano-enabled pesticides.

Besides helping to bolster the pesticide market, keeping pace with the evolution of encapsulated pesticides is vital for regulatory agencies. In this case, we demonstrated that encapsulated formulations may complicate the use of hydrophobicity metrics in modeling endeavors due to time-dependent and size-dependent changes to the active ingredient fate and toxicity. These

modifications can alter the risk profile of pesticide products by disrupting foundational assumptions about chemical behavior, such as the reliance upon a KOW value in active ingredient transport. Given concerns surrounding surface water pesticide contamination, recognizing these nuances may lead to more accurate environmental modeling and highlight scenarios in which other ingredients deserve unique attention.

2.6 Funding

This work was supported by a Cooperative Training Partnership between Oregon State University and the Environmental Protection Agency (83591301), USDA-NIFA (2013-67021-21181), and the Agricultural Research Foundation (ARF8301A). Further support was provided to M.S. by the ARCS Foundation.

2.7 Acknowledgments

The authors would like to thank the staff at the Aquatic Toxicology Laboratory at Oregon State University for supplying *C. dubia* for the experiments.

2.8 Conflicts of Interest

The authors declare no conflict of interest. The funders had no role in the design of the study; in the collection, analyses, or interpretation of data; in the writing of the manuscript, or in the decision to publish the results.

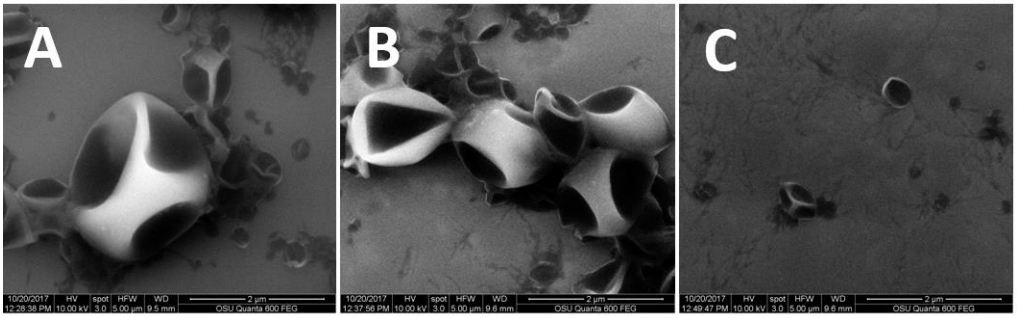

Figure 2.1. Representative SEM images of the encapsulated pesticide in each of the formulation fractions, showing the capsule morphology and size ranges. Scale bars are 2 µm. UF (A), LF (B), and SF (C).

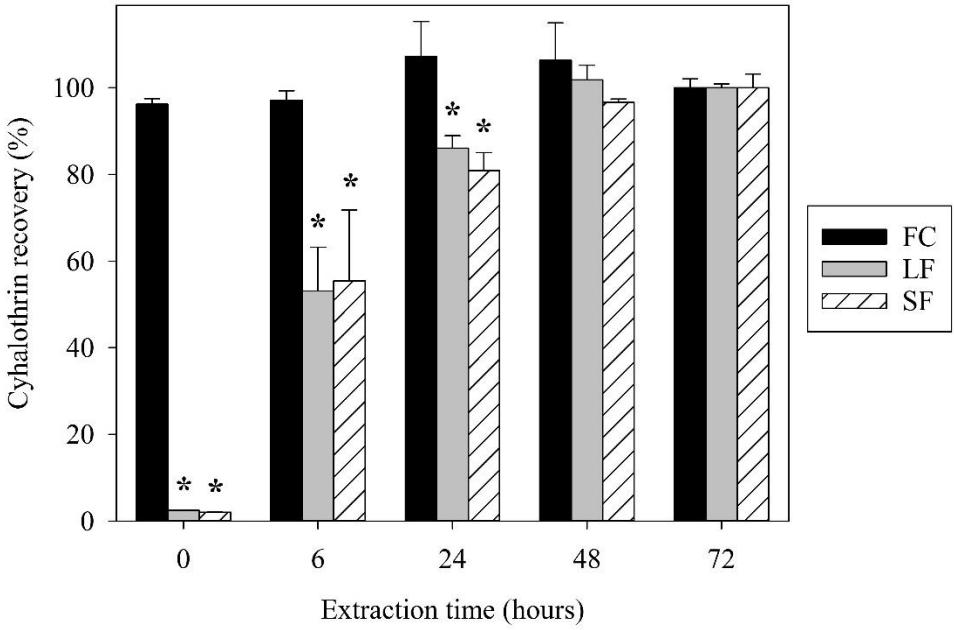

Figure 2.2. Recovery of total γ-cyhalothrin from FC, LF, and SF treatments at different extraction times. Bars represent standard error. * indicates significant difference from FC ($p \leq 0.05$).

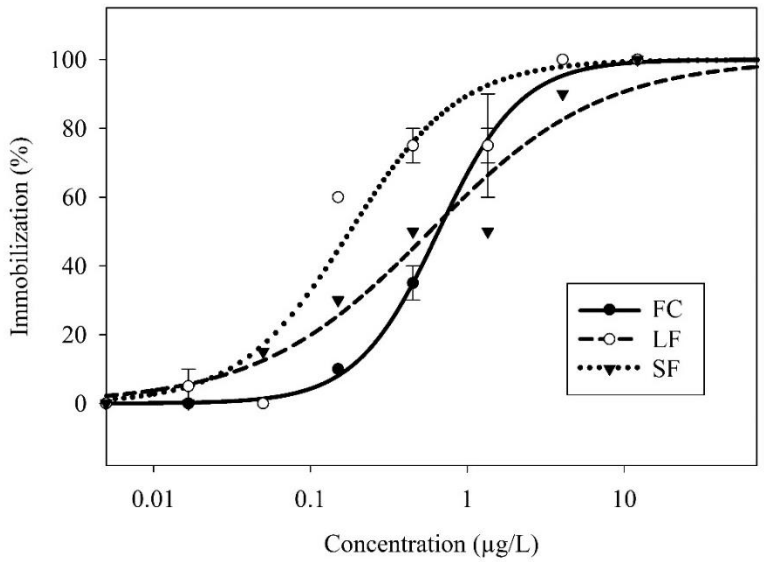

Figure 2.3. Two-parameter log-logistic regressions of *C. dubia* immobilization response to FC, LF, and SF as a function of γ-cyhalothrin concentration. Symbols represent sample means, bars represent standard error.

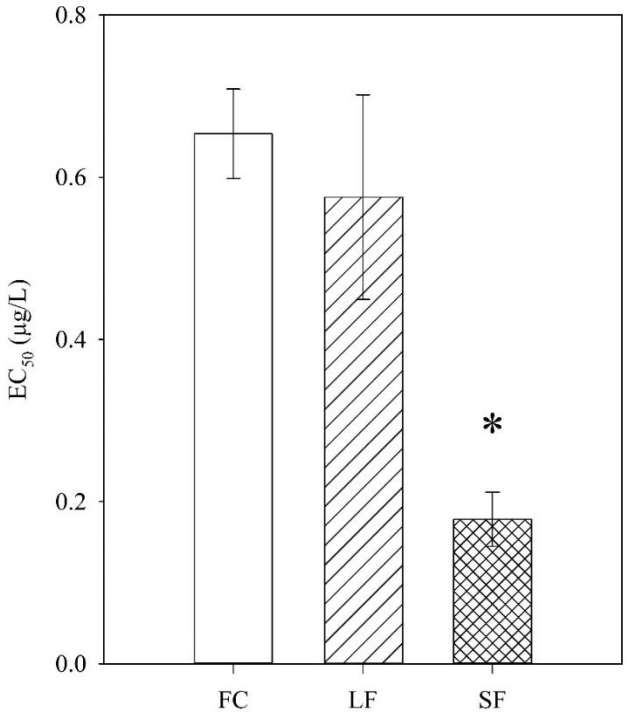

Figure 2.4. Estimated EC50 values for FC, LF, and SF. Bars represent standard error. * indicates significant difference from FC ($p \leq 0.05$).

Table 2.1. Average hydrodynamic diameter (HDD), zeta potential, and polydispersity index (PDI) for the UF, LF, and SF.

Fraction	HDD (nm)	Zeta Potential	PDI
UF	662 ± 9 [a]	−13.5 ± 2.6	0.291 ± 0.006 [a]
LF	758 ± 8 [b]	−11.0 ± 0.8	0.249 ± 0.013 [b]
SF	449 ± 2 [c]	−14.6 ± 1.6	0.264 ± 0.004

a, b, c Letters refer to statistical comparison among capsule fractions (Holm-Sidack multiple comparison); n = 3; ± standard error.

References Cited

1. Pesticide Industry Sales and Usage 2008 – 2012 Market Estimates. Office of Pesticide Programs. United States Environmental Protection Agency: Washington, DC, 2017; https://www.epa.gov/sites/production/files/2017-01/documents/pesticides-industry-sales-usage-2016_0.pdf.

2. Pesticide Registration Improvement Extension Act of 2012. Public Law 112-177, 2012. https://www.congress.gov/bill/112th-congress/senate-bill/3552

3. Surgan, M.; Condon, M.; Cox, C., Pesticide risk indicators: unidentified inert ingredients compromise their integrity and utility. Environ Manage 2010, 45, (4), 834-41.

4. Cowles, R. S.; Cowles, E. A.; McDermott, A. M.; Ramoutar, D., "Inert" Formulation Ingredients with Activity: Toxicity of Trisiloxane Surfactant Solutions to Twospotted Spider Mites (Acari: Tetranychidae). Journal of Economic Entomology 2000, 93, (2), 180-188.

5. Cox, C.; Surgan, M., Unidentified Inert Ingredients in Pesticides: Implications for Human and Environmental Health. Environmental Health Perspectives 2006.

6. Mullin, C. A.; Chen, J.; Fine, J. D.; Frazier, M. T.; Frazier, J. L., The formulation makes the honey bee poison. Pesticide biochemistry and physiology 2015, 120, 27-35.

7. Gish, T. G.; Shirmohammadi, A.; Wienhold, B. J., Field-Scale Mobility and Persistence of Commerical and Startch-Encapsulated Atrazine and Alachlor. J Environ Qual 1994, (23), 355-359.

8. Tsuji, K., Microencapsulation of pesticides and their improved handling safety. J Microencapsulation 2001, 18, (2), 137-147.

9. Hack, B.; Egger, H.; Uhlemann, J.; Henriet, M.; Wirth, W.; Vermeer, A. W. P.; Duff, D. G., Advanced Agrochemical Formulations through Encapsulation Strategies? Chemie Ingenieur Technik 2012, 84, (3), 223-234.

10. Kookana, R. S.; Boxall, A. B.; Reeves, P. T.; Ashauer, R.; Beulke, S.; Chaudhry, Q.; Cornelis, G.; Fernandes, T. F.; Gan, J.; Kah, M.; Lynch, I.; Ranville, J.; Sinclair, C.; Spurgeon, D.; Tiede, K.; Van den Brink, P. J., Nanopesticides: guiding principles for regulatory evaluation of environmental risks. Journal of agricultural and food chemistry 2014, 62, (19), 4227-40.

11. Wauchope, R.; Yeh, S.; Linders, J.; Kloskowski, R.; Tanaka, K.; Rubin, B.; Katayama, A.; Kordel, W.; Gerstl, Z.; Lane, M.; Unsworth, J., Pesticide soil sorption parameters: theory, measurement, uses, limitations, and reliability. Pest Manag Sci 2002, 58, 419-445.

12. Dubus, I. G.; Brown, C. D.; Beulke, S., Sources of uncertainty in pesticide fate modelling. Science of The Total Environment 2003, 317, (1-3), 53-72.

13. Pasquoto-Stigliani, T.; Campos, E. V. R.; Oliveira, J. L.; Silva, C. M. G.; Bilesky-Jose, N.; Guilger, M.; Troost, J.; Oliveira, H. C.; Stolf-Moreira, R.; Fraceto, L. F.; de Lima, R., Nanocapsules Containing Neem (Azadirachta Indica) Oil: Development, Characterization, And Toxicity Evaluation. Scientific reports 2017, 7, (1), 5929.

14. Tong, Y.; Wu, Y.; Zhao, C.; Xu, Y.; Lu, J.; Xiang, S.; Zong, F.; Wu, X., Polymeric Nanoparticles as a Metolachlor Carrier: Water-Based Formulation for Hydrophobic Pesticides and Absorption by Plants. Journal of agricultural and food chemistry 2017, 65, (34), 7371-7378.

15. Mohd Firdaus, M. A.; Agatz, A.; Hodson, M. E.; Al-Khazrajy, O. S. A.; Boxall, A. B. A., Fate, uptake, and distribution of nanoencapsulated pesticides in soil-earthworm systems and implications for environmental risk assessment. Environmental toxicology and chemistry 2018, 37, (5), 1420-1429.

16. Oliveira, J. L.; Campos, E. V. R.; Pereira, A. E. S.; Pasquoto, T.; Lima, R.; Grillo, R.; Andrade, D. J.; Santos, F. A. D.; Fraceto, L. F., Zein Nanoparticles as Eco-Friendly Carrier Systems for Botanical Repellents Aiming Sustainable Agriculture. Journal of agricultural and food chemistry 2018, 66, (6), 1330-1340.

17. Meredith, A. N.; Harper, B.; Harper, S. L., The influence of size on the toxicity of an encapsulated pesticide: a comparison of micron- and nano-sized capsules. Environment international 2016, 86, 68-74.

18. Son, J.; Hooven, L. A.; Harper, B.; Harper, S. L., Effect of pH and ionic strength on exposure and toxicity of encapsulated lambda-cyhalothrin to *Daphnia magna*. The Science of the total environment 2015, 538, 683-91.

19. Kah, M.; Beulke, S.; Tiede, K.; Hofmann, T., Nanopesticides: State of Knowledge, Environmental Fate, and Exposure Modeling. Critical Reviews in Environmental Science and Technology 2013, 43, (16), 1823-1867.

20. Nair, R.; Varghese, S. H.; Nair, B. G.; Maekawa, T.; Yoshida, Y.; Kumar, D. S., Nanoparticulate material delivery to plants. Plant Science 2010, 179, (3), 154-163.

21. Nuruzzaman, M.; Rahman, M. M.; Liu, Y.; Naidu, R., Nanoencapsulation, Nano-guard for Pesticides: A New Window for Safe Application. Journal of agricultural and food chemistry 2016, 64, (7), 1447-83.

22. Nel, A. E.; Madler, L.; Velegol, D.; Xia, T.; Hoek, E. M.; Somasundaran, P.; Klaessig, F.; Castranova, V.; Thompson, M., Understanding biophysicochemical interactions at the nano-bio interface. Nature materials 2009, 8, (7), 543-57.

23. Kah, M.; Kookana, R. S.; Gogos, A.; Bucheli, T. D., A critical evaluation of nanopesticides and nanofertilizers against their conventional analogues. Nature nanotechnology 2018.

24. Stone, D.; Harper, B. J.; Lynch, I.; Dawson, K.; Harper, S. L., Exposure assessment: recommendations for nanotechnology-based pesticides. International journal of occupational and environmental health 2010, 16, (4), 467-74.

25. Villaverde, J. J.; Sevilla-Moran, B.; Lopez-Goti, C.; Alonso-Prados, J. L.; Sandin-Espana, P., Considerations of nano-QSAR/QSPR models for nanopesticide risk assessment within the European legislative framework. The Science of the total environment 2018, 634, 1530-1539.

26. Methods for Measuring the Acute Toxicity of Effluents and Receiving Waters to Freshwater and Marine Organisms. Office of Water. United States Environmental Protection Agency: Washington, DC, 2002; https://www.epa.gov/sites/production/files/2015-08/documents/acute-freshwater-and-marine-wet-manual_2002.pdf

27. Control Solutions, Inc.: CapVantage; http://www.mypmp.net/2013/11/01/control-solutions-inc-capvantage.

28. Brady, J. A.; Wallender, W. W.; Werner, I.; Fard, B. M.; Zalom, F. G.; Oliver, M. N.; Wilson, B. W.; Mata, M. M.; Henderson, J. D.; Deanovic, L. A.; Upadhaya, S., Pesticide runoff from orchard floors in Davis, California, USA: A comparative

analysis of diazinon and esfenvalerate. Agriculture, Ecosystems & Environment 2006, 115, (1-4), 56-68.

29. Stehle, S.; Schulz, R., Agricultural insecticides threaten surface waters at the global scale. PNAS 2015, 112, (18), 5750-5755.

30. Campos, E. V. R.; de Oliveira, J. L.; Fraceto, L. F.; Singh, B., Polysaccharides as safer release systems for agrochemicals. Agronomy for Sustainable Development 2014, 35, (1), 47-66.

31. Gophen, M.; Geller, W., Filter mesh size and food particle uptake by Daphnia. Oecologia 1984, 64, 408-412

32. Mohd Firdaus, M. A.; Agatz, A.; Hodson, M. E.; Al-Khazrajy, O. S. A.; Boxall, A. B. A., Fate, uptake, and distribution of nanoencapsulated pesticides in soil-earthworm systems and implications for environmental risk assessment. Environmental toxicology and chemistry 2018, 37, (5), 1420-1429.

33. Zhao, C. M.; Wang, W. X., Size-dependent uptake of silver nanoparticles in Daphnia magna. Environmental science & technology 2012, 46, (20), 11345-51.

34. Ao, M.; Zhu, Y.; He, S.; Li, D.; Li, P.; Li, J.; Cao, Y., Preparation and characterization of 1-naphthylacetic acid-silica conjugated nanospheres for enhancement of controlled-release performance. Nanotechnology 2013, 24, (3), 035601.

35. Nasser, F.; Lynch, I., Secreted protein eco-corona mediates uptake and impacts of polystyrene nanoparticles on Daphnia magna. J Proteomics 2016, 137, 45-51.

NANO-SIZED COMPONENTS OF PESTICIDE FORMULATIONS MODULATE THE ENVIRONMENTAL RISK OF ACTIVE INGREDIENTS

Matthew R. Slattery, Bryan J. Harper, Vince L. Cataldi, Stacey L. Harper

In preparation for submission

Chapter 3 Nano-sized components of pesticide formulations modulate the environmental risk of active ingredients

3.1 Abstract

Nanopesticides, which capitalize on the highly customizable features of nanoparticles, are gaining interest in the agricultural marketplace. These products offer new strategies to modify the behavior of existing active ingredients, thereby improving their efficacy, reducing human exposure, and mitigating non-target effects. The differences between these nano-enabled products and their conventional counterparts, while identified, are poorly understood. Further, the role of particle size among nanopesticide products is also uncharacterized. Clarifying how nano-sized components in pesticide formulations impact the fate and behavior of active ingredients is important to maintain comprehensive and effective regulatory strategies. To investigate the influence of nanoparticles in current-use formulations, we isolated two distinct size fractions from a suspension concentrate variation of chlorothalonil: a large fraction (LF) with an average hydrodynamic diameter (HDD) of 381 nm, and a small fraction (SF) with an average HDD of 140 nm. These fractions were compared against a free chlorothalonil (FC) treatment using acetone as a carrier solvent. To determine whether the size of the chlorothalonil particulates influenced their toxicity, we conducted a 48-hour acute toxicity test with the freshwater macroinvertebrate *Dapnia magna*. We found that the LF was significantly more toxic than the SF or FC treatments (LC_{50} = 49.7 μg/L, 98.3 μg/L, and 113.7 μg/L respectively). In combination with the toxicological assessment, we also investigated differences in chlorothalonil degradation between the SF and LF particles. Our results showed that chlorothalonil was more stable in the LF treatment than the SF treatment over the course of 48 hours. This highlights that the environmental risk of nanopesticide formulations can be different from conventional formulations, warranting further investigation about the size ranges at which these effects diverge to inform manufacturers and regulators.

3.2 Introduction

Pesticides play an important role in mitigating catastrophic crop losses (Oerke 2006). The demand for pesticide products has consistently increased year by year, with current application rates over 1 billion pounds of active ingredients annually in the United States (Atwood 2017). In order to prevent unreasonable adverse effects on the environment, pesticide active ingredients receive extensive toxicological assessment. However, pesticides are often composed of a mixture of chemicals in a single formulation which complicates efforts to mitigate environmental risk. The potential for synergistic or additive effects of so called "other ingredients" is a contentious and concerning issue (Cowles 200, Cox 2006, Mullin 2015). Given the significant financial costs associated with registration of a novel active ingredient (PRIA 2012), reformulating existing active ingredients with unique combinations of other ingredients is common practice among major pesticide manufacturers.

Incorporation of nanotechnologies is one promising avenue for the reformulation of pesticide products that receives growing attention (Kah 2018). Nanopesticides represent a diverse category of products including a range of nanomaterials such as polymers, lipids, mesoporous clay, silica, and more (Kah 2013, Nair 2010, Naruzzaman 2016). Given the wide range of nanopesticide possibilities, a strict or consistent definition is difficult to assign. Nanoparticles in general exhibit high surface area and colloidal behavior (Nel 2009), which can be appealing features for modifying a pesticide product. By utilizing these properties, nanoparticle formulations can enhance the apparent solubility of an active ingredient (Tong 2017) and increase species selectivity (Anjali 2010), often through serving as a carrier of the active ingredient. In a comprehensive review, nanopesticide formulations were generally more efficacious than their conventional counterparts with the same active ingredient (Kah 2018).

While nanomaterials clearly have some potential benefit to the pesticide industry, nanopesticides may create gaps in pesticide regulation that warrant additional consideration (Stone 2010). For example, conventional metrics of chemical partitioning that are used to predict pesticide fate and transport, such as the octanol-water partitioning coefficient (K_{OW}), may not be applicable for

active ingredients when present as a nano-enabled formulation (Cornelis 2014). Conversely, nano-specific metrics such as particle size and shape are not reported, which are relevant for predictive modeling of nanopesticides (Villaverde 2018).

There is limited research into the effect of nanoparticle size on non-target toxicity of pesticide active ingredients. The relevance of particle size appears to be dependent on the test species. For example, fish responded similarly to an encapsulated formula at 250 nm and 2200 nm (Meredith 2015). Conversely, crustaceans were more sensitive to active ingredients contained in capsules averaging 449 nm as opposed to 758 nm (Slattery 2019). While the particles from these two examples were isolated from current-use insecticide products, only a small portion of the formulation was nano-sized (Meredith 2015, Slattery 2019). Estimating the number of pesticide products on the market with nanoparticles in their formulation is difficult considering the lack of reporting requirements from pesticide manufacturers, though these examples underscore the likelihood of other commercially-available formulations containing a nanoparticle constituent. In a preliminary assessment of nanoparticle prevalence in pesticide formulations, 8 out of 9 products examined with a scanning electron microscope (SEM) contained visible particles less than 1000 nm in diameter – none of which had any indication of nanoparticle presence on their labels (Supplemental Information, SEM figures). This suggests that nanoparticles may be a common constituent of modern formulations regardless of whether or not they are classified as a nanopesticide product.

Expanding pesticide assessments to a wide range of active ingredients is important to better understand how nanomaterials can influence their toxicity. For example, current-use formulations containing chlorothalonil, the most commonly applied fungicide in the United States (Atwood 2017), have not been evaluated for the presence of nanoparticles. Chlorothalonil is primarily applied in agricultural settings for pest control on peanuts, potatoes, and tomatoes, though use on golf courses and as antifouling paint is also common (EPA 1999). This fungicide is highly toxic to fish, birds, and aquatic invertebrates including *Daphnia magna* (Caux 1996). The detection of chlorothalonil in golf course runoff can exceed 96h LC_{50} (concentration required to cause 50% mortality in the test population) values for *Daphnia magna* (CA DPR).

Chlorothalonil is also found in nearly half of all honeybee wax samples in North America (Mullin 2010). Considering the broad use and apparent contamination of chlorothalonil in the United States, the presence and effect of nanoparticles in common formulations may be relevant information for mitigating environmental impacts.

Given the demand for nanopesticide research and lack of data comparing existing nano-sized components of registered pesticides, our objective here was to elaborate on the potential size-dependence of nanoparticle toxicity within a current-use fungicide marketed as a suspension concentrate. We accomplished this by (i) isolating and fractionating the nano-sized components from the full formulation in two distinct size ranges; (ii) assessing the effect of particle size on chlorothalonil partitioning behavior and degradation; and (iii) determining the sensitivity of a freshwater macroinvertebrate, *Daphnia magna*, to different nanoparticle sizes. These objectives were measured against a freely suspended chlorothalonil control to establish how a nanoparticle formulation of chlorothalonil might differ from a conventionally suspended product.

3.3 Materials and Methods

3.3.1 Chemicals

A commercially available, EPA-registered suspension concentrate (SC) fungicide (EPA Reg. No 50534-188) with 54% chlorothalonil was used. Analytical standard grade chlorothalonil [3-(2-chloro-3,3,3-triuoro-1-propenyl)-2,2-dimethyl,cyano(3-phenoxyphenyl) methyl ester], 99.3% purity (CAS number 1897-45-6) was purchased from Sigma Aldrich (St. Louis, MO, USA). Toluene (CAS number 108-88-3) was purchased from Fisher Scientific (Fair Lawn, NJ, USA).

3.3.2 Preparation of capsule fractions from commercial product

The pesticide formulation used here was sold as a suspension concentrate product (720 g chlorothalonil L^{-1} according to product label) which was diluted with deionized (DI) water to a 720 mg L^{-1} stock. Formulations designated as SC are typically composed of the active ingredient

milled down to microscopic particulates and suspended with the aid of other ingredients. To remove these soluble, other ingredients, 10x diluted stock samples were centrifuged for 30 minutes at 6960 Relative Centrifugal Force (RCF) with a benchtop Eppendorf 5430 centrifuge (Hamburg, Germany), effectively removing all chlorothalonil particles from suspension. Carefully, 8 mL of the resulting supernatant (containing soluble other ingredients) was removed from each sample and replaced with 8 mL of Moderately Hard Water (MHW, prepared according to EPA 2002) and then vortexed to resuspend the settled chlorothalonil particles. This resulted in "cleaned" chlorothalonil suspensions.

To isolate the nano-sized chlorothalonil particles from microparticles, two separate procedures were used to generate a large fraction (LF) and small fraction (SF). The LF was generated by centrifuging the cleaned samples for 7 minutes at 169 RCF, and the resulting supernatant was collected and saved as the LF. The SF was generated by centrifuging cleaned samples for 12 minutes at 5114 RCF, and the resulting supernatant was collected and pass through a 0.22 µm membrane filter, then saved as the SF. Both the LF and SF samples were wrapped in aluminum foil and stored at 4 °C for 48 hours to allow any remaining large particles to drop out of solution before aliquots were removed for characterization, extraction, degradation, and toxicity assessments.

3.3.3 Chlorothalonil nanoparticle characterization

The hydrodynamic diameter (HDD), zeta potential, and polydispersity index (PDI) of the SF and LF were measured in triplicate by dynamic light scattering (DLS) using a Zetasizer Nano ZS (Malvern Instruments, LTD., Worcestershire, UK) at 25 °C. Statistical differences between fractions were determined with a one-way ANOVA. Analyses were considered significantly different at $p \leq 0.05$. The size and morphology of capsules were verified using an FEI Quanta 600 FEG (FEI CO., Hillsboro, OR, USA) scanning electron microscope (SEM) operating at 10 kV with samples prepared by dropping 20 µL of each fraction onto a Si substrate and drying before imaging.

3.3.4 Quantification and partitioning of chlorothalonil

An Agilent Technologies 7820A GC (Agilent Technologies, Santa Clara, CA, USA) equipped with an Agilent Technologies 7963A Automatic Liquid Sampler, electron capture detector (ECD), and 25 m × 0.32 mm ID BPX35 column was used to quantify chlorothalonil. Standard grade chlorothalonil was run at 0.5, 2.5, and 12.5 mg L^{-1} to produce a calibration curve and verify retention times at the beginning of every run. Solutions of LF and SF were diluted to approximately 10 mg L^{-1} for chlorothalonil quantification. The LF and SF solutions were compared against a free chlorothalonil (FC) solution, prepared by adding chlorothalonil suspended in an acetone carrier solvent with MHW such that the concentration of acetone was 1 mL L^{-1}. For quantification of chlorothalonil in samples, 700 µL of toluene was mixed with 700 µL of the sample in 1.5 mL gas chromatography vials, in triplicate. Vials were placed on a SCILOGEX MX-T6-S Analog Tube Roller set to 30 rpm for 0 (2 min), 1, or 2 h to agitate samples during extraction and encourage migrate of chlorothalonil from the aqueous phase to the toluene phase. After agitation, 500 µL of toluene was aspirated from the vials and diluted with 500 µL of fresh toluene in a new GC vial for analysis. Extraction efficiency was calculated as a fraction of the chlorothalonil recovered from samples after a 72 h value with the assumption that this represents complete extraction of the chlorothalonil from suspension (verified using the full formulation and complete recovery of the label concentration).

3.3.5 Daphnid immobilization assay

Daphnia magna less than 24 h old were cultured in MHW according to EPA specifications (EPA 2002). Toxicity assessments at 48 h used mortality of *D. magna* as an endpoint, defined as no observable heartbeat. A total of five treatments were tested: MHW control, acetone carrier control, FC, SF, and LF. The chlorothalonil concentrations in the FC, SF, and LF stock solutions were verified by GC-ECD before dilution with MHW to concentrations of 25, 50, 100, 150, 200, 250, and 300 µg/L. For each treatment and control, 7 *D. magna* were placed in individual glass vials with 2 mL of treatment solution. There were three experimental replicates per concentration

and control, for a total of 18 *D. magna* per treatment. The test period was 48 h at 20 °C under 18 h light period with full-spectrum lights.

A one-way ANOVA was used to compare differences between experimental replicates. The *drc* package in R, version 3.0-1, was used to generate a two-parameter log-logistic model of the *D. magna* dose–response curve that was compared pairwise using a one-way ANOVA. Estimates of the LC_{50} for the FC, LF, and SF treatments were calculated using *drc*. These estimates were compared using a one-way ANOVA test. Analyses were considered significantly different at $p \leq 0.05$.

3.4 Results

3.4.1 Particle size and morphology

SEM images reveal the presence, size, and morphology of nanoparticles in the suspension concentrate fungicide prior to any cleanup or isolation methods (Figure 3.1A). This provides clear evidence that the full formulation has a wide range of granular particle sizes ranging from a few hundred nanometers up to 3 µm. The blotchy background is indicative of residue from the evaporation of soluble other ingredients in the formula mixture, perhaps organic solvents, that comprise the remaining 46% of the formulation that is not chlorothalonil. After cleanup and isolation, these residues are almost entirely eliminated in the LF and SF images (Figures 3.1B and 3.1C), suggesting that a majority of other ingredients were successfully removed. The LF and SF images also demonstrate that the particle sizes are smaller and more homogenous than the full formulation, such that overall particle size is ranked in order of full formulation > LF > SF. The granular surface and approximately spherical shape of the particles is preserved through the centrifugation and filtration steps that generate the SF and LF fractions.

Characterization of nanoparticles by DLS is impaired by microparticles (>1000 nm in diameter) or settling particles. This precludes the full formulation from measurement considering the microparticles visible in the SEM image and further corroborated by runtime errors on the DLS

when attempting to collect full formulation data. Despite the slightly uneven particle surfaces, the granular and roughly spherical shape of the SF and LF particles produced acceptable DLS data by the Zetasizer software. The PDI for all processed samples was below 0.3, indicating sufficiently homogenous distributions for DLS assessment. Particles in the LF were approximately twice as large as SF particles, at 386 and 191 nm respectively. The two fractions were significantly different.

3.4.2 Hydrophobic partitioning

The hydrophobicity of chlorothalonil when formulated as nanoparticles in the SF and LF was compared against the non-nano, freely suspended chlorothalonil in the FC using a time-dependent extraction method (Figure 3.3A). This method, based on the same partitioning principle as conventional liquid-liquid extraction procedures, provided a quantitative assessment of chlorothalonil's hydrophobic partitioning at 0, 1, and 2 h (Figure 3.3B). At the 0 h time point (2 minutes of extraction time), approximately 60% of the chlorothalonil in the FC and SF samples had hydrophobically partitioned into the non-polar (toluene) phase, whereas only 30% chlorothalonil in the LF samples had partitioned. This difference was statistically significant. After 1 and 2 h, these significant differences disappeared between samples with all of the chlorothalonil hydrophobically partitioning out of the aqueous phase and into the non-polar phase, regardless of whether or not the chlorothalonil was presented in FC, SF, or LF forms.

3.4.3 Degradation

The degradation of chlorothalonil was compared between the SF and LF treatments at 8, 24, and 48 h to identify differences in chlorothalonil chemical stability (Figure 3.4). The chlorothalonil recovery is a measure of the total chlorothalonil found in the sample and does not distinguish nanoparticle or freely dissolved forms. The starting concentration for chlorothalonil in SF and LF samples was adjusted to 1.8 mg L^{-1} at the start of the degradation experiment, which was necessarily higher than the toxicity exposure concentrations (0 mg L^{-1} to 0.3 mg L^{-1}) to accommodate the limits of detection for the gas chromatograph method. At the 8, 24, and 48 h time points, significantly less chlorothalonil was recovered from the SF than the LF. After 48 h,

24% of the chlorothalonil had degraded from the LF samples whereas the SF lost 31%. While there was a consistent trend of less chlorothalonil measured in the SF, the degradation kinetics did not appear to follow a typical exponential decay pattern, with degradation halting between 24 h and 48 h. Changes to particle size could not be investigated with DLS or SEM because the number of particles in a 1.8 mg L^{-1} solution was too low for detection.

3.4.4 *Daphnia* toxicity assay

The toxic response of the freshwater macroinvertebrate *D. magna* was assessed for the FC, SF, and LF treatments. Exposures for each of the treatments was normalized according to total chlorothalonil concentration. The shape of the fitted concentration-response curves for the FC and SF were similar (Figure 3.5A). In comparison, the LF slope of the concentration-response curve was steeper and begins at a lower chlorothalonil concentration. The two parameter log-logistic model that fit the data produced LC_{50} estimates for the FC, SF, and LF which were 105 ± 3 µg L^{-1}, 98 ± 5 µg L^{-1}, and 50 ± 2 µg L^{-1}, respectively (Figure 3.5B). The LC_{50} for the LF was significantly different than the FC.

3.5 Discussion

3.5.1 Characterization

The prime objective of this study was to investigate how particle size in a nanopesticide formulation influences the risk of the active ingredient. The SEM images demonstrate that the original agricultural product that we used in this study does not contain exclusively nanoparticles, rather it is a heterogeneous mixture of micro-scale and nano-scale particles (Figure 3.1A). This raises an important yet unresolved question of nanopesticide research: should pesticide products be classified as nanopesticides if they contain any nanoparticle components at all? If the pesticide nanoparticles elicit unique or distinct effects from their non-nano counterparts, identifying and labeling their presence may be relevant for effective regulation and

environmental risk management. A metanalysis of nanopesticide products suggests that this may be the case (Kah 2018). On the contrary, the presence of nanoparticles in formulations may be inconsequential for some full formulations if it represents a sufficiently small fraction of the total formulated product. Slattery et al (2019) found that only 2% of the total active ingredient in an encapsulated formulation was within the nano-scale, according to the methods used to isolate those particles. A comprehensive assessment of nanoparticle presence in conventional formulations would be important moving forward to determine if notification or labeling of nanoparticles in pesticide formulations would be useful or inconsequential.

Besides verifying that the commercial pesticide formulation used here contains chlorothalonil nanoparticles, the SEM images also validated our method as a successful means of removing microparticles and solvent residues (Figure 3.1B, 3.1C). The solvents likely aid in the dispersion of the particles throughout the formulation, though the ambiguous use of "other ingredients" on the pesticide label is not sufficient to determine this with any certainty. The particles themselves are presumably composed of chlorothalonil, based on the relatively high percentage of active ingredient (54%), retention of toxic activity after particle isolation, and classification as a SC formula which suggests that the active ingredient has been milled down to microscopic particles for suspension in solution rather than freely dissolved.

The DLS results (Figure 3.2) agree with the size ranges visible in the SEM images and offer a consistent measurement of their average diameter. The SF preparation included filtration through a 0.22 µm membrane filter, and the average particle size of 191 nm falls within what would be expected for a distribution of particles with an upper limit of 220 nm. The LF particles were roughly twice the size in both the SEM images and DLS data, which makes for a suitable comparison across chlorothalonil particles that span a portion of the nano-scale range.

3.5.2 Hydrophobicity

Chlorothalonil is a moderately hydrophobic active ingredient with a log K_{OW} of 2.88 (CDPR). The hydrophobic properties of this fungicide are desirable for reducing the likelihood of

environmental transport in rain or surface waters (Stehle 2015), and in general is considered an important variable for predicting environmental exposure (Wauchope 2002, Dubus 2003). The hydrophobic partitioning method used here is similar to the liquid-liquid extraction method used to determine a chemical's K_{OW}, with the important addition of multiple time point measurements to observe the hydrophobic behavior of active ingredients over time. Partitioning coefficients like K_{OW} are taken at equilibrium, but our data suggests that the time to equilibrium can be impacted by some size ranges of nanoparticle formulations (Figure 3.3). This indicates that log K_{OW} values may not provide a complete picture of hydrophobic partitioning, given that nanopesticide formulations at some sizes exhibit delayed hydrophobic movement. Active ingredients may be more likely to travel with water when formulated as large (>350 nm) nanoparticles rather than small nanoparticles (<200 nm) or freely dissolved active ingredients. In environmental scenarios, a 386 nm chlorothalonil nanoparticle that displays delayed hydrophobic activity may temporarily have increased mobility in rain or surface waters in comparison to a 191 nm nanoparticle. This could contribute to chlorothalonil contamination in the environment.

The duration of this hydrophobic delay is an important consideration. Previously, a pyrethroid active ingredient contained inside nano-sized capsules also exhibited a delay in hydrophobic partitioning (Slattery 2019). The duration of the delay was much longer (>24 h) and was not size-specific for particles ranging from 448 to 758 nm, whereas in this case the delay persists for less time (<1 h) and is only observed in the LF. This inconsistency among nanopesticide behavior (in this case, nanocapsules versus nanoparticle suspension concentrates) is reflective of the challenging nature of nanopesticide diversity. Regulating nanopesticides as a single class or category is problematic without acknowledging the variety of nanopesticide types. Comparison of these nanopesticide types is an important step towards comprehensive regulatory strategies. For example, encapsulated formulations may be less sensitive to particle size with respect to delays in hydrophobic partitioning of active ingredients, in contrast to suspension concentrates where the particle size is a significant factor.

3.5.3 Degradation

The environmental degradation of pesticide active ingredients is an important variable to consider for both pesticide efficacy and non-target risk. A persistent pesticide does not need to be re-applied as frequently but is also more likely to lead to chronic environmental exposures if the active ingredient is transported away from the application area. The half-life of chlorothalonil via varies widely depending on environmental conditions, ranging from 2 hours to 8 days in water, and significantly longer in soil (EPA 1999). However, there is no data available for the effect of particle size on chlorothalonil degradation.

Here, we show that chlorothalonil in the LF is more persistent under our static, laboratory exposure conditions than the SF (Figure 3.4). The 48 h timeline allows us to compare the degradation over the course of the acute toxicity exposures. Our results indicate a size-dependent effect on the degradation of the pesticide active ingredient. This can be explained by changes in the surface area to volume ratio of chlorothalonil nanoparticles. As the particles decrease in size, their surface area increases, which would also translate to an increased proportion of chlorothalonil molecules on the exterior of the nanoparticle that are available for chemical interaction. Chlorothalonil can be degraded via photolysis or chemical reactions with water (Caux 1996). Unless chlorothalonil and its degradants are released from the nanoparticle and dissolved into solution, they would create a semiprotective sheath around the chlorothalonil core. This is supported by Figure 3.4, as the LF shows relatively little degradation in comparison to the SF. The smaller particles also showed significant degradation until 24 h when the rate appeared to slow, which would be expected if the surface chlorothalonil is degraded and shields the core chlorothalonil from further degradation. Changes to particle size, either through release of chlorothalonil or agglomeration of the particles, could not be assessed because the concentration of particles was too low for DLS assessment.

3.5.4 Toxicity

In the 48 h mortality assay with *D. manga*, the filter-feeding organisms showed a concentration-dependent response to the FC, SF, and LF exposures. The published LC_{50} values for chlorothalonil toxicity to D. manga are 68 µg L^{-1} for the freely dissolved active ingredient

(analogous to the FC in our study) and 97 µg L^{-1} for the full formulation of the same pesticide product that we used in our study (EPA 1999). Those results suggest that the full formulation (including microparticles and other ingredients) is less toxic to the D. manga than chlorothalonil alone. Given the tendency for large (>1000 nm) particles to rapidly settle out of suspension, it is probable that aquatic assays using the full formulation reduce the exposure to organisms that swim through the water column, because many of the chlorothalonil particles sink to the base of the container where they are unavailable for consumption by *D. manga*. This would explain the reduced toxicity observed in a full formulation assessment. In comparison, the experimental design used in this study ensured that the SF and LF particles do not settle out of solution within 48 h.

We found a significant increase in toxicity for the LF compared to the FC or the SF (Figure 3.5). This shift in toxicity, despite the normalized chlorothalonil concentrations among the treatments, can be explained by the preferential uptake of specific particle sizes for *D. magna*, which most effectively uptake suspended particles near 500 nm in diameter (Gophen 1984). If we again compare these results to the previous nanopesticide study by Slattery et al. (2019), this trend towards increased toxicity at particle sizes that filter feeding organisms preferentially uptake holds true. While it is possible that the SF and LF particles are releasing chlorothalonil freely into suspension during the course of the 48 h assay, the degradation kinetics apparent in Figure 3.4 are not typical of a first-order degradation rate that would be expected of a freely dissolved chemical.

3.6 Conclusions

The role of nanopesticide products in the agricultural industry is receiving increased attention by manufacturers and researchers. The numerous advantages of nanopesticide formulations warrants a clear understanding of how these emerging products fit into our current regulatory framework. Comprehensive and effective regulation of nanopesticides is dependent on establishing general trends for the litany of nano-enabled pesticides that are either currently available or under development.

The data outlined in this study highlights that for nanopesticide formulations that feature an active ingredient nanoparticle, the size range of the particle is an relevant factor in environmental risk. Hydrophobic partitioning is delayed by large (~400 nm) nanoparticles whereas smaller (~200 nm) nanoparticles acted similarly to the freely dissolved active ingredient. In an aquatic setting, the degradation of the active ingredient is decreased with larger particle sizes, likely due to a shielding effect from degradants on the particle surface. Finally, the toxicity of pesticide active ingredients can be significantly altered by some particle sizes, depending on the preferential particle uptake of the test organism. Other pelagic organisms with filter feeding strategies may be susceptible to similar increases in toxic response based on this same mechanism, depending on if their preferred particle uptake dimensions are similar the particles found in a nanopesticide formulation. This information can be used toward the iterative improvement of nanopesticide products and the guidelines that will eventually come into place to regulate them.

3.7 Funding

This work was supported by a Cooperative Training Partnership between Oregon State University and the Environmental Protection Agency (83591301), USDA-NIFA (2013-67021-21181), and the Agricultural Research Foundation (ARF8301A). Further support was provided to M.S. by the ARCS Foundation.

3.8 Acknowledgments

The authors would like to thank Vince Cataldi for collecting the toxicity data on *D. magna*.

3.9 Conflicts of Interest

The authors declare no conflict of interest. The funders had no role in the design of the study; in the collection, analyses, or interpretation of data; in the writing of the manuscript, or in the decision to publish the results.

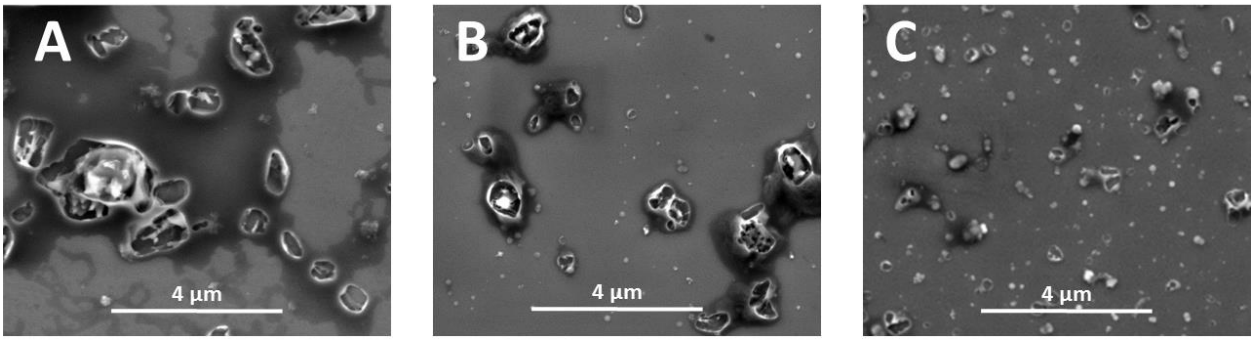

Figure 3.1. Representative SEM images of the particles observed in the suspension concentrate fungicide product before (A) and after cleanup and separation into the LF (B) and SF (C).

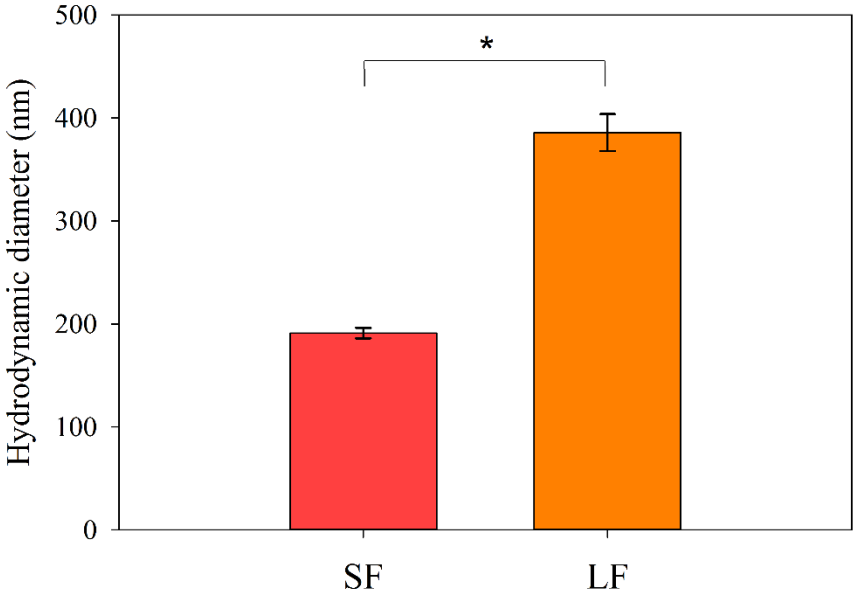

Figure 3.2. The average HDD of nanoparticles in the SF and LF treatments measured as the primary peak in DLS output (* indicates significant difference between treatments, $p \leq 0.05$).

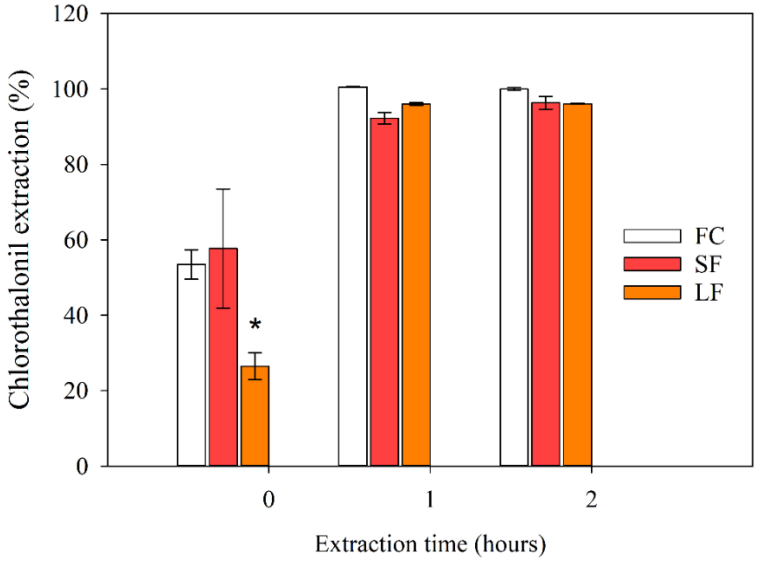

Figure 3.3. Recovery of chlorothalonil from aqueous mixtures of FC, SF, and LF over time using a liquid-liquid extraction with toluene. Chlorothalnil extraction is expressed as a percentage of total chlorothalonil present in each sample (* indicates significant difference from FC, $p \leq 0.05$).

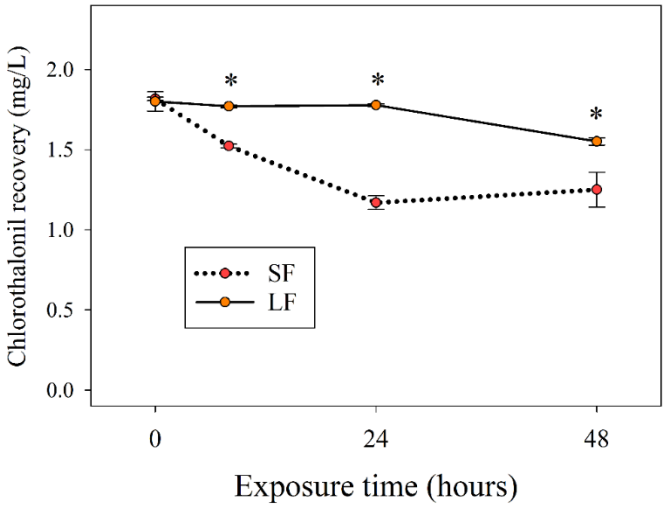

Figure 3.4. Recovery of chlorothalonil from SF and LF treatments over the course of 48 hours in MHW under a 18 h light period with full-spectrum lights (* indicates significant differences between treatments, $p \leq 0.05$).

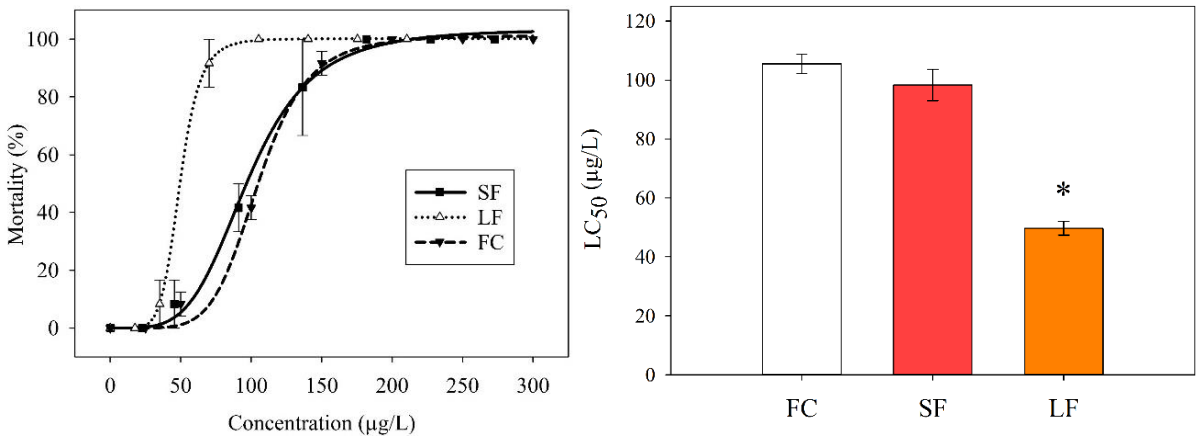

Figure 3.5. Acute toxicity of *D. magna* in response to FC, SF, and LF treatments. Two-parameter log-logistic regressions of neonate mortality overlaid onto sample means with standard error (A), and the estimated LC_{50} values from the regressions (B). (* indicates significant difference from FC, $p \leq 0.05$).

References Cited

1. Atwood, D., & Paisley-Jones, C. (2017). 2008-2012 Market Estimates. Pesticides Industry Sales and Usage.Caux, P.Y., Kent, R.A., Fan, G.T., Stephenson, G.L. (1996). Environmental Fate and Effects of Chlorothalonil: A Canadian Perspective. Critical Reviews in Environmental Science and Technology. 26(1):56-93.
2. Cornelis, G., Kookana, R. S., Fernandes, T. F., Van den Brink, P. J., Reeves, P. T., Spurgeon, D., … Beulke, S. (2014). Nanopesticides: Guiding Principles for Regulatory Evaluation of Environmental Risks. Journal of Agricultural and Food Chemistry, 62(19), 4227–4240. https://doi.org/10.1021/jf500232f
3. Cowles, R. S., Cowles, E. A., McDermott, A. M., & Ramoutar, D. (2009). "Inert" Formulation Ingredients with Activity: Toxicity of Trisiloxane Surfactant Solutions to Twospotted Spider Mites (Acari: Tetranychidae). Journal of Economic Entomology, 93(2), 180–188. https://doi.org/10.1603/0022-0493-93.2.180
4. Cox, C., & Surgan, M. (2006). Unidentified inert ingredients in pesticides: Implications for human and environmental health. Environmental Health Perspectives, 114(12), 1803–1806. https://doi.org/10.1289/ehp.9374
5. Dubus, I. G., Brown, C. D., & Beulke, S. (2003). Sources of uncertainty in pesticide fate modelling. Science of the Total Environment, 317(1–3), 53–72. https://doi.org/10.1016/S0048-9697(03)00362-0
6. EPA. (1999). Chlorothalonil reregistration eligibility decision (RED). EPA 738-R-99-004 U.S. Environmental Protection Agency, Washington, D.C.
7. Gophen, M., & Geller, W. (2018). International Association for Ecology Filter Mesh Size and Food Particle Uptake by Daphnia Author (s): Moshe Gophen and Walter Geller Published by : Springer in cooperation with International Association for Ecology Stable URL : https://www.jstor.org/st. 64(3), 408–412.
8. Kah, M., Kookana, R. S., Gogos, A., & Bucheli, T. D. (2018). A critical evaluation of nanopesticides and nanofertilizers against their conventional analogues. Nature Nanotechnology, 13(8), 677–684. https://doi.org/10.1038/s41565-018-0131-1

9. Meredith, A. N., Harper, B., & Harper, S. L. (2016). The influence of size on the toxicity of an encapsulated pesticide: A comparison of micron- and nano-sized capsules. Environment International, 86, 68–74. https://doi.org/10.1016/j.envint.2015.10.012
10. Mullin, C. A., Frazier, M., Frazier, J. L., Ashcraft, S., Simonds, R., Vanengelsdorp, D., & Pettis, J. S. (2010). High levels of miticides and agrochemicals in North American apiaries: implications for honey bee health. PloS One, 5(3), e9754. https://doi.org/10.1371/journal.pone.0009754
11. Nair, R., Varghese, S. H., Nair, B. G., Maekawa, T., Yoshida, Y., & Kumar, D. S. (2010). Nanoparticulate material delivery to plants. Plant Science, 179(3), 154–163. https://doi.org/10.1016/j.plantsci.2010.04.012
12. Nel, A. E., Mädler, L., Velegol, D., Xia, T., Hoek, E. M. V, Somasundaran, P., … Thompson, M. (2009). Understanding biophysicochemical interactions at the nano-bio interface. Nature Materials, 8(7), 543–557. https://doi.org/10.1038/nmat2442
13. Nuruzzaman, M., Rahman, M. M., Liu, Y., & Naidu, R. (2016). Nanoencapsulation, Nano-guard for Pesticides: A New Window for Safe Application. Journal of Agricultural and Food Chemistry, 64(7), 1447–1483. https://doi.org/10.1021/acs.jafc.5b05214
14. Oerke, E. C. (2006). Crop losses to pests. Journal of Agricultural Science, 144(1), 31–43. https://doi.org/10.1017/S0021859605005708
15. Pesticide Registration Improvement Extension Act of 2012. Public Law 112-177, 2012. https://www.congress.gov/bill/112th-congress/senate-bill/3552
16. Slattery, M., Harper, B., & Harper, S. (2019). Pesticide Encapsulation at the Nanoscale Drives Changes to the Hydrophobic Partitioning and Toxicity of an Active Ingredient. Nanomaterials, 9(1), 81. https://doi.org/10.3390/nano9010081
17. Stehle, S., & Schulz, R. (n.d.). Supporting Information. 1–45.
18. Stone, D., Harper, B. J., Lynch, I., Dawson, K., & Harper, S. L. (2010). Exposure assessment: Recommendations for nanotechnology-based pesticides. International Journal of Occupational and Environmental Health, 16(4), 467–474. https://doi.org/10.1179/oeh.2010.16.4.467

19. Tong, Y., Wu, Y., Zhao, C., Xu, Y., Lu, J., Xiang, S., … Wu, X. (2017). Polymeric Nanoparticles as a Metolachlor Carrier: Water-Based Formulation for Hydrophobic Pesticides and Absorption by Plants. Journal of Agricultural and Food Chemistry, 65(34), 7371–7378. https://doi.org/10.1021/acs.jafc.7b02197
20. USEPA. (2002). Methods for Measuring the Acute Toxicity of Effluents and Receiving Waters to Freshwater and Marine Organisms Fifth Edition October 2002. United States Environmental Protection Agency Office of Water, Washington(October), 1–275.
21. Villaverde, J. J., Sevilla-Morán, B., López-Goti, C., Alonso-Prados, J. L., & Sandín-España, P. (2018). Considerations of nano-QSAR/QSPR models for nanopesticide risk assessment within the European legislative framework. Science of the Total Environment, 634, 1530–1539. https://doi.org/10.1016/j.scitotenv.2018.04.033
22. Wauchope, R. D., Yeh, S., Linders, J. B. H. J., Kloskowski, R., Tanaka, K., Rubin, B., … Unsworth, J. B. (2002). Pesticide soil sorption parameters: Theory, measurement, uses, limitations and reliability. Pest Management Science, 58(5), 419–445. https://doi.org/10.1002/ps.489

CeO_2 NANOPARTICLES AFFECT SOYBEANS AND THEIR ROOT-ASSOCIATED MICROBIOME AT LOW, ENVIRONMENTALLY RELEVANT CONCENTRATIONS

Matthew R Slattery., Stacey L. Harper, Mark G. Johnson, Christian P. Andersen, Jay R. Reichman

In preparation for submission

Chapter 4 CeO_2 nanoparticles affect soybeans and their root-associated microbiome at low, environmentally relevant concentrations

4.1 Abstract

The use of cerium oxide nanoparticles (CeNPs) in fuel additives and other industrial products may result in the accumulation of these nanoparticles in soils. The biological interaction between CeNPs, plants, and the root-associated microbiome is poorly understood. Complicating the issue, the use of pristine nanoparticles in toxicity tests may not be realistic because complex interactions with environmental media can alter the fundamental properties of a nanoparticle over time. Here, soybeans were grown to maturity in a natural soil with either aged CeNPs (3 month incubation in soil) or pristine CeNPs (no incubation in soil) at low (1 mg kg^{-1}) or high (100 mg kg^{-1}) soil concentrations, then compared to control soybeans grown with no CeNPs. The CeNP exposures caused significant changes to the soybean yield and biomass, especially among the pristine-low treatments. Non-monotonic responses were apparent for certain phenotypic endpoints, particularly among the pristine CeNPs. To identify associations between plant growth and the root-associated microbiome, root samples were processed for 16S rDNA amplicon sequencing. The root microbiome structure shifted dramatically in the pristine CeNP exposures, whereas the aged CeNP communities were more similar to the control. However, aged treatments caused a significant loss of bacterial richness when compared to the control, and the magnitude of these effect was somewhat dependent on spatial proximity to the root surface. Overall, impacts to soybeans and their root-associated microbiome are dependent on the concentration and age of CeNPs. In this case, CeNPs produced agriculturally and ecologically relevant changes in the plant-soil system. These results highlight the non-monotonic effects of CeNPs in soil that may change dramatically over time and the potential for microbiome-mediated plant toxicity.

4.2 Introduction

Rapid implementation of nanotechnology worldwide (Roco 2011) will inevitably increase the amount of engineered nanomaterials found in the environment (Gottschalk 2013). Among these are cerium oxide nanoparticles (CeNPs) with up to 10,000 metric tons produced each year for use in fuel additives, chemical planarization, and UV-coatings (Piccinno 2012, Keller 2013). Life-cycle analyses predict that 14% of total manufactured CeNPs will contaminate soils through a variety of environmental vectors (Keller 2013). For example, the atmospheric deposition of CeNPs from diesel fuel along roadways could result in concentrations above 1 mg kg^{-1} dry soil (Park 2008) before accounting for other contamination vectors. Biosolids application may also increase soil CeNP concentrations, considering 90% of CeNPs introduced to wastewater treatment plants remain in biosolids after processing (Barton 2014, Gomez-Rivera 2012) and more than 40% of biosolids generated in the United States are applied as fertilizer (US EPA 1999). With the potential for CeNP contamination in soil established, it is important to understand how these nanomaterials can influence terrestrial life including plants and microbes.

Soybeans (*Glycine max*) offer an agriculturally and ecologically relevant system to explore the relationships between plants, microbes, and CeNPs. A record 4.54 billion bushels of soybeans were produced by the United States in 2018 (USDA 2019). Soybeans are an attractive agricultural commodity in part because they facilitate a symbiotic relationship with nitrifying bacteria that is responsible for 77% of the total nitrogen fixed by leguminous crops (Herridge 2008), significantly reducing the need for nitrogenous fertilizer application (Salvagiotti 2008). Importantly, the nodules that facilitate this symbiosis are a part of the greater root-associated microbiome (also known as the rhizosphere) that is vital for carbon sequestration, ecosystem functioning, and nutrient cycling in plant systems (Berg 2009). Past research identified that soybeans respond to terrestrial CeNPs in a myriad of ways including reductions in plant growth, yield, and nitrogen fixation (Priester 2012, Preister 2017), altered nutrient profiles (Peralta-Videa 2014), and changes in the rate of net photosynthesis (Cao 2017). Studies investigating the potential mediating role of microbes in CeNP effects on soybeans are limited. One study attempted to isolate the role of the root microbiome by autoclaving soil prior to CeNP amendment (Stowers 2018), but the comparison of autoclaved and non-autoclaved soils is inherently problematic due to dramatic changes in soil structure and microbial respiration in the

wake of this extreme sterilization process (Shaw 1998). Nonetheless, it is important to continue probing this system to reveal what mediating role, if any, the soil microbiome plays in CeNP toxicity.

The gap in literature covering the interactions between CeNPs, soybeans, and their microbial communities is exacerbated by other factors. The existing research has failed to capture environmentally realistic doses if the 1 mg kg^{-1} concentration iterated above is accurate; in fact, very few studies incorporate concentrations below 100 mg kg^{-1}. This is problematic in light of other nanomaterial research indicating that soil exposures can display atypical dose-response relationships where lower concentrations elicit stronger effects on microbial communities (Simonin 2017) and soybean nodulation (Wang 2017). Some of the aforementioned soybean studies with CeNP observed stronger effects at lower concentrations (Priester 2012). Further, most studies focus on exposures with pristine CeNP amendment at the start of the soybean exposure, disregarding the potential for both biotic and abiotic nanomaterial transformations over time that can significantly alter nanomaterial-biological interactions (Lowry 2012).

The aim of this study was to address the lack of CeNP studies that holistically assess CeNP-soybean interactions, with particular attention to the potential mediating role of the microbial community that exists along the root-soil interface. A combination of soybean phenotypic metrics of plant growth and microbial sequencing from the soybean roots will help to elucidate if soil communities influence nanomaterial toxicity to plants. The authors selected CeNP concentrations at the upper limit of environmental concentrations and the lower limit of concentration ranges utilized in most other studies. Finally, this study incorporated long-term aging of particles in soil prior to soybean exposure to determine if pristine CeNPs are sufficiently representative of chronic environmental exposures.

4.3 Materials and methods

4.3.1 Nanoparticles

The CeNPs were purchased from Sigma Aldrich (St Louis, MO, USA) in powder form with a primary particle size of 16 nm, verified by the manufacturer using X-ray diffraction and Brunauer–Emmett–Teller (BET) analysis (batch number MKCB0040V). For soil amendments, CeNPs were suspended in deionized (DI) water at either 125 mg L^{-1} (for low concentration soils) or 12,500 mg L^{-1} (for high concentration soils), then sonicated for 5 minutes at 100% intensity with a VCX 750 Vibra-Cell sonicator (Sonics and Materials Inc., Newton, CT, USA) with a cup-horn style high intensity probe in a recirculating bath.

4.3.2 Soil Preparation

A natural soil was collected in the Willamette Valley flood plain in Western Oregon to ensure the complexity of typical soil matrices along with an existing microbial community. The soil characteristics are presented in Table S4.2. This soil was sieved with a 6.35 mm sieve and stored in a closed container for at least two years prior to use in this experiment. In order to accommodate two CeNP concentrations and two CeNP ages, 25 kg aliquots of soil were added to individual plastic tubs for each of the 5 treatments: control, low-pristine, high-pristine, low-aged, and high-aged (described below).

The soil for all tubs was prepared in two steps. The first step occurred 106 days prior to the transfer of soybeans into potted soil. All soil tubs were inoculated at the first step with a rhizobia inoculant (America's Best Soybean Inoculant® batch #2G18210) from Advanced Biological Marketing, Van Wert, Ohio, USA at a rate of ~1,600 CFU *Bradyrhizobium japonicum* cm^{-3}. This is also when CeNPs were added to the tubs for the 2 aged treatments, at low (1 mg kg^{-1} dry soil) and high (100 mg kg^{-1}) concentrations. All tubs were watered to 75% of their field capacity (0.32 m^3 m^{-3}), thoroughly homogenized with a shovel, and then placed in a temperature controlled incubation chamber set to 25 °C with lids on.

The second soil preparation step occurred 106 days later. At this time, CeNPs were added to the pristine tubs at low and high concentrations. All tubs were watered to 85% of field capacity and thoroughly homogenized a second time, at which point they were ready for transfer to plastic

pots. Each pot contained 3 cm of crushed gravel at its base, a polyethylene grow bag with 12 holes at the bottom for drainage, and 2.5 kg of prepared soil in the bag. Each of the 5 treatments had 10 replicates.

4.3.3 Soybean cultivation

Soybean seeds (*Glycine max,* Beer Friend variety, lot #3301001) were purchased from Victory Seeds, Molalla, Oregon, USA. This variety was selected for its rapid time to maturity. An excess of 200 seeds were rinsed with DI water before placement into peat starter pellets in a greenhouse under natural lighting. After 7 days, 50 healthy seedlings at the same developmental stage were selected for transfer to the prepared pots. Soybeans were watered once per week from below by submerging the pots in 10 cm of water until the topsoil was visibly moistened. Soybean plants were harvested for processing after 84 days of growth, at which point plants were in the R6/R7 stage of growth.

At harvest, the stem length was measured, and the above-ground tissues were separated into stems, leaves, pods, and beans, then dried and weighed. Soil was gently shaken loose from the root mass, and nodules were excised from the roots. Nodules were counted, sliced open to ensure a red color (indicating active and healthy nodules), then dried and weighed. A 5 cm section of root material was excised from each root mass for DNA extraction.

4.3.4 Soybean microbiome compartments

To generate spatially distinct microbiome data, we adapted a method from Edwards et al (2014). Briefly, 1 g of root material (including loosely bound soil) was placed in a 50 mL falcon tube with 40 mL of phosphate buffered saline (PBS) solution (8 g L^{-1} NaCl, 0.2 g L^{-1} KCl, 1.42 g L^{-1} Na_2HPO_4, 0.24 g L^{-1} KH_2PO_4). Sterile forceps were used to stir the root material in the vial, releasing some of the soil into solution representing the “rhizosphere” compartment. Next, the rinsed roots were placed in a new falcon tube with 40 mL PBS and sonicated for 45 s in a bath ultrasonicator, releasing more tightly bound soil representing the “rhizoplane” compartment.

Finally, the root was placed in 40 mL of fresh PBS and sonicated for 45 s, placed in fresh PBS buffer and sonicated for 45 s again, then removed and placed in a dry falcon tube representing the “root” compartment. All soil compartment samples were stored at 4 °C for three days until being frozen at –20 °C awaiting DNA extraction the following week.

4.3.5 DNA extraction and sequence library preparation

Following the manufacturer’s instructions (MO BIO Labratories, Inc., Carlsbad, CA, USA) total DNA was extracted from 250 mg of rhizosphere, rhizoplane, or root material from 4 randomly selected plants in each treatment using MoBio PowerSoil® DNA Isolation Kits. This resulted in 60 total samples that were stored at –20 °C until further processing. Extracted DNA was processed according to the Illumina MiSeq preparation guide (Part # 15044223 Rev. B). Briefly, amplicon PCR targeted the V3/V4 hypervariable region of the 16S rDNA gene with S-D-Bact-0341-b-S-17 and S-D-Bact-0785-a-A-21 primers adapted from Klindworth et al (2013) with Illumina overhang sequences attached, supplied by Eurofins Genetics (Louisville, KY, USA). An Agilent Technologies (Santa Clara, CA, USA) 2100 Bioanalyzer verified the fragment size and distribution of the amplicons prior to the index PCR (using Nextera N7XX and S5XX index kits) process, and a Qubit 3.0 Flurometer (Thermo Fisher Scientific, Waltham, MA, USA) was used to normalize final DNA concentrations prior to injection into a MiSeq v3 Reagent Tray (Illumina, San Deigo, CA, USA). The reagent tray was analyzed with a MiSeq sequencer (version 3.1.0.13). The sequence output can be accessed in GenBank as a Sequence Read Archive (SUB5818994).

4.3.6 QIIME2 analysis

Sample sequences were analyzed using the QIIME 2 2018.11 (Boylen 2018) software package. The raw data from the MiSeq instrument was quality filtered with q2-deblur (Amir 2017). The resulting amplicon sequence variance were aligned with mafft (Katoh 2002) and placed into a phylogenetic tree with fasttree (Price 2010). Metrics of alpha diversity (observed operational taxonomic units (OTUs) and Shannon diversity index), beta diversity (weighted UniFrac

(Lozupone 2007)), and a principal coordinate analysis (PCoA) were estimated using the q2-diversity plugin after samples were rarefied to 13,611 sequences per sample (the minimum observed in any given sample). Taxonomic assignment of the amplicon sequence variants was conducted with the q2-feature-classifier (Bokulich 2018) trained against the Greengenes 13_8 99% OTUs reference sequences (McDonald 2012).

4.3.7 Statistical analysis

Soybean phenotypic endpoints (biomass measurements, nodule count, bean count) and microbial population abundancies were compared between CeNP treatments and the control using the student's t-test. Observed OTUs and the Shannon diversity values were compared using Kruskal-Wallis pairwise comparisons. Changes in microbial community structure were calculated with a pairwise PERMANOVA test. Differences were considered significant when $p \leq 0.05$.

4.4 Results and Discussion

The findings from this study are divided into two general sections: the phenotypic observations of soybean growth and yield, and the assessment of the root-associated microbiome via the QIIME 2 software package and associated plugins.

4.4.1 Soybean phenotypic observations

CeNPs generally reduce soybean yield

In response to all of the tested CeNP exposures, average bean mass generally decreased regardless of concentration or aging treatment (Figure 4.1A). The low-pristine treatment had a statistically significant 23% reduction in bean mass, but other CeNPs merely trended towards a decrease without reaching significance ($p=0.052$ for the high-pristine treatment). Considering that beans are rich in nitrogen and roughly half of nitrogen in soybeans is sourced from biological nitrogen fixation (Salvagiotti 2008), the significant reduction in overall yield observed

in the low-pristine treatment may indicate disruption of symbiotic exchange between soybeans and nitrogen fixing bacteria.

Impacts to bean production, measured by the average bean count, was also generally reduced by all CeNP exposures (Figure 4.1B). This reduction was statistically significant at the low CeNP concentrations for both the pristine and aged treatments. This data for bean mass and bean count suggests an atypical dose-response curve, in which lower concentration treatments can elicit a stronger effect than higher concentrations. This would not be the first instance of such phenomenon, as experiments with soybeans and CeNPs have noted a similar trend for plant growth metrics (Priester 2012) and reactive oxygen species (Priester 2017) in which the highest dose does not represent the strongest response. Other researchers have pointed to an increase in particle agglomeration with higher concentrations as a driver of this atypical dose-response (Wang 2017). However, this study stands apart in that the lowest dose tested was within the environmental estimate of 1 mg kg^{-1} in soils, which is one estimate provided for CeNP accumulation in soils near roadways with heavy diesel traffic (Park 2008).

CeNP impact to soybean growth is dependent on particle aging

Other phenotypic metrics conveyed trends in soybean response that were dependent on particle aging. Stem biomass was strongly reduced in the high-aged treatment, which was the only significant treatment for that endpoint (Figure 4.1C). Interestingly, low-pristine treatment had an opposite effect and trended towards an increase in stem biomass ($p=0.087$). Other phenotypic metrics, such as average pod mass, indicated trends towards distinct aged and pristine CeNP effects that did not achieve statistical significance (SI).

Nodule biomass is affected by pristine but not aged CeNPs

The biomass of root nodules in soybeans presented here showed a significant increase in the low-pristine treatment and a similar increase for the high-pristine CeNPs (failed equal variance test, Mann-Whitney rank sum test $p=0.252$) (Figure 4.1D). In contrast, the aged CeNPs did alter the

nodule biomass. This increase in nodule mass for pristine treatments was unexpected given past research suggesting that CeNP reduced nodule biomass, albeit at extremely high concentrations of 1000 mg kg^{-1} (Priester 2012). A study with carbonaceous nanomaterials also reduced soybean nodulation at very low concentrations under 1 mg kg^{-1} (Wang 2017).

Changes to nodule mass are important in light of their support role for the relationship with nitrogen fixing bacteria, such that soybean growth models incorporate the nodule biomass as a predictor of nitrogen fixation potential (Baddeley 2011). The abundance of nitrogen fixing bacteria found in the microbial component of this study corroborates the nodule data here and is discussed at length in a later section. Notably, the increased nodule mass was not accompanied by an increase in yield – instead, the yield dropped. This fact, coupled with the general trend towards reduced bean mass, suggests that CeNP treatments may be disrupting soybean nitrogen assimilation beyond modifying the abundance of nitrogen fixing bacteria.
Collectively, the phenotypic data demonstrates that CeNP's effect on soybean growth and yield is dependent on both the concentration and age of the particles. Different plant metrics reveal different trends following CeNP amendment to soil, but a non-monotonic response influenced by particle aging is likely.

The subsequent sections will focus on the results of the microbiome investigation. These are divided into alpha diversity (absolute measures of community structure that do not directly compare samples) and beta diversity (relative measures of community similarity).

4.4.2 CeNPs affect alpha diversity

Spatial compartmentalization produces a bacterial richness gradient

Acknowledging that the spatial heterogeneity of soil microbes is a problematic limitation of most microbiome research (Prosser 2015), this study divided the root-associated microbiome into three compartments in order of increasing proximity to the root surface: rhizosphere, rhizoplane, and root (representative cross-section displayed in Figure 4.2) as an adaptation from the work of

Edwards et al (2014). Comparing the observed OTUs – a metric for assessing the richness of microbial communities – shows significant differences across all three of the compartments, such that the bacterial richness decreased with closer proximity to the root surface (Figure S4.4). This suggests that the compartmental separation process was successful, considering that the community is likely to become more specialized in close proximity to root tissues which release mucilage and exudates to shape the community (Edwards 2014).

Changes in bacterial richness are spatially dependent

Comparison of the control, pristine, and aged communities within each compartment is displayed in Figure 2. The low and high concentrations were paired for simplicity and because there was no significant difference in bacterial richness between low and high concentrations, though the low concentration trended towards a greater reduction (Figure S4.5). Interestingly, the pristine group in all compartments trended towards the highest bacterial richness, though this was not statistically significant. The aged treatments all had significantly fewer observed OTUs than their pristine counterparts. For the rhizosphere, the aged OTUs were also significantly different from the control. The rhizosphere compartment appears to have the most dramatic bacterial richness response to aged CeNPs, which are similar but muted in the rhizoplane and root compartments.

Pristine and aged CeNPs produce opposite effects on microbial diversity

When analyzing the Shannon diversity – a metric that incorporates both bacterial richness and community evenness – the low and high concentrations were again grouped for simplicity and because there was no significant difference between low and high CeNP treatments (see SI). Neither the pristine nor the aged CeNP treatments diverged significantly from control with respect to this diversity metric in any compartment. However, the pristine and aged treatments were different from each other in all three compartments. While no CeNP treatments were different from the control diversity baseline, there was a consistent trend towards increasing diversity in pristine treatments and decreased diversity in aged treatments. This highlights that nanoparticle aging can produce diametrically opposite trends in microbial community structure.

In comparison to the bacterial richness, it is also clear that overall metrics of diversity are conserved between compartments more so than community richness, where root proximity appears to be more important.

The fact that bacterial community response to CeNPs is spatially dependent is probably linked to the accumulation of CeNPs at the root-soil interface. A previous CeNP study with soybeans did not produce any changes to the soil community unless a soybean was in the same pot (Ge 2014). Another study with canola plants asserted that proximity to plant roots was a significant factor in determining the impacts of CeNPs to microbial communities (Hamidat 2016). This is probably because CeNPs are concentrated at the root-soil interface; a synchrotron study shows that CeNPs tend to accumulate at soybean roots in concentrations several orders of magnitude higher than above-ground tissues (Hernandez-Viezcas 2014). Based on this information, it is probable that soybean roots act as a sieve for CeNPs traveling in soil water that is moving towards the plant, where they are excluded by the plant and accumulate along the root surface as water and other nutrients are taken up by the plant.

The loss of microbial diversity and richness in the aged treatments suggests a reduction in the reservoir of genetic and functional diversity, which contributes to the resilience of soil ecosystems (Lynch 2015). Further, the loss of microbial diversity can lead to lower potential denitrification activity in soil (Philippot 2013), which may have specific relevance to soybeans and other plants that rely upon nitrogen fixing microbes for nitrogen assimilation.

Alpha diversity positively correlates with soybean phenotypes

Correlating the phenotypic soybean metrics with bacterial richness and the Shannon diversity helps to determine the relevance of root microbiome diversity with practical plant implications. A significant, positive correlation exists between the Shannon diversity and the shoot biomass, stem biomass, and number of beans produced by soybeans (Table 4.1). The number of OTUs significantly correlates in the same manner with number of beans. These correlations affirm the relevance of the microbial community diversity with respect to soybean growth and yield.

4.4.3 CeNPs affect beta diversity

Spatial compartments harbor distinct communities

Microbial communities were compared across samples using a weighted Unifrac approach, which accounts for phylogenetic relatedness among individual microbes. A visual representation of these comparisons is provided as a PCoA plot (Figure 4.4). The compartments separate into two general groups, with the root samples located near the top of the plot and the rhizosphere and rhizoplane samples grouped more similarly along the bottom. This separation corroborates the bacterial richness and diversity data, indicating that distinct bacterial communities can be found along a spatial gradient perpendicular to the root surface. A PERMANOVA analysis shows that root communities are statistically different from both the rhizosphere and rhizoplane communities. There appears to be relatively little difference between the rhizoplane and rhizosphere communities, which did not differ statistically based on the weighted Unifrac metric. This is somewhat surprising considering how dissimilar the root compartment was to these outer compartments, and the rhizoplane would presumably be compositionally between the rhizosphere and root compartments.

Aged communities nearly recover to baseline composition

In Figure 4.4, the pristine communities are separated to the right of the plot in purple and are significantly different from both the control and aged samples represented by orange and green. The control and aged samples overlap, but analysis revealed that these two are indeed significantly different ($p=0.049$). The aged group's similarity to the control community is suggestive of an incomplete reversion to the control baseline structure in the timeline of our experiment (3 month incubation and 3 month soybean cultivation). This failure to recover completely is not entirely surprising given that the bacterial richness decreased significantly in the aged communities, which may make total recovery impossible if certain microbes are eradicated from the soil. An alternative explanation is that the soybean microbiome community

in the aged treatments did not dramatically diverge from the baseline to begin with, due to a reduction in CeNP biological activity resulting from environmental transformations over the course of the 3 month soil incubation. Perhaps a layer of soil matter (analogous to a protein corona) prevents direct contact of the CeNPs with bacteria, which is in line with experimental data suggesting that direct spatial contact with bacteria is necessary to provoke cytotoxicity (Thill 2006). However, the general loss of bacterial richness in aged groups suggests otherwise.

Not shown in the coordinate plot is the difference between low and high communities, which both showed significant differences from the control community structure. However, the low and high groups were not significantly different from each other, suggesting that the 100-fold difference between low and high concentrations was not sufficient to generate distinct community structures. This agrees with the alpha diversity and phenotypic metrics, which also showed relatively limited differences between low and high concentrations.

4.4.4 CeNPs alter taxonomic hierarchy of the soybean microbiome

The 16S rDNA sequences collected across 60 samples were classified with a reference library (Greengenes 13_8) to generate a taxonomic bar plot (Figure 4.5). Assignment to known taxonomic identities is important for identifying microbes that are susceptible to CeNP exposure. For example, pristine treatments of CeNPs strongly reduced the abundance of gammaproteobacteria, represented by purple in the Figure 5.

Bacilli sensitivity to pristine CeNP exposure

Abundance of bacteria in the Bacillaceae family is significantly reduced by pristine CeNP exposure (Figure 4.6A). Recent studies have noted that bacteria in the *Bacilli* class, a subset of the Bacillaceae family, can reduce surface cerium of CeNPs from Ce^{+4} to Ce^{+3} and subsequently chelate Ce^{+3} ions, resulting in toxic effects to the microbe(Xie 2019). While no specific enzymatic processes are indicated for Ce^{+3} susceptibility, metal toxicity is often the result of metal ions interfering with endogenous ions of similar charge and size. This could explain the

sensitivity of Bacillaceae in the soybean microbiome exposed to CeNPs. However, there is a rebound in Bacillaceae abundance for the low-aged treatment. Over time, CeNPs may either be transformed in a way that reduces the interaction with Bacillaceae, perhaps through a complete reduction of available Ce on the particle surface, or a surface coating that mitigates bacterial interaction. Dissolution of CeNPs in an artificial soil solution demonstrates that these nanoparticles are extremely resilient to degradation, with undetectable dissolution after 28 days at neutral or alkaline pH and only 3.1% dissolution at pH of 4 (Cornelis 2014). While the *Bacilli* may have one mechanism that contributes to CeNP degradation, it is unlikely to completely degrade these particles over the course of this experiment in light of this resilience to degradation. That said, unexpected dissolution of nanoparticles by microbiomes is not unheard of, as gold nanoparticles were unexpectedly dissolved in the presence of a freshwater microbiome (Avellan 2018). Other studies have also observed reductions in *Bacilli* microbes and overall decrease in bacterial richness in periphytic communities (Tang 2017). This suggests that *Bacilli* microbes are indeed a highly susceptible microbe to CeNP exposure, with a proposed mechanism of toxicity available.

Bradyrhizobiaceae sensitivity to pristine CeNP exposure

One important element of this study was to cross reference the abundance of nitrogen fixing bacteria with the observations of nodule mass. The natural soils used in this study were inoculated with a *Bradyrhizobia* inoculant to ensure that these microbes would be present in sufficient numbers so as to facilitate soybean nodulation, and these nitrogen fixing organisms were present in all samples (Figure 4.6B). The abundance of these microbes in the rhizosphere compartment matched the results of the nodule biomass in that the pristine exposures were higher than the control, and the aged treatments were not significantly different. Comparison of abundance in the rhizoplane and root compartments yielded no statistically significant differences, again acknowledging the role of spatial heterogeneity as a factor in experimental outcomes.

There are multiple explanations for the increased abundance of rhizobia microbes. First, a reduction in other bacteria that utilize the same resources could improve growth conditions for rhizobia by reducing competition. Second, CeNPs could interact with the root signaling processes, i.e. the release of flavonoids by the plants and nodulation factors by the rhizobia. This isn't necessarily supported by the nodule count observed in the soybeans in which no significant changes were observed (Figure S4.1). Perhaps the nodules that are successfully formed receive a disproportion amount of resources in the pristine treatments as an attempt to increase biological nitrogen fixation because their nitrogen assimilation was otherwise inhibited. Third, the soil rhizobia might directly benefit from interaction with the CeNPs, as some studies have showed that CeNPs can serve as scavengers of reactive oxygen species and mimetic of antioxidant enzymes (Lee 2013, Wang 2017, Korsvik 2007).

4.5 Conclusions

Three important ideas emerge from the findings of this experiment. First, soil amendments of CeNPs can modulate biological systems at low, environmentally relevant concentrations that are rarely included in terrestrial assessments. Importantly, the low concentrations sometimes elicit a stronger response, indicating a non-monotonic or atypical dose-response curve. This introduces uncertainty into the prediction of CeNP impacts to the environment, which generally operate on the assumption of increased effects at higher concentrations. Derivation of a threshold or no adverse effect concentration is impossible without establishing the shape of the dose-response curve. Other studies incorporating CeNP concentrations at 1 mg kg^{-1} and lower are needed.

Second, CeNPs incubated in a natural soil can produce opposite effects on plant growth and microbial community structure when compared with their pristine counterparts. The notion of environmental transformations that influence the behavior and toxicity of nanomaterials is not new, but this study presents a case in which three months of CeNP-soil interaction can fundamentally alter the conclusion of a terrestrial toxicity assessment.

Finally, the soybean microbiome is strongly impacted by CeNPs. Modulation of this root-associated soil community is primarily dependent on the aging status of the CeNPs and the proximity to the root surface. Despite a 100-fold difference in CeNP concentrations, the microbiome response to high and low concentrations was similar.

In future studies, determining the functional implications of the microbiome community shifts elicited by CeNP exposures will fill important gaps about the relevance of CeNP contamination. Considering the significant changes apparent with a 16S marker gene analysis, a transcriptomic survey would almost certainly yield an array of functional changes that accompany the community shifts. Alternatively, the use of predictive bioinformatics software such as Phylogenetic Investigation of Communities by Reconstruction of Unobserved States 2 (PICRUSt2) may validate the notion of functional impacts without the need for supplemental experiments.

4.6 Funding

This work was supported by a Cooperative Training Partnership between Oregon State University and the Environmental Protection Agency (83591301), USDA-NIFA (2013-67021-21181), and the Agricultural Research Foundation (ARF8301A). Further support was provided to M.S. by the ARCS Foundation.

4.7 Acknowledgments

The authors would like to thank Andrew Bird and AMBI for supplying the soybean inoculant.

4.8 Conflicts of Interest

The authors declare no conflict of interest.

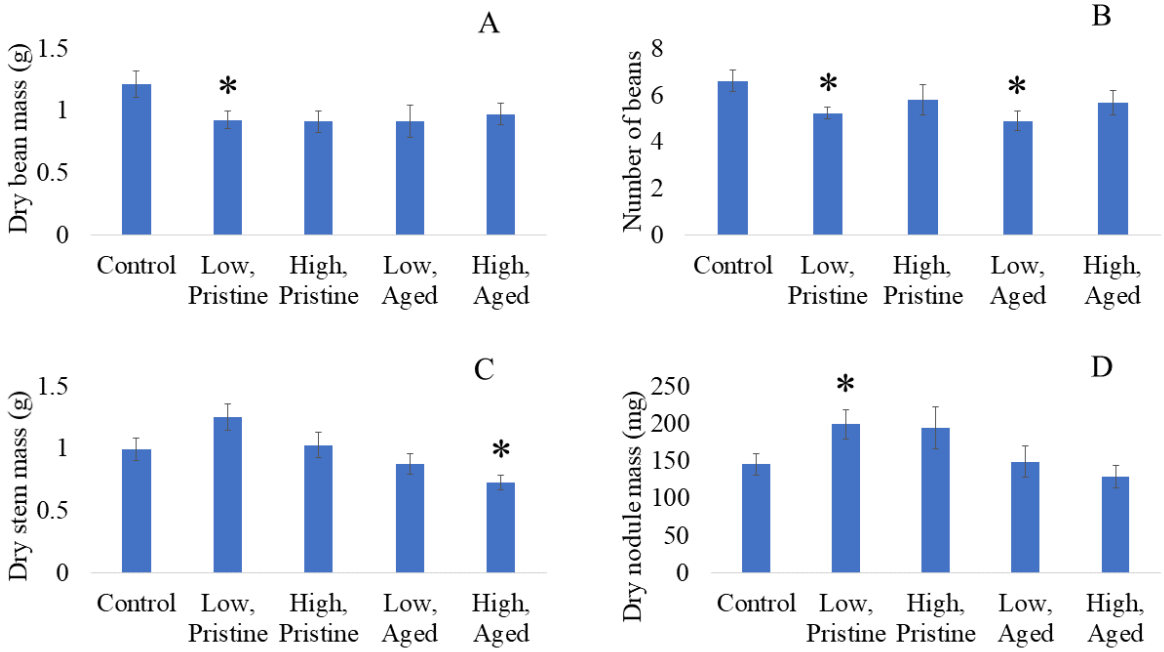

Figure 4.1. Phenotypic responses of soybeans exposed to pristine or aged (3 month incubation) CeNPs at low (1 ppm) or high (100 ppm) concentrations. The average soybean bean mass (A), bean count (B), stem mass (C), and nodule mass (D) are represented here (n=9 except for control where n=10, bars represent SE, * indicates significant difference from control based on t-test, $p \leq 0.05$).

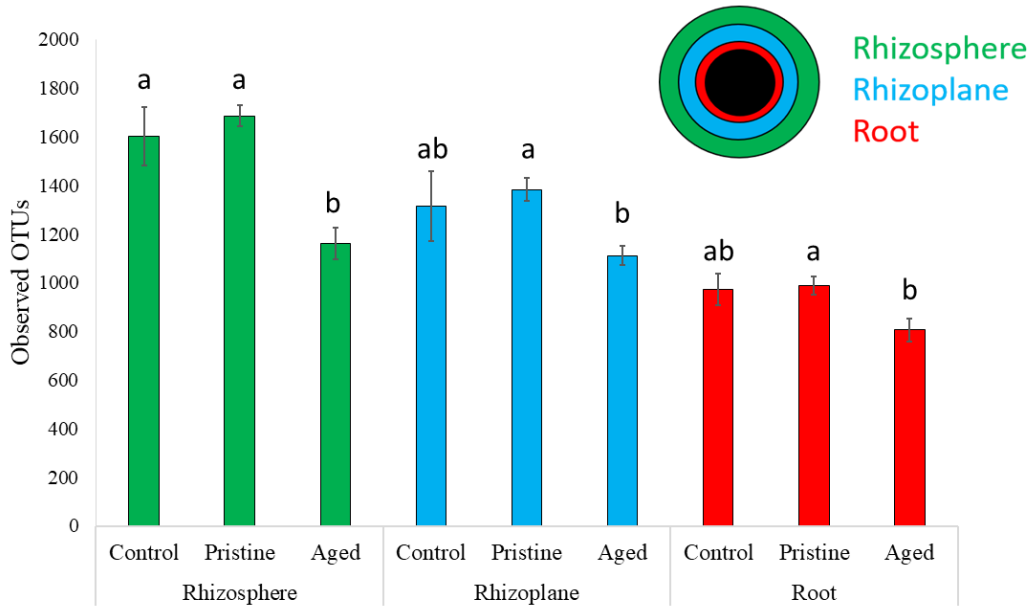

Figure 4.2. Average number of OTUs in soybean root-associated microbiome, separated by the three spatial compartments (rhizosphere, rhizoplane, and root) and subdivided into control, pristine (combined low and high concentrations), and aged (combined low and high concentrations) treatments (n=8 except for controls where n=4, error bars ± SE, Kruskal-Wallis pairwise comparison within compartments, corrected $p \leq 0.05$)

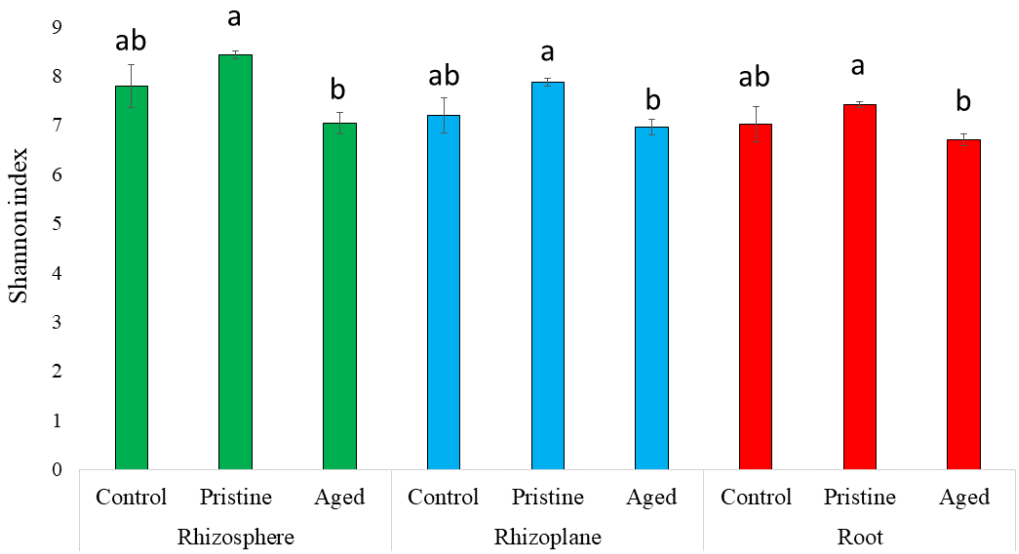

Figure 4.3. Shannon diversity index in soybean root-associated microbiome, separated by the three spatial compartments (rhizosphere, rhizoplane, and root) and subdivided into control, pristine (combined low and high concentrations), and aged (combined low and high concentrations) treatments (n=8 except for controls where n=4, error bars ± SE, Kruskal-Wallis pairwise comparison within compartments, corrected $p \leq 0.05$)

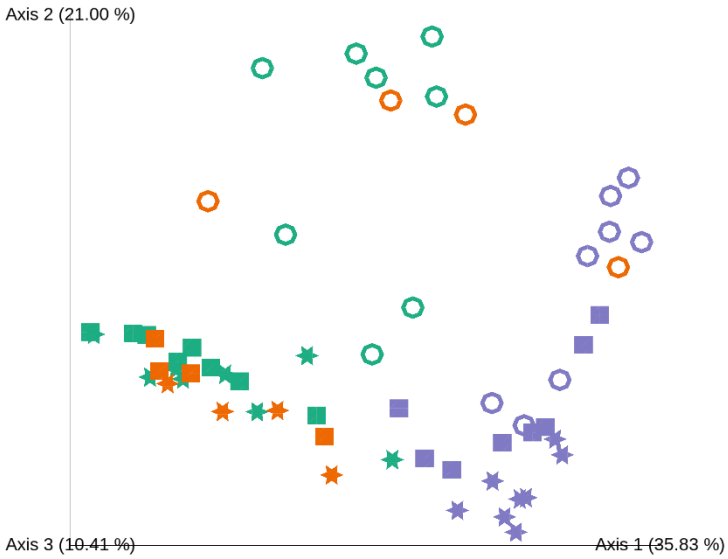

Figure 4.4. PCoA plot depicting the clusters of bacterial communities across spatial compartments (stars=rhizosphere, squares=rhizoplane, rings=root) and particle age (control=orange, pristine=purple, aged=green) based on their weighted UniFrac distance metrics. The percent variation along each axis refers to the fraction of total variance.

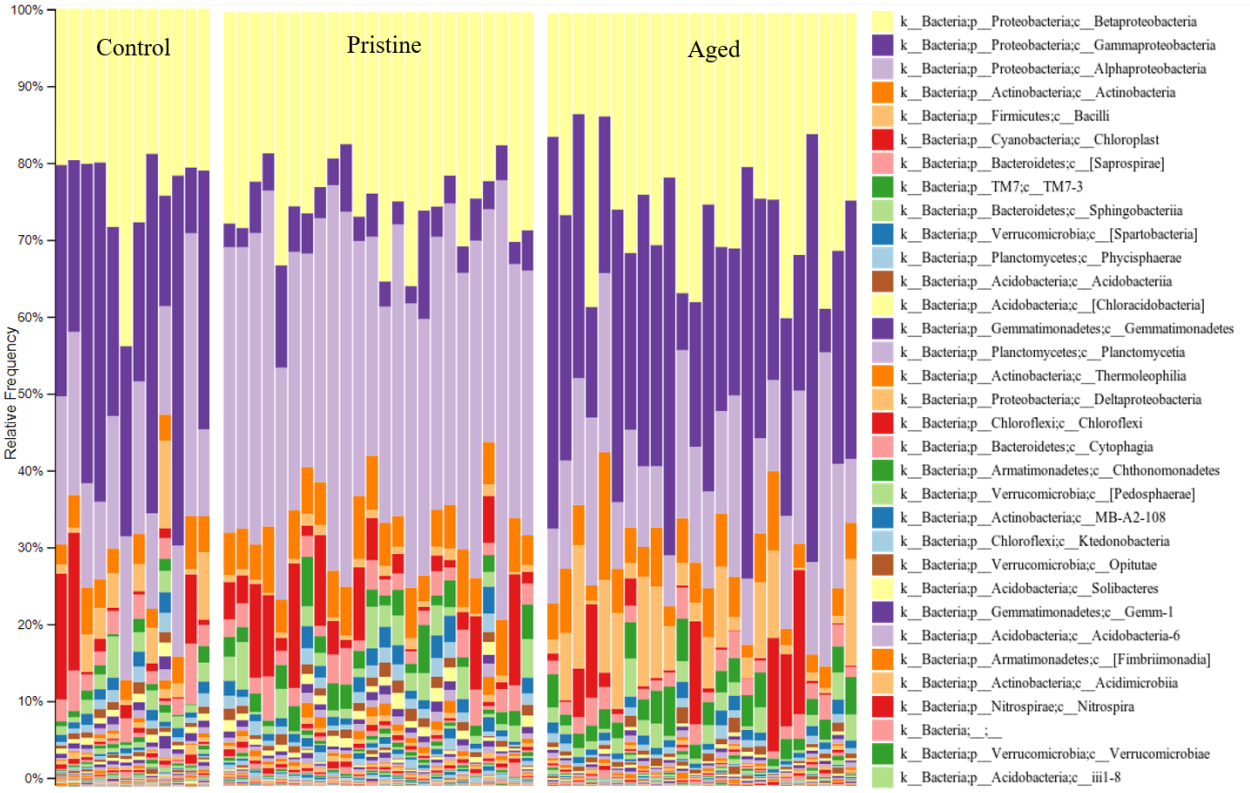

Figure 4.5. Taxonomic distribution of bacteria, classified by bacterial Class in accordance the Greengenes database (version 13.8). Samples are grouped by control, pristine, and aged CeNP treatments.

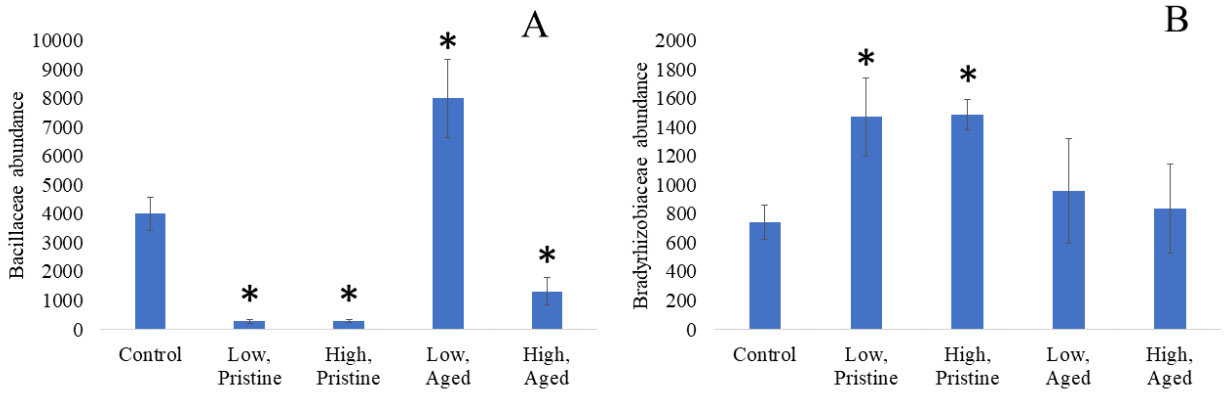

Figure 4.6 Comparison of microbial abundance in the rhizosphere compartment across all treatments for bacteria in the Bacillaceae family (A) and Bradyrhizobiaceae family (B).

Table 4.1. Spearman's correlation values between alpha diversity metrics and soybean growth and yield metrics. Bolded values are significant ($p \leq 0.05$)

	Bean mass	Bean count	Stem mass	Nodule mass
Observed OTUs	0.211	**0.029**	0.299	0.619
Shannon diversity	0.242	**0.033**	**0.026**	0.336

References Cited

1. Avellan, A., Simonin, M., McGivney, E., Bossa, N., Spielman-Sun, E., Rocca, J. D., … Lowry, G. V. (2018). Gold nanoparticle biodissolution by a freshwater macrophyte and its associated microbiome. Nature Nanotechnology, 13(11), 1072–1077. https://doi.org/10.1038/s41565-018-0231-y
2. Baddeley, J., Watson, C., Baddeley, J., Watson, C., Yanyan, L., Lianhai, W., … Christine, A. W. (2011). Models of biological nitrogen fixation of legumes . A review To cite this version : HAL Id : hal-00930470 Review article Models of biological nitrogen fixation of legumes . A review.
3. Barton, L. E., Auffan, M., Bertrand, M., Barakat, M., Santaella, C., Masion, A., … Bottero, J. Y. (2014). Transformation of pristine and citrate-functionalized CeO2 nanoparticles in a laboratory-scale activated sludge reactor. Environmental Science and Technology, 48(13), 7289–7296. https://doi.org/10.1021/es404946y
4. Berg, G., & Smalla, K. (2009). Plant species and soil type cooperatively shape the structure and function of microbial communities in the rhizosphere. FEMS Microbiology Ecology, 68(1), 1–13. https://doi.org/10.1111/j.1574-6941.2009.00654.x
5. Cao, Z., Stowers, C., Rossi, L., Zhang, W., Lombardini, L., & Ma, X. (2017). Physiological effects of cerium oxide nanoparticles on the photosynthesis and water use efficiency of soybean (: Glycine max (L.) Merr.). Environmental Science: Nano, 4(5), 1086–1094. https://doi.org/10.1039/c7en00015d
6. Cornelis, G., Kookana, R. S., Fernandes, T. F., Van den Brink, P. J., Reeves, P. T., Spurgeon, D., … Beulke, S. (2014). Nanopesticides: Guiding Principles for Regulatory Evaluation of Environmental Risks. Journal of Agricultural and Food Chemistry, 62(19), 4227–4240. https://doi.org/10.1021/jf500232f
7. Edwards, J., Johnson, C., Santos-Medellín, C., Lurie, E., Podishetty, N. K., Bhatnagar, S., … Sundaresan, V. (2015). Structure, variation, and assembly of the root-associated microbiomes of rice. Proceedings of the National Academy of Sciences, 112(8), E911–E920. https://doi.org/10.1073/pnas.1414592112

8. Ge, Y., Priester, J. H., Werfhorst, L. C. Van De, Walker, S. L., Nisbet, R. M., An, Y., … Holden, P. A. (2014). Cerium_particles_soybean.
9. Gómez-Rivera, F., Field, J. A., Brown, D., & Sierra-Alvarez, R. (2012). Fate of cerium dioxide (CeO 2) nanoparticles in municipal wastewater during activated sludge treatment. Bioresource Technology, 108, 300–304. https://doi.org/10.1016/j.biortech.2011.12.113
10. Gottschalk, F., Sun, T., & Nowack, B. (2013). Environmental concentrations of engineered nanomaterials: Review of modeling and analytical studies. Environmental Pollution, 181, 287–300. https://doi.org/10.1016/j.envpol.2013.06.003
11. Hamidat, M., Barakat, M., Ortet, P., Chanéac, C., Rose, J., Bottero, J. Y., … Santaella, C. (2016). Design Defines the Effects of Nanoceria at a Low Dose on Soil Microbiota and the Potentiation of Impacts by the Canola Plant. Environmental Science and Technology, 50(13), 6892–6901. https://doi.org/10.1021/acs.est.6b01056
12. Hernandez-Viezcas, J. A., Castillo-Michel, H., Andrews, J. C., Cotte, M., Rico, C., Peralta-Videa, J. R., … Gardea-Torresdey, J. L. (2013). In situ synchrotron X-ray fluorescence mapping and speciation of CeO 2 and ZnO nanoparticles in soil cultivated soybean (Glycine max). ACS Nano, 7(2), 1415–1423. https://doi.org/10.1021/nn305196q
13. Herridge, D. F., Peoples, M. B., & Boddey, R. M. (2008). Global inputs of biological nitrogen fixation in agricultural systems. Plant and Soil, 311(1–2), 1–18. https://doi.org/10.1007/s11104-008-9668-3
14. Keller, A. A., McFerran, S., Lazareva, A., & Suh, S. (2013). Global life cycle releases of engineered nanomaterials. Journal of Nanoparticle Research, 15(6). https://doi.org/10.1007/s11051-013-1692-4
15. Korsvik, C., Patil, S., Seal, S., & Self, W. T. (2007). Superoxide dismutase mimetic properties exhibited by vacancy engineered ceria nanoparticles. Chemical Communications, (10), 1056–1058. https://doi.org/10.1039/b615134e
16. Lee, S. S., Song, W., Cho, M., Puppala, H. L., Nguyen, P., Zhu, H., … Colvin, V. L. (2013). Antioxidant properties of cerium oxide nanocrystals as a function of nanocrystal diameter and surface coating. ACS Nano, 7(11), 9693–9703. https://doi.org/10.1021/nn4026806

17. Lynch, M. D. J., & Neufeld, J. D. (2015). Ecology and exploration of the rare biosphere. Nature Reviews Microbiology, 13(4), 217–229. https://doi.org/10.1038/nrmicro3400
18. Park, B., Donaldson, K., Duffin, R., Tran, L., Kelly, F., Mudway, I., … Martin, P. (2008). Hazard and risk assessment of a nanoparticulate cerium oxide-based diesel fuel additive - A case study. Inhalation Toxicology, 20(6), 547–566. https://doi.org/10.1080/08958370801915309
19. Peralta-Videa, J. R., Hernandez-Viezcas, J. A., Zhao, L., Diaz, B. C., Ge, Y., Priester, J. H., … Gardea-Torresdey, J. L. (2014). Cerium dioxide and zinc oxide nanoparticles alter the nutritional value of soil cultivated soybean plants. Plant Physiology and Biochemistry, 80, 128–135. https://doi.org/10.1016/j.plaphy.2014.03.028
20. Philippot, L., Spor, A., Hénault, C., Bru, D., Bizouard, F., Jones, C. M., … Maron, P. A. (2013). Loss in microbial diversity affects nitrogen cycling in soil. ISME Journal, 7(8), 1609–1619. https://doi.org/10.1038/ismej.2013.34
21. Piccinno, F., Gottschalk, F., Seeger, S., & Nowack, B. (2012). Industrial production quantities and uses of ten engineered nanomaterials in Europe and the world. Journal of Nanoparticle Research, 14(9). https://doi.org/10.1007/s11051-012-1109-9
22. Priester, J. H., Ge, Y., Mielke, R. E., Horst, A. M., Moritz, S. C., Espinosa, K., … Holden, P. A. (2012). Soybean susceptibility to manufactured nanomaterials with evidence for food quality and soil fertility interruption. Proceedings of the National Academy of Sciences, 109(37), E2451–E2456. https://doi.org/10.1073/pnas.1205431109
23. Priester, J. H., Moritz, S. C., Espinosa, K., Ge, Y., Wang, Y., Nisbet, R. M., … Holden, P. A. (2017). Damage assessment for soybean cultivated in soil with either CeO2 or ZnO manufactured nanomaterials. Science of the Total Environment, 579, 1756–1768. https://doi.org/10.1016/j.scitotenv.2016.11.149
24. Prosser, J. I. (2015). Dispersing misconceptions and identifying opportunities for the use of “omics” in soil microbial ecology. Nature Reviews Microbiology, 13(7), 439–446. https://doi.org/10.1038/nrmicro3468
25. Roco, M. C. (2011). The long view of nanotechnology development: The National Nanotechnology Initiative at 10 years. Journal of Nanoparticle Research, 13(2), 427–445. https://doi.org/10.1007/s11051-010-0192-z

26. Salvagiotti, F., Cassman, K. G., Specht, J. E., Walters, D. T., Weiss, A., & Dobermann, A. (2008). Nitrogen uptake, fixation and response to fertilizer N in soybeans: A review. Field Crops Research, 108(1), 1–13. https://doi.org/10.1016/j.fcr.2008.03.001
27. Shaw, L. J., Beaton, Y., Glover, L. A., Killham, K., & Meharg, A. A. (1999). Re-inoculation of autoclaved soil as a non-sterile treatment for xenobiotic sorption and biodegradation studies. Applied Soil Ecology, 11(2–3), 217–226. https://doi.org/10.1016/S0929-1393(98)00149-8
28. Simonin, M., Martins, J. M. F., Le Roux, X., Uzu, G., Calas, A., & Richaume, A. (2017). Toxicity of TiO2 nanoparticles on soil nitrification at environmentally relevant concentrations: Lack of classical dose–response relationships. Nanotoxicology, 11(2), 247–255. https://doi.org/10.1080/17435390.2017.1290845
29. Stowers, C., King, M., Rossi, L., Zhang, W., Arya, A., & Ma, X. (2018). Initial Sterilization of Soil Affected Interactions of Cerium Oxide Nanoparticles and Soybean Seedlings (Glycine max (L.) Merr.) in a Greenhouse Study. ACS Sustainable Chemistry and Engineering, 6(8), 10307–10314. https://doi.org/10.1021/acssuschemeng.8b01654
30. Tang, J., Zhu, N., Zhu, Y., Zamir, S. M., & Wu, Y. (2018). Sustainable pollutant removal by periphytic biofilm via microbial composition shifts induced by uneven distribution of CeO2 nanoparticles. Bioresource Technology, 248, 75–81. https://doi.org/10.1016/j.biortech.2017.07.064
31. Thill, A., Zeyons, O., Spalla, O., Chauvat, F., Rose, J., Auffan, M. (2006). Cytotoxicity of CeO 2 Nanoparticles Physico-Chemical Insight of the Cytotoxicity Mechanism. Environmental Science & Technology, 6151–6156.
32. US EPA. (1999). Biosolids Generation, Use, and Disposal in The United States Solid Waste and Emergency Response (5306W) Biosolids Generation, Use, and Disposal in the United States. (September). Retrieved from www.epa.gov
33. USDA. (2019). Crop Production 2018 Summary. (February). Retrieved from https://www.nass.usda.gov/Publications/Todays_Reports/reports/cropan19.pdf
34. Wang, G., Zhang, J., He, X., Zhang, Z., & Zhao, Y. (2017). Ceria Nanoparticles as Enzyme Mimetics. Chinese Journal of Chemistry, 35(6), 791–800. https://doi.org/10.1002/cjoc.201600845

35. Wang, Y., Chang, C. H., Ji, Z., Bouchard, D. C., Nisbet, R. M., Schimel, J. P., … Holden, P. A. (2017). Agglomeration Determines Effects of Carbonaceous Nanomaterials on Soybean Nodulation, Dinitrogen Fixation Potential, and Growth in Soil. ACS Nano, 11(6), 5753–5765. https://doi.org/10.1021/acsnano.7b01337
36. Xie, C., Zhang, J., Ma, Y., Ding, Y., Zhang, P., Zheng, L., … He, X. (2019). Bacillus subtilis causes dissolution of ceria nanoparticles at the nano-bio interface. Environmental Science: Nano, 6(1), 216–223. https://doi.org/10.1039/C8EN01002A

PREDICTIVE METAGENOMIC ANALYSIS REVEALS HOW CEO2 NANOPARTICLES ALTER MICROBIAL FUNCTION IN THE SOYBEAN MICROBIOME

Matthew R Slattery., Stacey L. Harper, Mark G. Johnson, Christian P. Andersen, Jay R. Reichman

In preparation for submission

Chapter 5. Predictive metagenomic analysis reveals how CeO_2 nanoparticles alter microbial function in the soybean microbiome

5.1 Introduction

Cerium oxide nanoparticles (CeNPs) are used in a variety of industrial applications including fuel additives, chemical planarization, and UV-coatings (Piccinno 2012, Keller 2013). Among the 10,000 metric tons of CeNPs produced every year, roughly 14% are expected to contaminate soils (Keller 2013). One proposed vector of contamination includes biosolids application, in which up to 90% of CeNPs that travel through wastewater treatment plants are deposited into the biosolids (Barton 2014) and are subsequently applied to farmland as fertilizer. Another significant route of contamination is through atmospheric deposition from diesel exhaust aerosols, as diesel engines burning fuel containing CeNPs could result in soil concentrations up to 1 mg kg^{-1} along roadways (Park 2008).

Given the potential for CeNPs to accumulate in soil compartments, it is important to understand how they interact with microbial communities. Soil bacteria are a massively diverse group of organisms which have historically remained mysterious in their functional capacities (Fierer 2007), though modern sequencing technologies offer one avenue to resolve these mysteries (Prosser 2017). Microbes that exist in mutualistic relationships with plants have garnered particular attention because they play a critical role in carbon sequestration, ecosystem functioning, and nutrient cycling (Berg 2009). For example, nitrogen fixing bacteria including *Bradyrhizobia* transform elemental nitrogen in the atmosphere to ammonia for their soybean hosts. This symbiotic relationship significantly reduces the need for nitrogenous fertilizer application (Salvagiotti 2008), reflecting the agricultural relevance of soil microbes in addition to their ecological importance. In fact, plants excrete 10-44% of their photosynthetically derived carbon into soils to promote the enrichment of beneficial microorganisms (Guttman 2014).

It is important to consider the interaction between microbial communities and engineered nanomaterials because bacteria serve as both targets of nanomaterial toxicity and, simultaneously, as influencers of nanomaterial behavior (Holden 2014). Evidence suggests that

CeNPs have the capacity to disrupt the soybean-microbe relationship, as early evaluation by Priester et al (2012) suggested that soybean nodulation – the process by which soybeans facilitate nitrogen fixation – could be affected by CeNP exposure. In particular, this study aims to build upon the work of a previous experiment in which soybeans were grown in a natural soil amended with CeNPs at environmentally relevant concentrations and soil incubation regimes that established an aged and pristine exposure scenario (Chapter 4). The results of that investigation relied on phylogenetic and taxonomic assessment of the soybean microbiome to determine the extent of response by the bacterial community.

To validate the phylogenetic findings of that study and further differentiate the biological activity of the various CeNP treatments in the soybean microbiome, the 16S universal marker data collected previously was fed to the Phylogenetic Investigation of Communities by Reconstruction of Unobserved States 2 (PICRUSt2) software package. PICRUSt2 is based on the original PICRUSt program, which makes accurate predictions about the functional capacity of a given community based on 16S data (Langille 2013). The output of this package is interpreted in both the enzymatic and pathway-based changes that PICRUSt2 predicts. The data output is based on bacteria with fully sequenced genomes when available and interpolates what a bacteria's genome would look like based on its nearest known taxonomic neighbor. In the context of the CeNP exposed soybean microbiomes, the predicted abundance of enzymes and pathways were compared to explore what functional changes occurred.

5.2 Methods

5.2.1 Collection of soybean microbiome 16S data

The 16S dataset used in this study was generated in a previous experiment. An overview of the study design is presented here for context, and a detailed description of the methods can be found in Chapter 4 (CeO2 nanoparticles affect soybeans and their root-associated microbiome at low, environmentally relevant concentrations).

CeNPs with a primary particle size of 16 nm were supplied from Sigma Aldrich (St Louis, MO, USA). Two amendment timelines were followed for particle aging. In the aged treatments, CeNPs were added to the soil 106 days prior to soybean planting. In the pristine treatments, CeNPs were added on the same day as soybean planting. The CeNPs were added to the soil in a deionized water suspension such that the soil concentration was either 1 mg kg^{-1} (low) or 100 mg kg^{-1} (high). Soybeans were grown in greenhouse conditions for 84 days before being harvested at the R6/R7 stage.

At harvest, 4 soybeans from each of the 5 treatments (4 CeNP treatments plus control) were randomly selected. Approximately 1 g of root material (with loosely bound soil still attached) from each soybean was collected for DNA extraction. A sequential washing and sonication procedure was followed to establish three distinct spatial compartments in each plant, in order of proximity to the root surface: rhizosphere, rhizoplane, and root. This produced 60 samples (5 treatments x 4 plants per treatment x 3 compartments per plant) for 16S amplicon sequencing using an Illumina MiSeq (San Diego, CA, USA). The output from the MiSeq was processed in the QIIME 2 bioinformatic package to produce a set of amplicon sequence variants (ASVs) and their associated frequency table.

5.2.2 PICRUSt2 pipeline

The PICRUSt2 suite is a compilation of other tools listed here. Sample amplicon sequence variants (ASVs) were aligned to reference sequences using HMMER (Eddy 2011) and placed into a reference tree using EPA-NG (Barbera 2018) and gappa (Czech 2019). PICRUSt2 normalizes for multiple 16S gene copies in bacteria using the hidden state prediction tool, castor (Louca 2018). The normalized data was used to predict gene family profiles, and mapped onto gene pathways using MinPath (Ye 2009). The default protocols outlined on the PICRUSt2 GitHub page (https://github.com/picrust/picrust2/wiki) were followed.

5.2.3 Statistical comparisons

The Statistical Analysis of Metagenomic Profiles (STAMP) bioinformatics software package (Parks 2010) was used to determine statistically significant results from the PICRUSt2 output, for both the enzyme and pathway abundances. Significant changes in multiple group comparisons were determined with a Tukey-Kramer comparison ($p \leq 0.05$). For comparison of two groups, Welch's t-test was used ($p \leq 0.05$). Enzyme abundance in rhizosphere communities were compared with a student's t-test ($p \leq 0.05$). When indicated, some analyses restricted the significant results to those with a minimum effect size (the ratio of proportions between two enzymes or pathways) of 2.

5.3 Results and Discussion

There were two main outputs from PICRUSt2 to analyze: predicted enzyme abundances (listed according to their Enzyme Commission number (EC)) and predicted pathway abundances (generated by mapping EC abundances into the MetaCyc reactions database). Analyzing enzymes offers fine resolution of predicted changes within the metagenome, whereas the pathways give a broader sense of ecological functioning. Both categories will be considered in the context of community shifts elicited by CeNPs within the soybean root-associated microbiome.

5.3.1 CeNPs alter the abundance of a large suite of enzymes and pathways

Multiple group comparison across the control and all four CeNP treatments (low-pristine, high-pristine, low-aged, high-aged) revealed substantial changes to predicted abundance of enzymes and their associated metabolic pathways. The overall similarity of the enzymatic and pathway profiles is displayed as PCoA plots in Figure 5.1. The dissimilarity of both enzymatic and pathway profiles for the treatments appears comparable to the taxonomic findings from Chapter 4, in that the control and aged samples grouped separately from the pristine samples.

Statistical comparison of all treatments shows that out of 2305 enzymes identified by the PICRUSt2 analysis, 71% (1652 enzymes) showed different abundancies. Comparatively, 77% of

the 421 pathways identified were significantly different (326 pathways in total). Both of these metrics indicate that the presence of CeNPs in soil produces substantial changes across the metabolic profile of the soil metagenomes, and that soil functionality is probably more affected by pristine CeNPs than their aged counterparts based on their dissimilarity in the PCoA plot.

5.3.2 Aged treatments are more sensitive to CeNP concentration

In Table 5.1, the enzyme and pathway abundances were compared between the control and each of the individual treatments, providing a metric for the magnitude of metabolic change that occurs in response to CeNPs. The pristine treatments produced more significant differences in both enzyme and pathway abundance than either of the aged treatments. The low concentrations also produced more changes than the high concentration in both aging scenarios, though this was particularly apparent for the aged CeNPs where the number of significantly different enzymes or pathways more than tripled. By comparison, the low-pristine treatments showed roughly a 10% increase in enzyme and pathway abundance versus high-pristine. This complicates the concern over differential effects observed between pristine and aged particles by demonstrating that the metabolic activity of a soil microbiome might be more susceptible to changes in CeNP concentration if the particles are aged.

5.3.3 Distinct pathway modulation between pristine and aged CeNPs at low concentrations

When compared to control and filtered for features with a minimum 2-fold difference in abundance, the low-pristine treatment changed 51 pathways (Figure S5.1) whereas the low-aged treatment changed 19 pathways (Figure 5.2). Among these, 6 of the pathways were unique to the aged treatment suggesting a distinct response to the aged nanoparticles. Unique pathways included vitamin B12 biosynthesis (Figure S5.2) and chitin degradation (Figure S5.3). In the pristine treatment, unique pathways included denitrification (Figure S5.4) and gallate degradation (Figure S5.5). In future studies, these pathways may be useful starting points for

further analysis to differentiate the effects of aged and pristine CeNPs. Below, the enzymes involved in denitrification and other nitrogen cycling enzymes are evaluated.

5.3.4 Pristine CeNP exposure affects nitrogen cycling enzymes

One advantage to the PICRUSt2 analysis is the capacity to evaluate specific enzymes or pathways. This approach is superior for determining the practical impact of CeNPs to soil ecosystem functionality over a normal phylogenetic or taxonomic assessment, because a different community structure does not necessarily indicate a different functional capacity due to functional redundancy in soil communities (Allison 2008). Based on Chapter 4, the rhizosphere compartment (the outermost compartment tested) was the most sensitive spatial compartment with regard to CeNP response, and therefore the enzyme abundance comparisons shown here are calculated on the rhizosphere compartment predictions.

Nitrogen fixation is a biochemical process converting elemental nitrogen to ammonia, a form bioavailable to plants. This reaction is catalyzed by nitrogenase, which is in turn regulated by dinitrogen reductase 1 and 2 enzymes (Nordlund 2013). As seen in Figure 5.3A, there is a significant increase in the abundance of nitrogenase in the pristine treatments (significantly different in low-pristine) that would be expected considering the increased abundance of *Bradyrhizobia* observed in Chapter 4. The dinitrogen reductase enzymes (Figure 5.4B and C) decline in abundance, especially for dinitrogen reductase 2. These reductase enzymes block the activity of nitrogenase in the presence of sufficient ammonia concentrations, serving as a brake system for nitrogen fixation. This data suggests that nitrogen fixation processes are likely increasing in the presence of the pristine CeNPs, due to both an increase in nitrogenase and a decrease in the enzymes that block its activity. Aged treatments do not show the same trend.

In Figure 5.5A, the abundance of urease is significantly decreased in the pristine CeNP treatments. Urease is responsible for oxidizing urea, a nitrogen fertilizer whose use has increased tremendously in the last 50 years and is considered a significant contributor towards eutrophication issues in coastal areas (Glibert 2006). The reduced abundance of urease in the

pristine CeNP amendments could exacerbate problematic nutrient loading of waterways by mitigating the capacity for soils to compensate for overwhelming urea application. This is an example of how CeNPs might affect soil functionality with downstream effects other than disrupting mutualistic relationships with plants.

Other nitrogen cycling enzymes were also impacted significantly, notably those involved with denitrification – which returns ammonia to elemental nitrogen. Ammonia monooxygenase is one such denitrifying enzyme that significantly increased in the presence of low concentrations of pristine CeNPs (Figure 5.5B). This might suggest an increase in overall denitrification, but that is contradicted by significant decreases in the abundance of nitrite reductase and nitrate reductase (Figure 5.4) and the reduction in the overall denitrification pathway in the low-pristine treatment (Figure S5.5).

Collectively, the shift in nitrogen cycle enzyme abundance indicates that CeNPs significantly alter the functional capacity of soil communities to participate in nitrogen cycling. During the soil incubation process that the aged particles undergo, this effect disappears. Modification of nitrogen cycling functionality may help to explain the effects on soybean growth observed in Chapter 4: if normal nitrogen cycling processes are disrupted, there could be an associated disruption in nitrogen assimilation by plant species. The practical implications of this disruption are complicated by the fact that nitrogen use efficiency of plants changes depending on which forms are available and at what concentrations (Xu 2012). The decrease in abundance of nitrite and nitrate reductase enzymes, for example, could reduce the amount of nitrate in the soil. As a response to reduced nitrate availability, soybeans may devote additional resources to their *Bradyrhizobia* symbionts, thereby explaining the increase in nodule mass of the soybeans in the pristine CeNP treatments.

5.3.5 Evaluating the difference between pristine and aged CeNP effects

Based on the findings from PICRUSt2, it is apparent that the phylogenetic and taxonomic changes demonstrated in Chapter 4 can lead to changes in the functional capacities of the soil

community. Importantly, these functional changes are highly dependent on whether or not the CeNPs were aged via the 3 month soil incubation process. There are three possible explanations for this phylogenetic and functional distinction.

First, the aged particles could modify the community from which the soybean rhizosphere is generated. The root-associated microbiome of soybeans is a subset of the available microbes in the bulk soil community (Mendes 2014). If CeNPs change the composition of the bulk soil community, then the plants would not have the same source community of microbes to select from to generate their rhizosphere. This line of thought is not well supported by other studies: Ge et al (2014) found that CeNPs did not modify the bacterial community of bulk soils if a plant was not present, and different study with canola plants emphasized that proximity to the root surface was a relevant factor driving significant community changes (Hamidat 2016). However, the outermost compartment (which would be most similar to the bulk soil) appeared the most sensitive to CeNP exposure.

A second explanation is a transformation of the CeNP particles that results in a muted effect on microbial community shifts. There is a two-way interaction between nanomaterials and bacterial communities that can result in changes to nanoparticle characteristics (Holden 2014). In CeNPs specifically, mechanisms have been proposed for the reduction of Ce^{+4} to Ce^{+3} at the surface of CeNPs (Xie 2019). This could change the reactivity of the CeNPs in a manner analogous to the aging of silver nanoparticles, which undergo anaerobic sulfidation thereby reducing their cytotoxicity (Levard 2013). Environmental transformation of nanoparticles can include a multitude of interactions that affect surface coating, surface chemistry, and agglomeration (Lowry 2012). This is supported by the functionally distinct profiles of the microbial communities that PICRUSt2 predicted.

Finally, difference in soil mobility for the aged CeNPs could be a significant contributor. While CeNPs are known to accumulate at the root surface (Hernandez-Viezcas 2014), the extent of

accumulation could differ between aged and pristine particles. If this were the primary reason behind the difference, then the aged particles would need to be significantly less mobile than the pristine particles to display such a difference in the magnitude of their effect. In support of this, other studies have shown that bacteria can help to disperse nanoparticles and prevent their agglomeration (Horst 2010). However, PICRUSt2 predicted unique changes in enzyme and pathway abundance between the aged and pristine treatments, suggesting that CeNP mobility cannot completely explain the differences between biological responses to pristine and aged particles. In later investigations, measuring the concentration of CeNPs at the root-soil interface could provide valuable insight into the mobility of aged versus pristine particles. It's worth noting that cerium is the most abundant rare earth metal in soils (Dahle 2015), and therefore indiscriminate quantification of cerium in soils may not identify CeNPs at the relatively low concentrations (1 mg kg^{-1}) in which it was added in this study.

5.4 Conclusions

In this analysis, we revealed that CeNPs can elicit strong changes to the predicted abundance of enzymes and metabolic pathways in the soybean microbiome. Comparing these functional metrics demonstrates that aged CeNP treatments are more susceptible to changes in concentration than pristine particles, though pristine particles produce many more enzymatic and pathway responses in general. In particular, the pristine CeNPs appear to strongly impact the nitrogen cycle in a more substantial way than was originally expected based on the increased abundance of nitrogen fixing bacteria.

This follow-up study demonstrates the utility of the PICRUSt2 software to generate additional insights into the potential impacts of CeNPs on terrestrial systems. As with the previous study upon which it is based, we see again that the outcome of nano-biological interactions cannot be adequately described without considering the complex environmental interactions that can mediate nanomaterial behavior. Further, it provides supplemental evidence for the notion of atypical dose response curves and points out that this unusual phenomenon may be more likely to be significant after nanoparticles have aged in natural environments.

5.5 Funding

This work was supported by a Cooperative Training Partnership between Oregon State University and the Environmental Protection Agency (83591301), USDA-NIFA (2013-67021-21181), and the Agricultural Research Foundation (ARF8301A). Further support was provided to M.S. by the ARCS Foundation.

5.6 Conflicts of Interest

The authors declare no conflict of interest.

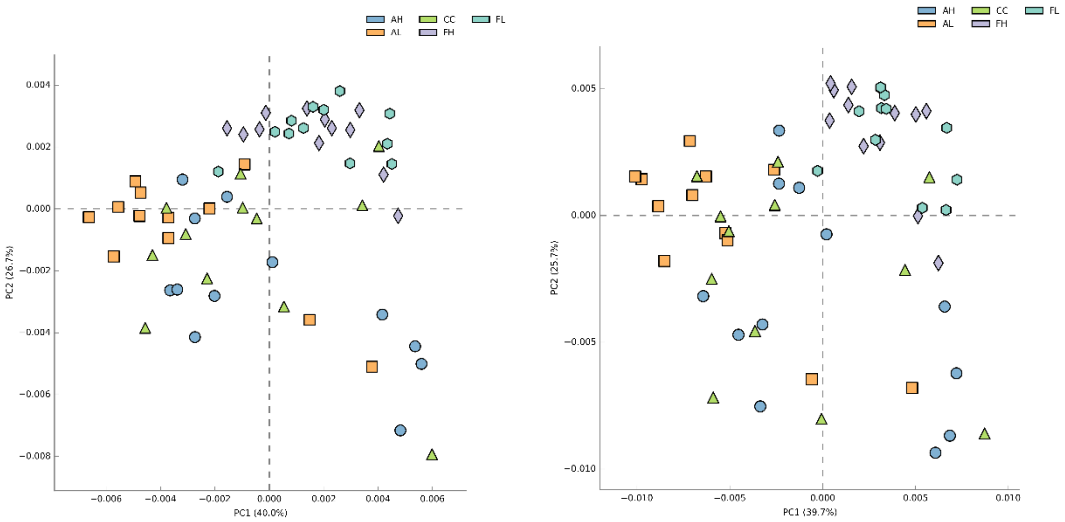

Figure 5.1. PCoA plots depicting the similarity of enzymatic (left) and metabolic pathway (right) samples across all treatments (green triangles=control, low-pristine=light blue hexagons, high-pristine=purple diamonds, low-aged=orange squares, high-aged=blue circles) based on their enzymatic or pathway abundance profiles.

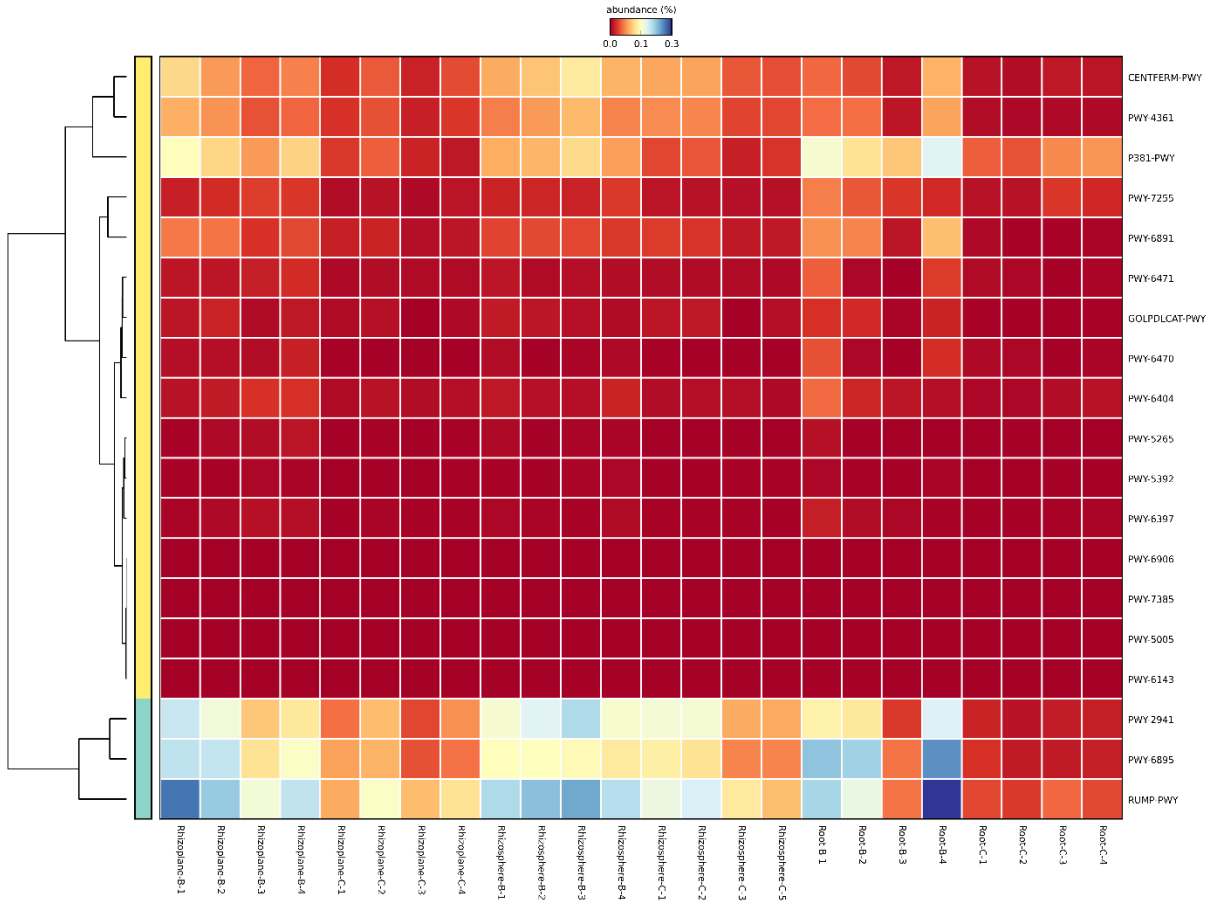

Figure 5.2. Heatmap of 19 significantly altered pathways ($p \leq 0.05$) with a minimum effect size (ratio of proportions between pathways) of 2, compared between control and low-aged CeNP treatment. All compartments are included.

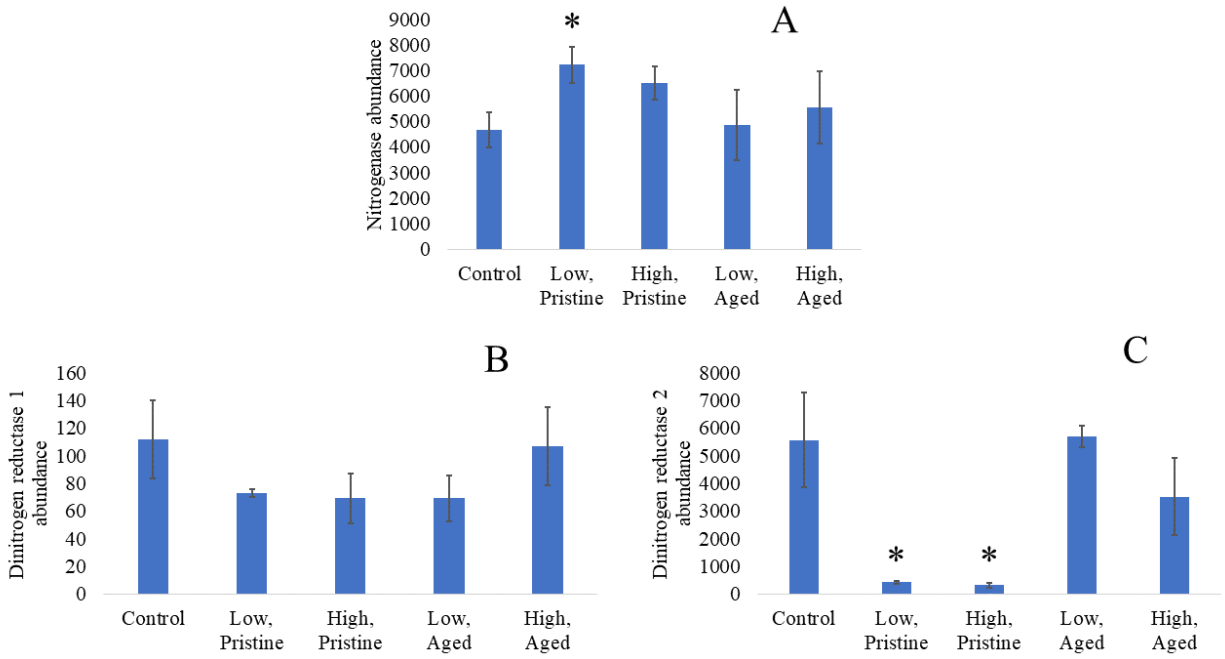

Figure 5.3. Comparison of predicted enzyme abundance across all treatments for nitrogenase (A), dintritrogen reductase 1 (B), dinitrogen reductase 2 (C) (* indicates significant difference from control, $p \leq 0.05$).

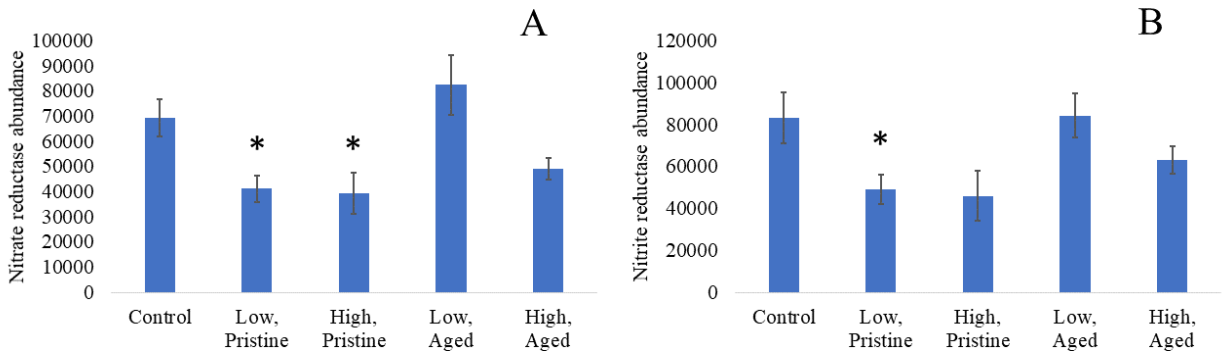

Figure 5.4. Comparison of predicted enzyme abundance across all treatments for nitrate reductase (A) and nitrite reductase (B) (* indicates significant difference from control, $p \leq 0.05$).

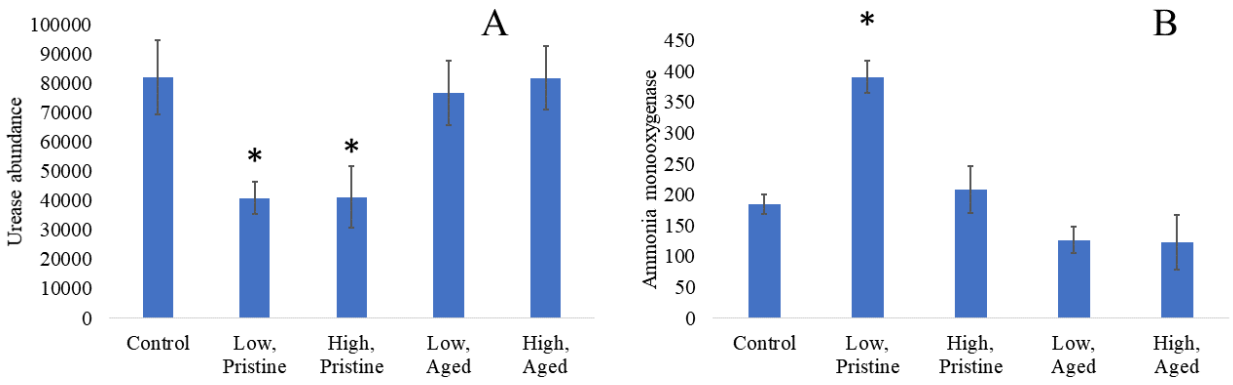

Figure 5.5. Comparison of predicted enzyme abundance across all treatments for urease (A), ammonia monooxygenase (B) (* indicates significant difference from control, $p \leq 0.05$).

Table 5.1 Summary of Welch's t-test comparisons between control group and the designated treatment, including both the number of significant enzymes and number of significant pathways that changed in abundance.

Treatment	Number of significant enzymes	Number of significant pathways
Low-pristine	1151	214
High-pristine	1030	199
Low-aged	840	188
High-aged	277	55

References Cited

1. Barbera, P., Kozlov, A. M., Czech, L., Morel, B., Darriba, D., Flouri, T., & Stamatakis, A. (2019). EPA-ng: Massively Parallel Evolutionary Placement of Genetic Sequences. Systematic Biology, 68(2), 365–369. https://doi.org/10.1093/sysbio/syy054
2. Barton, L. E., Auffan, M., Bertrand, M., Barakat, M., Santaella, C., Masion, A., … Bottero, J. Y. (2014). Transformation of pristine and citrate-functionalized CeO2 nanoparticles in a laboratory-scale activated sludge reactor. Environmental Science and Technology, 48(13), 7289–7296. https://doi.org/10.1021/es404946y
3. Berg, G., & Smalla, K. (2009). Plant species and soil type cooperatively shape the structure and function of microbial communities in the rhizosphere. FEMS Microbiology Ecology, 68(1), 1–13. https://doi.org/10.1111/j.1574-6941.2009.00654.x
4. Czech, L., & Stamatakis, A. (2019). Scalable methods for analyzing and visualizing phylogenetic placement of metagenomic samples. BioRxiv, 346353. https://doi.org/10.1101/346353
5. Eddy, S. R. (2011). Accelerated profile HMM searches. PLoS Computational Biology, 7(10). https://doi.org/10.1371/journal.pcbi.1002195
6. Ge, Y., Priester, J. H., Werfhorst, L. C. Van De, Walker, S. L., Nisbet, R. M., An, Y., … Holden, P. A. (2014). Cerium_particles_soybean.
7. Glibert, P. M., Harrison, J., Heil, C., & Seitzinger, S. (2006). Escalating worldwide use of urea - A global change contributing to coastal eutrophication. Biogeochemistry, 77(3), 441–463. https://doi.org/10.1007/s10533-005-3070-5
8. Guttman, D. S., McHardy, A. C., & Schulze-Lefert, P. (2014). Microbial genome-enabled insights into plant-microorganism interactions. Nature Reviews Genetics, 15(12), 797–813. https://doi.org/10.1038/nrg3748
9. Hamidat, M., Barakat, M., Ortet, P., Chanéac, C., Rose, J., Bottero, J. Y., … Santaella, C. (2016). Design Defines the Effects of Nanoceria at a Low Dose on Soil Microbiota and the Potentiation of Impacts by the Canola Plant. Environmental Science and Technology, 50(13), 6892–6901. https://doi.org/10.1021/acs.est.6b01056
10. Hernandez-Viezcas, J. A., Castillo-Michel, H., Andrews, J. C., Cotte, M., Rico, C., Peralta-Videa, J. R., … Gardea-Torresdey, J. L. (2013). In situ synchrotron X-ray

fluorescence mapping and speciation of CeO 2 and ZnO nanoparticles in soil cultivated soybean (Glycine max). ACS Nano, 7(2), 1415–1423. https://doi.org/10.1021/nn305196q

11. Holden, P. A., Schimel, J. P., & Godwin, H. A. (2014). Five reasons to use bacteria when assessing manufactured nanomaterial environmental hazards and fates. Current Opinion in Biotechnology, 27, 73–78. https://doi.org/10.1016/j.copbio.2013.11.008
12. Horst, A. M., Neal, A. C., Mielke, R. E., Sislian, P. R., Suh, W. H., Mädler, L., … Holden, P. A. (2010). Dispersion of TiO 2 nanoparticle agglomerates by Pseudomonas aeruginosa. Applied and Environmental Microbiology, 76(21), 7292–7298. https://doi.org/10.1128/AEM.00324-10
13. Keller, A. A., McFerran, S., Lazareva, A., & Suh, S. (2013). Global life cycle releases of engineered nanomaterials. Journal of Nanoparticle Research, 15(6). https://doi.org/10.1007/s11051-013-1692-4
14. Langille, M. G. I., Zaneveld, J., Caporaso, J. G., McDonald, D., Knights, D., Reyes, J. A., … Huttenhower, C. (2013). Predictive functional profiling of microbial communities using 16S rRNA marker gene sequences. Nature Biotechnology, 31(9), 814–821. https://doi.org/10.1038/nbt.2676
15. Levard, C., Hotze, E. M., Colman, B. P., Truong, L., Yang, X. Y., Bone, A., … Lowry, G. V. (2014). toxicity. 47(23), 13440–13448. https://doi.org/10.1021/es403527n.Sulfidation
16. Louca, S., & Doebeli, M. (2018). Efficient comparative phylogenetics on large trees. Bioinformatics, 34(6), 1053–1055. https://doi.org/10.1093/bioinformatics/btx701
17. Nordlund, S., & Högbom, M. (2013). ADP-ribosylation, a mechanism regulating nitrogenase activity. FEBS Journal, 280(15), 3484–3490. https://doi.org/10.1111/febs.12279
18. Park, B., Donaldson, K., Duffin, R., Tran, L., Kelly, F., Mudway, I., … Martin, P. (2008). Hazard and risk assessment of a nanoparticulate cerium oxide-based diesel fuel additive - A case study. Inhalation Toxicology, 20(6), 547–566. https://doi.org/10.1080/08958370801915309

19. Parks, D. H., & Beiko, R. G. (2010). Identifying biologically relevant differences between metagenomic communities. Bioinformatics, 26(6), 715–721. https://doi.org/10.1093/bioinformatics/btq041
20. Piccinno, F., Gottschalk, F., Seeger, S., & Nowack, B. (2012). Industrial production quantities and uses of ten engineered nanomaterials in Europe and the world. Journal of Nanoparticle Research, 14(9). https://doi.org/10.1007/s11051-012-1109-9
21. Priester, J. H., Ge, Y., Mielke, R. E., Horst, A. M., Moritz, S. C., Espinosa, K., … Holden, P. A. (2012). Soybean susceptibility to manufactured nanomaterials with evidence for food quality and soil fertility interruption. Proceedings of the National Academy of Sciences, 109(37), E2451–E2456. https://doi.org/10.1073/pnas.1205431109
22. Salvagiotti, F., Cassman, K. G., Specht, J. E., Walters, D. T., Weiss, A., & Dobermann, A. (2008). Nitrogen uptake, fixation and response to fertilizer N in soybeans: A review. Field Crops Research, 108(1), 1–13. https://doi.org/10.1016/j.fcr.2008.03.001
23. Xie, C., Zhang, J., Ma, Y., Ding, Y., Zhang, P., Zheng, L., … He, X. (2019). Bacillus subtilis causes dissolution of ceria nanoparticles at the nano-bio interface. Environmental Science: Nano, 6(1), 216–223. https://doi.org/10.1039/C8EN01002A
24. Xu, G., Fan, X., & Miller, A. J. (2012). Plant nitrogen assimilation and use efficiency. Annual Review of Plant Biology, 63, 153–182. https://doi.org/10.1146/annurev-arplant-042811-105532
25. Ye, Y., & Doak, T. G. (2011). A Parsimony Approach to Biological Pathway Reconstruction/Inference for Metagenomes. Handbook of Molecular Microbial Ecology I: Metagenomics and Complementary Approaches, 5(8), 453–460. https://doi.org/10.1002/9781118010518.ch52

Chapter 6 Conclusions

This dissertation explores the nuances of nanotoxicology with two distinct applications of nanomaterials: nanopesticides and cerium based nanoparticles (CeNPs).

In Chapters 2 and 3, two distinct nanopesticide products were evaluated. The first was a nano-sized encapsulation, in which the active ingredient was contained in a polymeric shell. The second was a milled active ingredient, ground down to nanoparticle sized granules. Each of these products modified the active ingredient toxicity, presumably due to the three-dimensional structure of the nanoparticles. The daphnids used in these assessments are filter feeding organisms with a preferential uptake of particles near 500 nm in diameter, which was similar to the dimensions isolated in the large granules and small capsules (approximately 400 and 450 nm, respectively). This is one example by which nanopesticide formulations could exert unusual or unexpected toxicity, demonstrating that the physical properties of nanomaterial constuents might be relevant information in addition to active and other ingredients. In the case of nanopesticides, the physical structure of the formulation appears to be a relevant factor in establishing risk to organisms that exhibit size-selective feeding behavior.

Another important consideration that emerges from the pesticide studies is how nanoparticles can influence the hydrophobic partitioning of active ingredients. In the nano-encapsulated product, it was not entirely surprising to find that the active ingredient's partitioning behavior was significantly delayed, because the capsule itself was intended to preserve the active ingredient from degradation (for marketing as a slow release product). This effect did not appear to be size-dependent between different nano-sized particles. In general, consideration of how encapsulated products modify the apparent hydrophobicity of pyrethroids and other hydrophobic active ingredients may help to improve our current regulatory strategies. However, these judgements cannot be based on size alone, because the second pesticide study revealed that not all nanopesticide particles can be expected to behave the same way. In that case, the milled version of the active ingredient showed changes in the hydrophobic partitioning only in the larger of the size ranges. This suggests that if new regulations are established for management of

nanopesticide products, it may be necessary to categorize the large variety of formation types that are emerging. For example, a different set of rules might regulate nanopesticides that incorporate nano-sized capsules versus a formulation that arises from nano-sized granules of the active ingredient. Capsules appear more likely to modify the hydrophobic behavior of active ingredients, and therefore the capsule formulations might need more stringent application windows that avoid rainfall events.

Chapters 4 and 5 explored the complex interactions between soybeans, microbes, and CeNPs. There are a number of important takeaways from these studies, beginning with the concentration of CeNPs tested. As noted previously, many other CeNP studies overlook environmentally relevant concentration ranges, presumably raising concentrations in an attempt to ensure biological responses. Yet our studies reflected that this conventional toxicology logic may not be valid for CeNPs applied to soil, and that lower doses may actually elicit stronger effects. This is concerning because a) previous literature of CeNPs may not be capturing important biological responses and b) establishing an acceptable concentration of CeNPs is not currently possible without knowing the shape of the concentration-response curve at these low concentrations.

In addition to showcasing why lower CeNP concentrations are relevant, these soybean studies also provide compelling evidence for the difference between pristine and aged nanomaterial exposures. While there are a number of possible explanations for why this difference occurs, it is important to keep this phenomenon in mind when designing future experiments, especially when working with nanomaterials that are resistant to degradation and prone to accumulation (such as CeNPs).

Finally, the soybean studies applied state-of-the-art sequencing technologies to learn more about how microbes might mediate CeNP toxicity to plants. The combination of phenotypic plant data, microbiome taxonomic data, and predicted soil functionality metrics offer a rare vertical integration of a biological system that is broadly perturbed by nanomaterials. Exactly how CeNPs are modulating the soybean-bacteria relationship is far from understood, but this combination of approaches pointed to future research areas that are likely to be fruitful. The

interaction of CeNPs with the nitrogen cycle appears to be a promising candidate based on multiple affects to the soybean-bacteria system: soybean yield, soybean nodule mass, abundance of nitrogen fixing bacteria, and nitrogen cycling enzyme abundances.

All together, these chapters represent a broad but unified exploration of nanomaterial nuances from a toxicological perspective. The results of the nanopesticide and CeNP experiments exemplify why reliance on the concentration of a substance is not sufficient to accurately predict its toxic effects in complex environmental systems. The disconnect between nanomaterial dosimetry and biological responses is derived from nanomaterials that can modify the behavior of other toxicants or display their own atypical concentration-response behavior. The lessons outlined from this dissertation contribute to our evolving knowledge of nanomaterials and bring environmental toxicologists one step closer towards a mastery of nanotoxicology.

APPENDICES

Appendix A. Supplemental information for Chapter 4

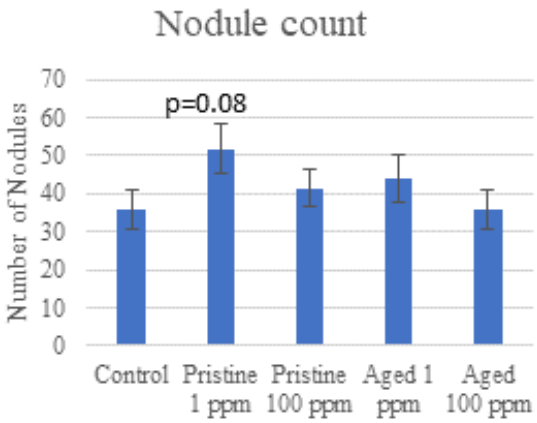

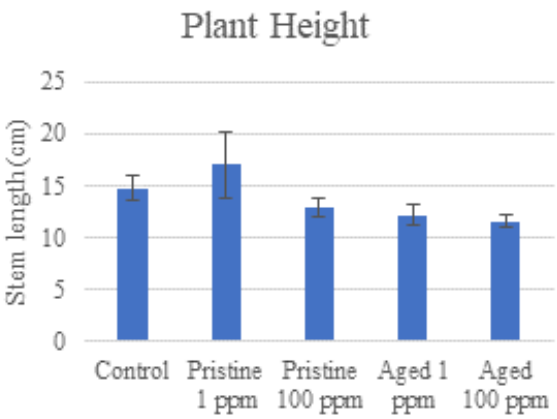

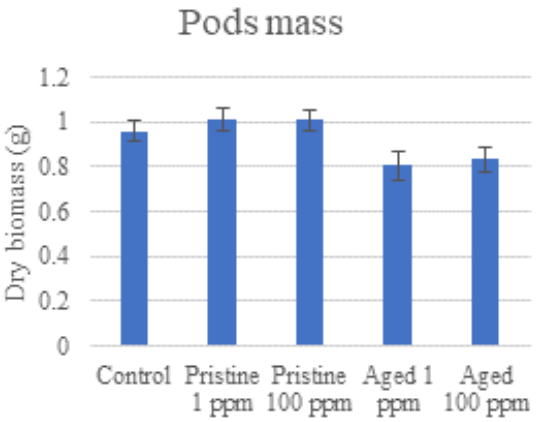

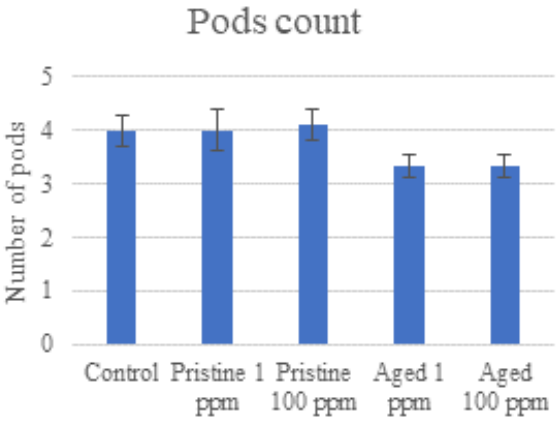

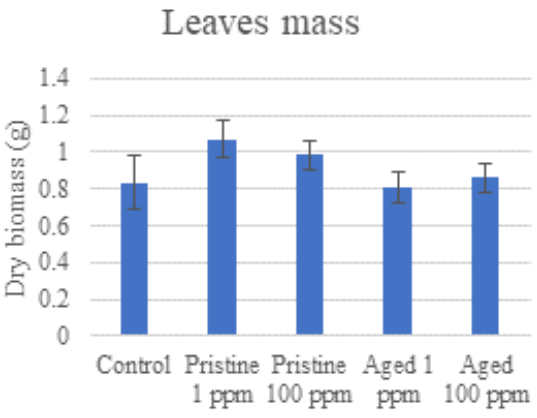

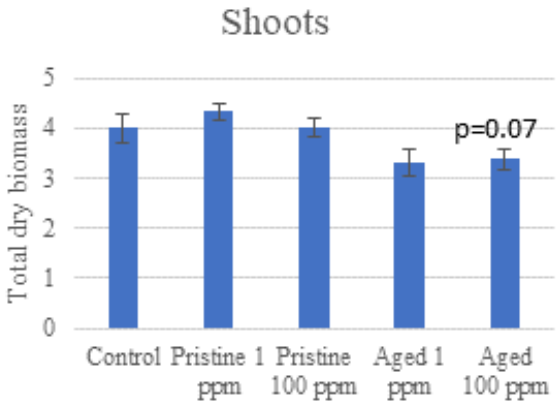

Figure S4.1. Supplemental phenotypic responses of soybeans exposed to pristine or aged (3 month incubation) CeNPs at low (1 ppm) or high (100 ppm) concentrations. The average nodule count (A), stem height (B), pods mass (C), pod count (D), leaf mass (E), total shoot mass (F) are represented here (n=9 except for control where n=10, bars represent SE, no significant differences observed between control and CeNP treatments, p-values indicated when $p<0.1$).

Sequencing and post-run analysis

A total of 60 samples were run, generating 9,711 features from 3,569,763 unique reads. The minimum reads in a sample was 13,611 and the maximum was 107,650, with an average of 59,496. The sampling depth was set to 13,611 to ensure that all samples were retained in for analysis. Rarefaction curves are displayed below to verify that the sampling depth was sufficient to capture a representative subset of reads from each sample.

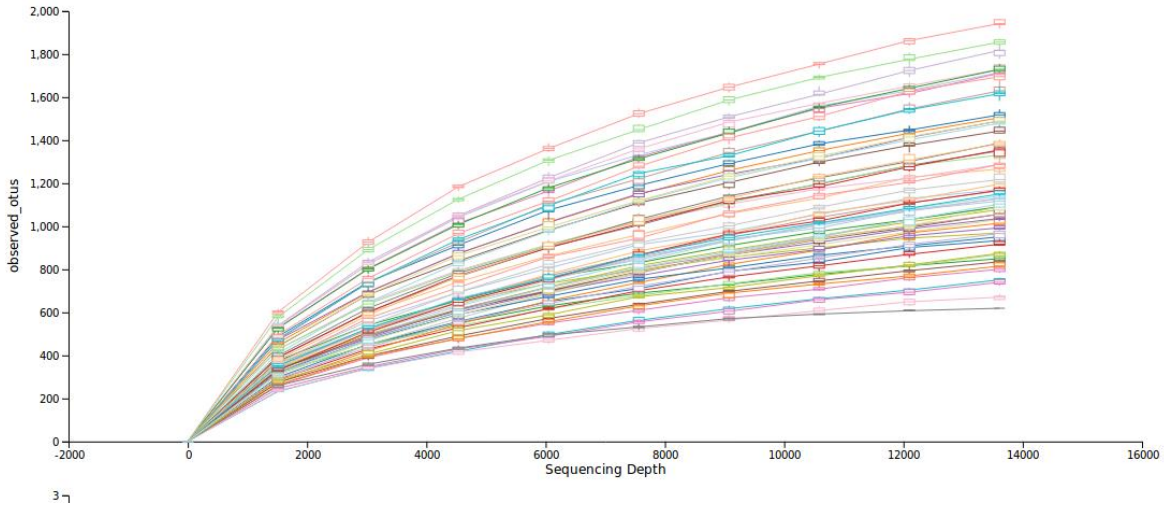

Figure S4.2. Observed OTUs measured across various sampling depths (maximum set to 13,611) for all samples.

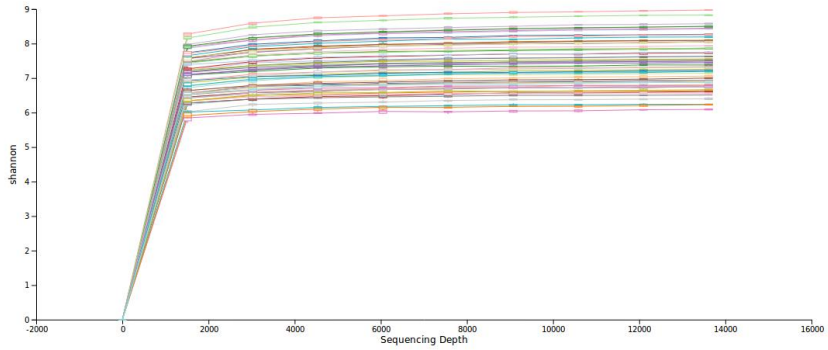

Figure S4.3. Shannon diversity measured across various sampling depths (maximum set to 13,611) for all samples.

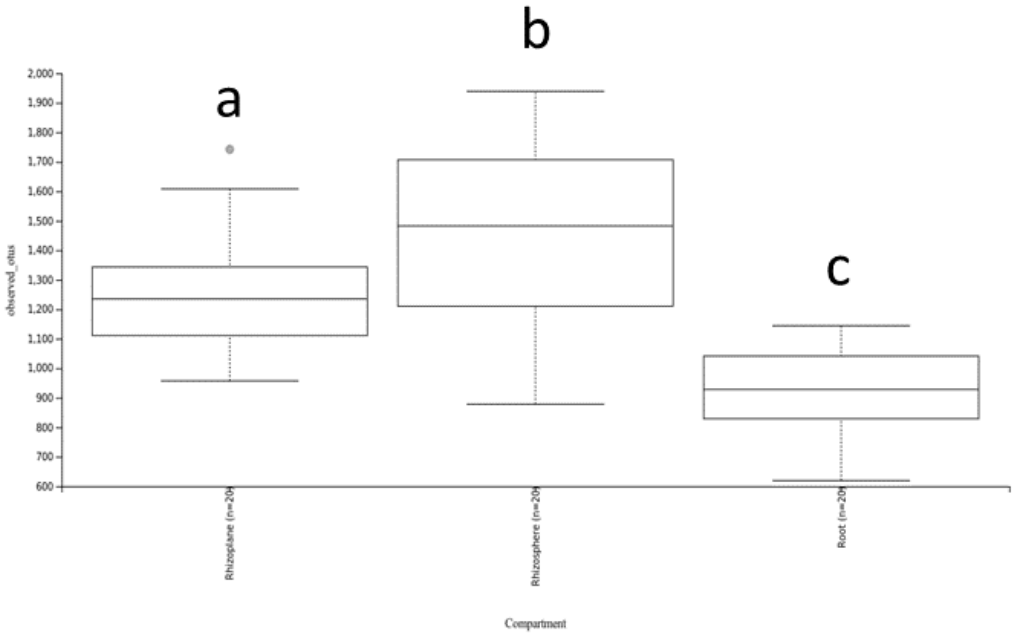

Figure S4.4. Observed OTUs in the rhizoplane, rhizosphere, and root compartments (note that the order is alphabetical, not spatially correct). Groups were compared with Kruskal-Wallis test, with letters indicating significant differences between groups (adjusted $p \leq 0.05$).

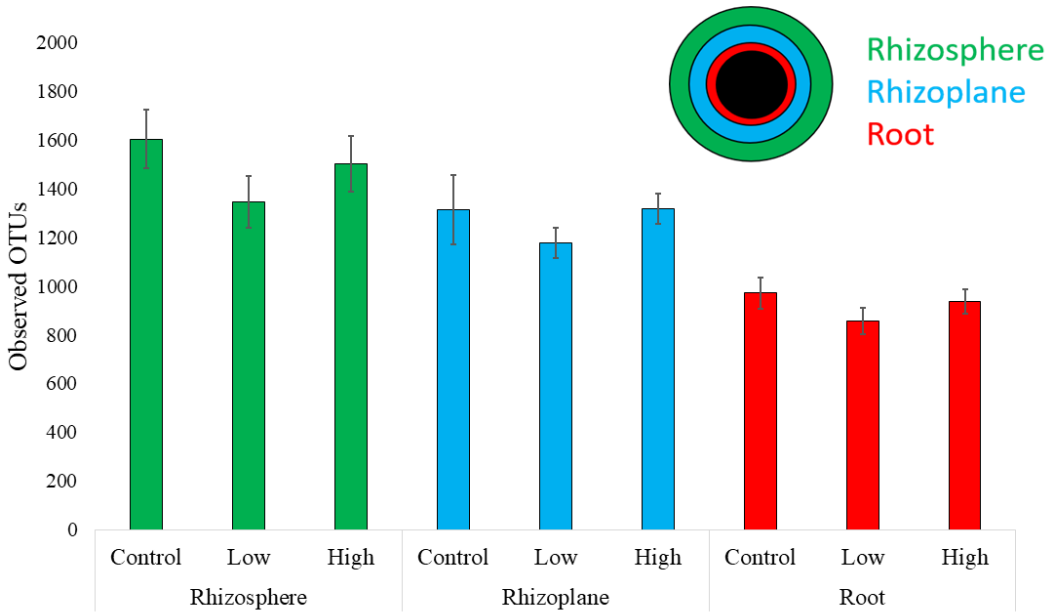

Figure S4.5. Average number of OTUs in soybean root-associated microbiome, separated by the three spatial compartments (rhizosphere, rhizoplane, and root) and subdivided into control, low (combined pristine and aged), and high (combined pristine and aged) treatments (n=8 except for control where n=4, bars represent SE, no significant differences within compartments according to Kurskal-Wallis comparison).

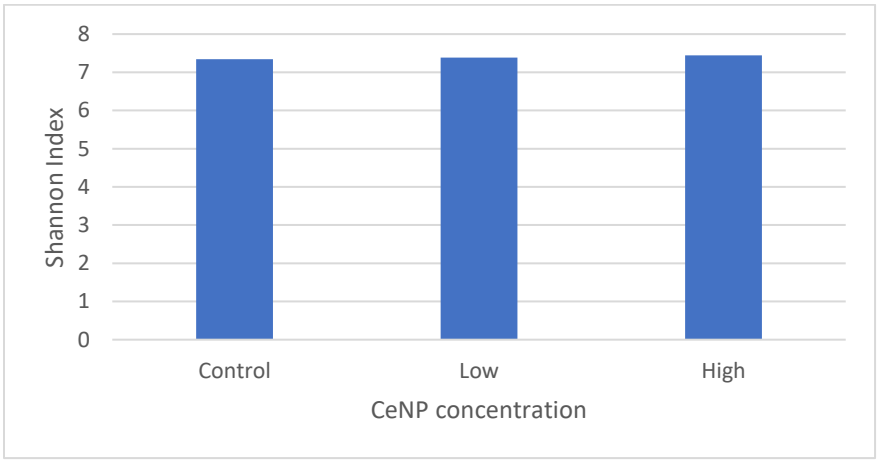

Figure S4.6. Shannon diversity index for the low (grouped pristine and aged) and high (grouped pristine and aged) treatments, no significant differences within compartments according to Kurskal-Wallis comparison.

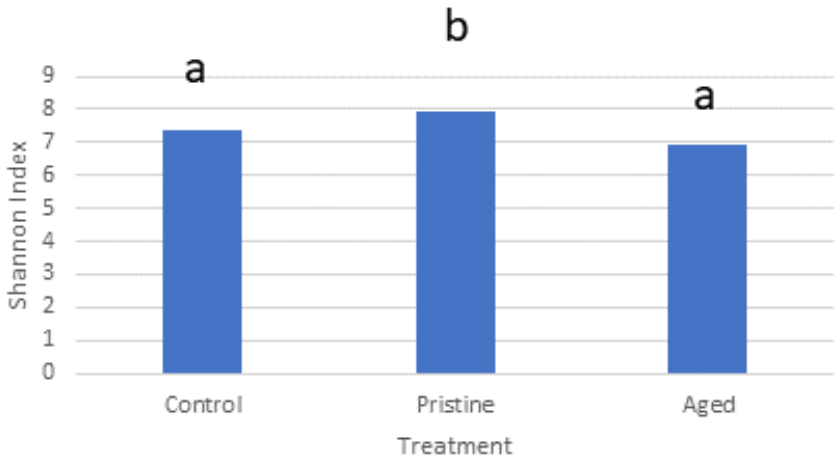

Figure S4.7. Shannon diversity index for the pristine (grouped low and high) and aged (grouped low and high) treatments. Groups were compared with Kruskal-Wallis test, with letters indicating significant differences between groups (adjusted $p \leq 0.05$).

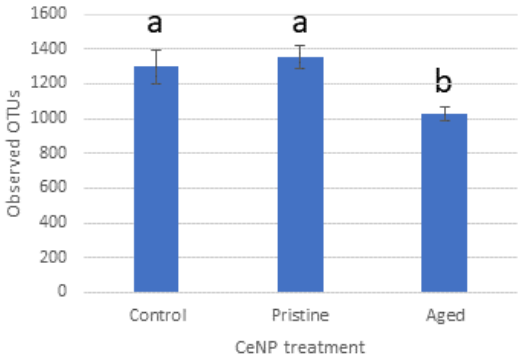

Figure S4.8. Observed OTUs for the pristine (grouped low and high) and aged (grouped low and high) treatments. Groups were compared with Kruskal-Wallis test, with letters indicating significant differences between groups (adjusted $p \leq 0.05$).

Table S4.1 Statistics for PERMANOVA comparison of weighted UniFrac distances.

Group 1	Group 2	Sample size	Permutations	pseudo-F	p-value	q-value
Rhizoplane	**Rhizosphere**	40	999	1.919128	0.120	0.1200
	Root	40	999	9.405614	0.001	0.0015
Rhizosphere	**Root**	40	999	12.410115	0.001	0.0015

Group 1	Group 2	Sample size	Permutations	pseudo-F	p-value	q-value
Aged	**Control**	36	999	2.169211	0.046	0.0460
	Fresh	48	999	22.780535	0.001	0.0015
Control	**Fresh**	36	999	14.077861	0.001	0.0015

Group 1	Group 2	Sample size	Permutations	pseudo-F	p-value	q-value
Control	**High**	36	999	2.865701	0.021	0.0315
	Low	36	999	3.642408	0.012	0.0315
High	**Low**	48	999	1.945974	0.093	0.0930

Table S4.2 Characterization of Oregon soil used for CeNP incubation and soybean cultivation.

Moisture	Sand	Silt	Clay	pH	BpH	EC	
4.1%	63.8%	20.1%	16.1%	6.59	7.03	0.393	
C	N	C:N	Active C	NO_3-N	NH_4-N	P	S
0.49%	0.035%	13.9	135.1ppm	54.6ppm	0.9ppm	10.8ppm	BQL
K	Ca	Mg	Na	K	Ca	Mg	CEC
49.0ppm	2032ppm	589ppm	178ppm	0.13 meq/100g	10.16 meq/100g	4.91 meq/100g	15.19 meq/100g
B	Mn	Cu	Zn	Al	Co	Ni	Pb
0.08ppm	22.0ppm	1.84ppm	1.26ppm	1110ppm	10.9ppm	22.3ppm	2.1ppm

Moisture	Gravimetric moisture as sample is received. All other data reported on a dry matter basis
Texture	Determined with hydrometer method after cementing and flocculating agents removed
pH EC	1:1 water:soil ratio, measured on a Hanna benchtop meter
BpH	Sikora buffered pH for determining lime requirement
Active Carbon	Readily oxidizable carbon measured by potassium permanganate reduction
NO_3, NH_4	Extracted with 2M KCl, measured on Lachat autoanalyzer
CEC	Sum of bases estimation of CEC
K, Ca, Mg, Mn, Zn, Cu, Fe	Extracted with Mehlich 3 solution, measured on Agilent 5110 ICP-OES
B	Extracted with 0.01M $CaCl_2$ solution, measured on Agilent 5110 ICP-OES

Na	Extracted with 1M ammonium acetate solution, measured on Agilent 5110 ICP-OES
Al, Co, Ni, Pb	Microwave digestion for total nutrient content, measured on Agilent 5110 ICP-OES
BQL	Below quantifiable limits

QIIME 2 Commands

##Soybean 16S Metagenomic Analysis on QIIME2
First processed 12/2018
##Illumina data stored at /media/sf_F_DRIVE/Amplicon-Metagenomics-Seq-Data/WED-MiSeq-amplicon-seq-data/181102_M04214_0013_000000000-B5RYW

#File directory
mkdir /media/sf_G_DRIVE/Soybean-16S-Metagenomics-120718
cd /media/sf_G_DRIVE/Soybean-16S-Metagenomics-120718

##
Import Illumina fastq files
##

#MiSeq data is imported as paired end reads with quality scores
#that have already been demultiplexed

qiime tools import \
--type 'SampleData[PairedEndSequencesWithQuality]' \
--input-path /media/sf_F_DRIVE/Amplicon-Metagenomics-Seq-Data/WED-MiSeq-amplicon-seq-data/181102_M04214_0013_000000000-B5RYW \
--source-format CasavaOneEightSingleLanePerSampleDirFmt \
--output-path demux-paired-end-soybeans.qza

#Create a summary of the demultiplexed data
qiime demux summarize \
--i-data demux-paired-end-soybeans.qza \
--o-visualization demux-paired-end-soybeans.qzv

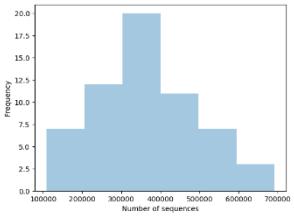

qiime tools view demux-paired-end-soybeans.qzv

```
#########################################################
                Quality Trimming and Processing
#########################################################

#Truncate sequences that have a successive run of low PHRED scores
qiime quality-filter q-score \
--i-demux demux-paired-end-soybeans.qza \
--o-filtered-sequences demux-filtered-soybeans.qza \
--o-filter-stats demux-filter-stats-soybeans.qza

#Deblur sequences and truncate at specified base position
qiime deblur denoise-16S \
--i-demultiplexed-seqs demux-filtered-soybeans.qza \
--p-trim-length 222 \
--p-jobs-to-start 10 \
--o-representative-sequences rep-seqs-deblur-soybeans.qza \
--o-table table-deblur-soybeans.qza \
--p-sample-stats \
--o-stats deblur-stats-soybeans.qza

# Visualize the q-score filtering result
qiime metadata tabulate \
--m-input-file demux-filter-stats-soybeans.qza \
--o-visualization demux-filter-stats-soybeans.qzv
```

qiime tools view demux-filter-stats-soybeans.qzv

sample-id (#q2:types)	total-input-reads (numeric)	total-retained-reads (numeric)	reads-truncated (numeric)	reads-too-short-after-truncation (numeric)	reads-exceeding-maximum-ambiguous-bases (numeric)
Rhizoplane-1-1	423774	423711	34	34	29
Rhizoplane-1-2	196809	196781	22	22	6
Rhizoplane-1-3	296446	296410	12	12	24

```
#Visualize the denoise filtering result
qiime deblur visualize-stats \
--i-deblur-stats deblur-stats-soybeans.qza \
--o-visualization deblur-stats-soybeans.qzv
```

qiime tools view deblur-stats-soybeans.qzv

	sample-id	reads-raw ▾	fraction-artifact-with-minsize	fraction-artifact	fraction-missed-reference	unique-reads-derep	reads-derep	unique-reads-deblur	reads-deblur	unique-reads-hit-artifact	reads-hit-artifact
40	Root-C-3	692537	0.421839	0.0	0.000374	32855	400398	5178	121672	0	0
23	Rhizoplane-C-4	632893	0.444036	0.0	0.000422	34911	351866	8932	112447	0	0
52	Rhizoplane-A-2	625420	0.403145	0.0	0.000348	28232	373285	5934	125856	0	0

```
#########################################################
                    Review filtered data
#########################################################

#Review filtered data and associated features

qiime feature-table summarize \
--i-table table-deblur-soybeans.qza \
--o-visualization rep-seqs-deblur-soybeans.qzv \
```

Frequency per sample

	Frequency
Minimum frequency	13,611.0
1st quartile	43,238.0
Median frequency	57,389.0
3rd quartile	74,791.0
Maximum frequency	107,650.0
Mean frequency	59,496.05

--m-sample-metadata-file soybean-metadata-120718.txt

qiime tools view rep-seqs-deblur-soybeans.qzv

##
Phylogenetic Tree
##

#Create a phylogenetic tree from the representative sequences
qiime alignment mafft \
--i-sequences rep-seqs-deblur-soybeans.qza \
--o-alignment aligned-rep-seqs-soybeans.qza

qiime alignment mask \
--i-alignment aligned-rep-seqs-soybeans.qza \
--o-masked-alignment masked-aligned-rep-seqs-soybeans.qza

qiime phylogeny fasttree \
--i-alignment masked-aligned-rep-seqs-soybeans.qza \
--o-tree unrooted-tree.qza

qiime phylogeny midpoint-root \
--i-tree unrooted-tree.qza \
--o-rooted-tree rooted-tree.qza

##
Alpha rarefaction
##

#Generate rarefaction curves to verify that the sampling depth is
#high enough to sufficiently represent the whole community.
#The max depth 13611 is chosen from the lowest number of
#features from rep-seqs-deblur-soybeans.qza
qiime diversity alpha-rarefaction \
--i-table table-deblur-soybeans.qza \
--i-phylogeny rooted-tree.qza \
--p-max-depth 13611 \
--m-metadata-file soybean-metadata-120718.txt \
--o-visualization alpha-rarefaction.qzv

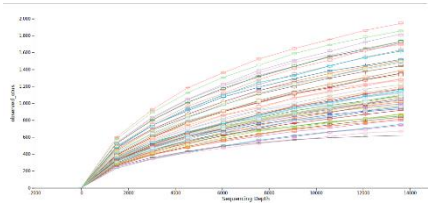

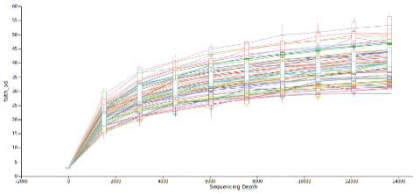

qiime tools view alpha-rarefaction.qzv

```
#########################################################
                    Phylogenetic core metrics
#########################################################

#Calculate the core metrics for phylogenetic diversity comparisons
#using the sampling depth verified above
qiime diversity core-metrics-phylogenetic \
--i-phylogeny rooted-tree.qza \
--i-table table-deblur-soybeans.qza \
--p-sampling-depth 13611 \
--m-metadata-file soybean-metadata-020719.txt \
--output-dir core-metrics-results
```

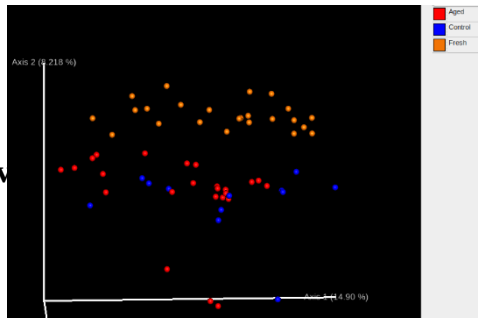

qiime tools view core-metrics-results/unweighted_unifrac_emperor.qzv
qiime tools view core-metrics-results/weighted_unifrac_emperor.qzv
qiime tools view core-metrics-results/jaccard_emperor.qzv
qiime tools view core-metrics-results/bray_curtis_emperor.qzv

```
qiime diversity alpha-group-significance \
--i-alpha-diversity core-metrics-results/faith_pd_vector.qza \
--m-metadata-file soybean-metadata-020719.txt \
--o-visualization core-metrics-results/faith-pd-group-significance.qzv

qiime diversity alpha-group-significance \
--i-alpha-diversity core-metrics-results/observed_otus_vector.qza \
--m-metadata-file soybean-metadata-020719.txt \
--o-visualization core-metrics-results/observed-otus-group-significance.qzv

qiime diversity alpha-group-significance \
--i-alpha-diversity core-metrics-results/shannon_vector.qza \
--m-metadata-file soybean-metadata-020719.txt \
--o-visualization core-metrics-results/shannon-group-significance.qzv

qiime diversity alpha-group-significance \
--i-alpha-diversity core-metrics-results/evenness_vector.qza \
--m-metadata-file soybean-metadata-020719.txt \
--o-visualization core-metrics-results/evenness-group-significance.qzv

qiime tools view core-metrics-results/faith-pd-group-significance.qzv
qiime tools view core-metrics-results/observed-otus-group-significance.qzv
qiime tools view core-metrics-results/shannon-group-significance.qzv
qiime tools view core-metrics-results/evenness-group-significance.qzv
```

```
#######################################################
            Beta diversity categorical comparisons
#######################################################

#Age-Comp unweighted
qiime diversity beta-group-significance \
--i-distance-matrix core-metrics-results/unweighted_unifrac_distance_matrix.qza \
--m-metadata-file soybean-metadata-020719.txt \
--m-metadata-column Compartment-Age \
--o-visualization core-metrics-results/unweighted-unifrac-distance-matrix-Compartment-Age.qzv
\
--p-pairwise

qiime tools view core-metrics-results/unweighted-unifrac-distance-matrix-Compartment-
Age.qzv


#######################################################
                  Alpha diversity correlations
#######################################################

#Correlate measures of alpha diversity with continuous
#variables such as bean biomass and nodule count

#Faith PD
qiime diversity alpha-correlation \
--i-alpha-diversity core-metrics-results/faith_pd_vector.qza \
--m-metadata-file soybean-metadata-020719.txt \
--o-visualization core-metrics-results/faith-pd-correlation.qzv

qiime tools view core-metrics-results/faith-pd-correlation.qzv


#Observed OTUs
qiime diversity alpha-correlation \
--i-alpha-diversity core-metrics-results/observed_otus_vector.qza \
--m-metadata-file soybean-metadata-020719.txt \
--o-visualization core-metrics-results/observed-otus-correlation.qzv

qiime tools view core-metrics-results/observed-otus-correlation.qzv
```

```
#Shannon
qiime diversity alpha-correlation \
--i-alpha-diversity core-metrics-results/shannon_vector.qza \
--m-metadata-file soybean-metadata-020719.txt \
--o-visualization core-metrics-results/shannon-correlation.qzv

qiime tools view core-metrics-results/shannon-correlation.qzv


#Evenness
qiime diversity alpha-correlation \
--i-alpha-diversity core-metrics-results/evenness_vector.qza \
--m-metadata-file soybean-metadata-020719.txt \
--o-visualization core-metrics-results/evenness-correlation.qzv

qiime tools view core-metrics-results/evenness-correlation.qzv


######################################################
                    Taxonomic analysis
######################################################

qiime feature-classifier classify-sklearn \
--i-classifier gg-13-8-99-OTUS-classifier.qza \
--i-reads rep-seqs-deblur-soybeans.qza \
--o-classification taxonomy.qza

qiime metadata tabulate \
--m-input-file taxonomy.qza \
--o-visualization taxonomy.qzv

qiime tools view taxonomy.qzv


qiime taxa barplot \
--i-table table-deblur-soybeans.qza \
--i-taxonomy taxonomy.qza \
--m-metadata-file soybean-metadata-120718.txt \
--o-visualization taxa-bar-plots.qzv

qiime tools view taxa-bar-plots.qzv
```

Appendix B. Supplement for Chapter 5

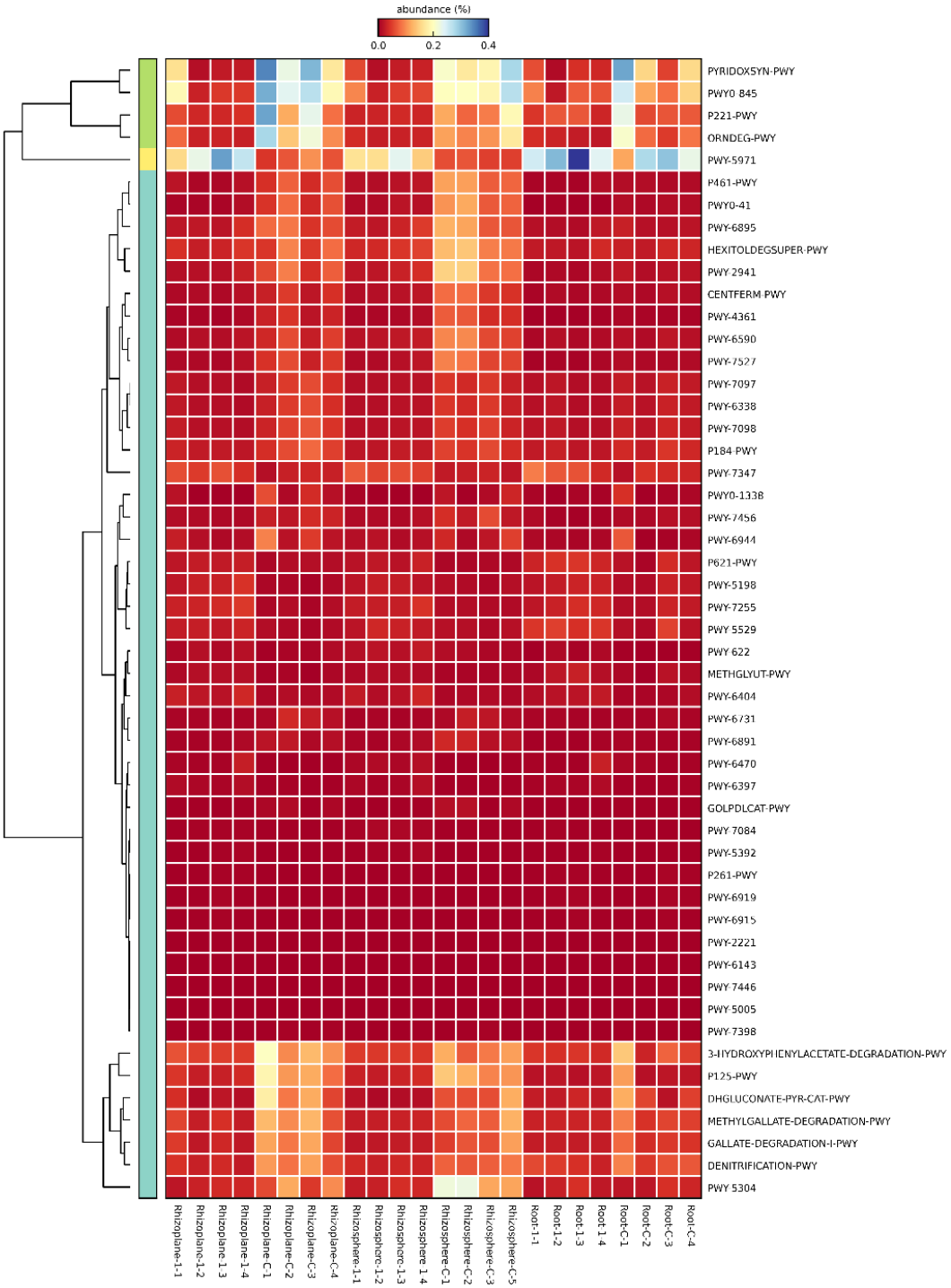

Figure S5.1. Heatmap of 51 significantly altered pathways ($p \leq 0.05$) with a minimum effect size (ratio of proportions between pathways) of 2, comparing control and low-aged CeNP treatments. All compartments are included.

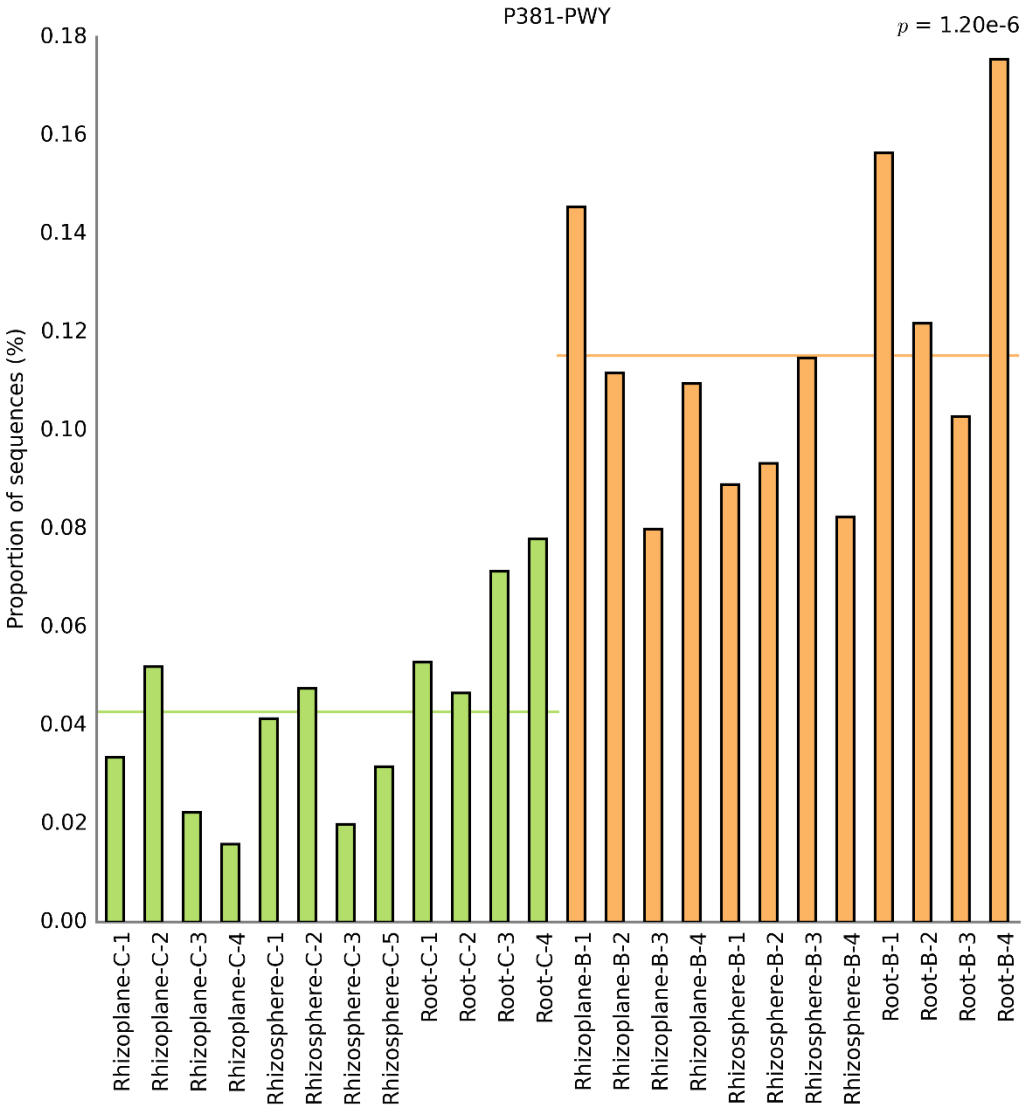

Figure S5.2 Abundance of P381-PWY, vitamin B12 biosynthesis, across control (green) and low-aged (orange) samples. ($p<0.001$)

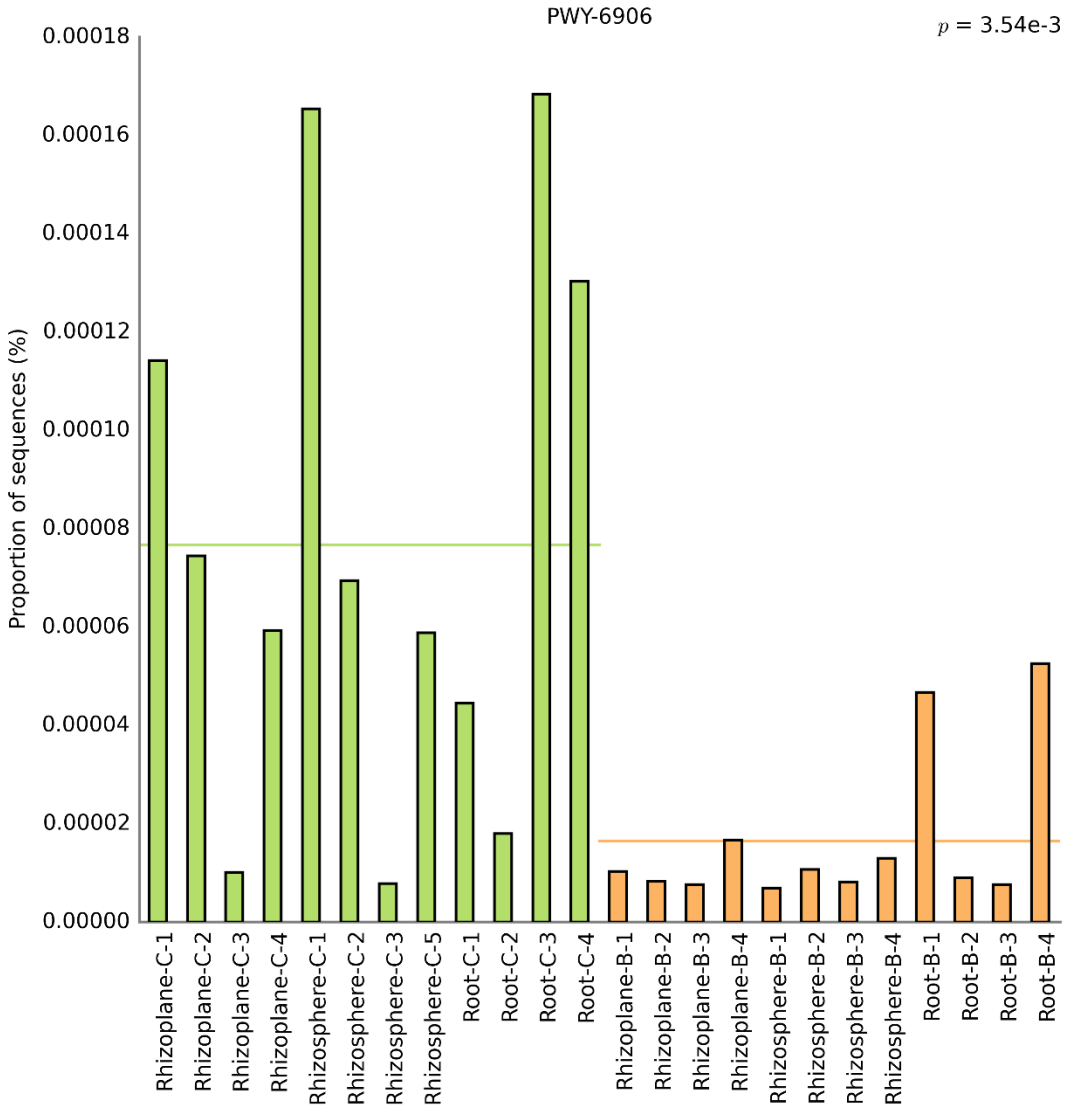

Figure 5.3 Abundance of PWY-6906, chitin degradation, across control (green) and low-aged (orange) samples. (p=0.004)

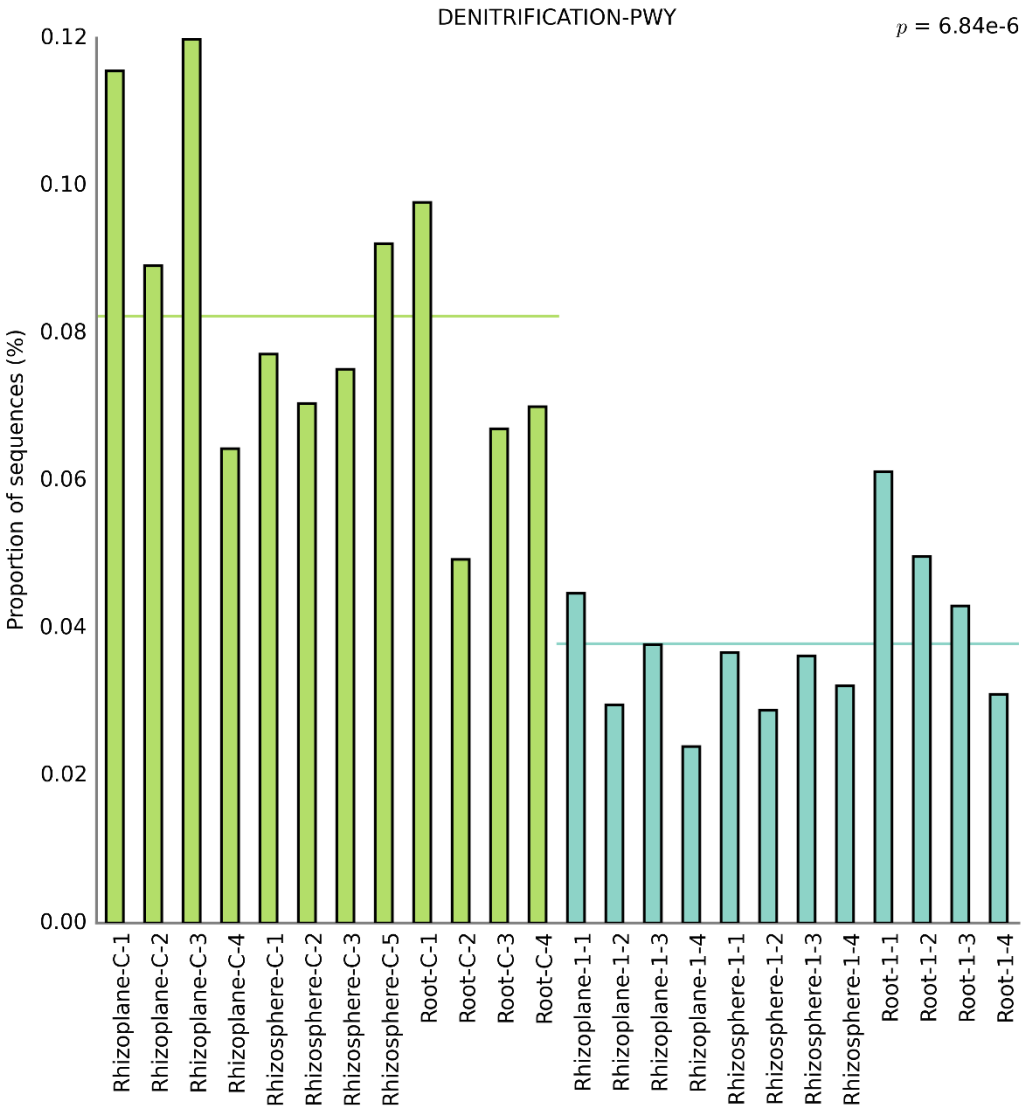

Figure S5.4 Abundance of DENITRIFICATION-PWY, denitrification of nitrate, across control (green) and low-pristine (blue) samples. ($p<0.001$)

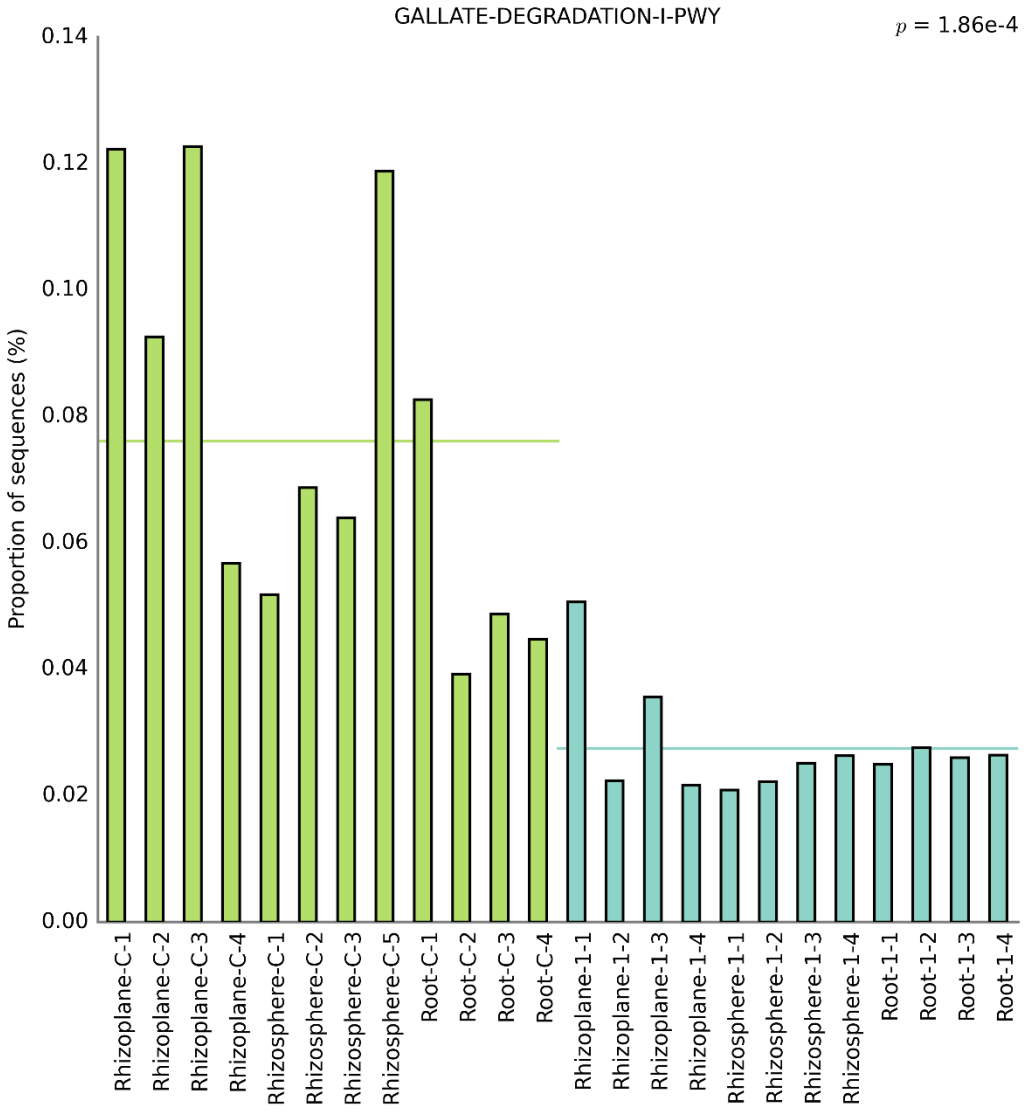

Figure S5.5 Abundance of GALLATE-DEGRADATION-I-PWY, degradation of gallic acid derivatives, across control (green) and low-pristine (blue) samples. ($p<0.05$)